Title

Investigating Combinatorial Extrinsic Regulation of Pluripotent and Neural Stem Cells for Applications in Regenerative Medicine

Author

Muckom, Riya J

Publication Date

2018

Peer reviewed|Thesis/dissertation

Investigating Combinatorial Extrinsic Regulation of Pluripotent and Neural Stem Cells for Applications in Regenerative Medicine

by

Riya J Muckom

A dissertation submitted in partial satisfaction of the

requirements for the degree of

Doctor of Philosophy

in

Chemical Engineering

in the

Graduate Division

of the

University of California, Berkeley

Committee in Charge:

Professor Douglas Clark, Co-Chair

Professor David Schaffer, Co-Chair

Professor Sanjay Kumar

Professor Henk Roelink

Summer 2018

Abstract

Investigating Combinatorial Extrinsic Regulation of Pluripotent and Neural Stem Cells for Applications in Regenerative Medicine

by

Riya J Muckom

Doctor of Philosophy in Chemical Engineering

University of California, Berkeley

Professor Douglas Clark, Co-Chair

Professor David Schaffer, Co-Chair

The potential for a biological stem cell to replenish itself as well as create diverse functional cell types leads to many applications in the field of regenerative medicine, such as disease modeling or cell replacement therapies. However, many of these applications rely on clear understanding and efficient control of regulatory processes that govern expansion and differentiation of stem cells. In its natural environment, a stem cell resides in a complex niche that presents multiple forms of instructive or selective signals simultaneously that act as "inputs" for cellular biochemical processes. Interestingly, combinatorial presentation of multiple signals have reported synergistic effects that cannot be predicted from linear addition of the signals in isolation. Here, we apply a novel *in vitro* culture system to systematically and effectively dissect combinatorial signaling environments for adult hippocampal neural stem cells and pluripotent stem cells to advance our fundamental understanding of these cellular systems as well as derive insights to aid in the clinic translation of potential cell replacement therapies.

Numerous biochemical cues from the endogenous hippocampal NSC niche have been identified as modulators of NSC quiescence, proliferation, and differentiation; however, the complex repertoire of signaling factors within stem cell niches raises the question of how cues act in combination with one another to influence NSC physiology. To help overcome experimental bottlenecks in studying this question, we adapted a high-throughput microculture system, with over 500 distinct microenvironments, to conduct a systematic combinatorial screen of key signaling cues and collect high-content phenotype data on endpoint NSC populations. This novel application of the platform consumed only 0.2% of reagent volumes used in conventional 96-well plates, and resulted in the discovery of numerous statistically significant interactions among key endogenous signals. Antagonistic relationships between FGF-2, TGF-β, and Wnt-3a were found to impact NSC proliferation and differentiation, whereas a synergistic relationship between Wnt-3a and Ephrin-B2 on neuronal differentiation and maturation was found. Furthermore, TGF-β and BMP-4 combined with Wnt-3a and Ephrin-B2 resulted in a coordinated effect on neuronal

differentiation and maturation. Overall, this study offers candidates for further elucidation of significant mechanisms guiding NSC fate choice and contributes strategies for enhancing control over stem cell based therapies for neurodegenerative diseases.

Additionally, the promising outlook for hPSC-derived cell therapies leads many to consider the development of manufacturing processes to meet the patient demand for such therapeutics. Toward this aim, 3D culture systems for hPSC differentiation are emerging because of their potential for higher expansion and yield of target cell types compared to 2D culture systems. Therefore, the ability to screen through a multifactorial parameter space of exogenous chemical cues for 3D hPSC cultures would greatly accelerate the pace of discovery and development of efficient in vitro differentiation protocols for target cell types of interest. Here, we demonstrate the advanced capabilities of a 3D micro-culture platform that we employ to screen through more than 1000 unique combinations of 12 independent 3D culture parameters to derive Olig2+Nkx2.2+ oligodendrocyte progenitor cells (OPCs) from hPSCs with 0.2% of the reagent volumes used in 96-well plates. We leverage novel fluorescent hPSC reporter cell lines to live-monitor proliferation and differentiation for over 80 days in the 3D micro-culture system. The robust data set enabled statistical modeling of the OPC differentiation process to uncover interactions and differential sensitivities to culture parameters such as hPSC seeding density, Retinoic Acid dose, Wnt pathway agonist CHIR dose and duration, SHH pathway agonist SAG dynamics, and combinations thereof. To show the generalizability of the platform, we then applied it to simultaneously assay 90 unique differentiation protocols to derive TH+ midbrain dopaminergic neurons from hPSCs. Overall, we demonstrate a strong methodology for upstream microscale screening/optimization to inform downstream scale-up processes to improve 3D production strategies of hPSC-derived CRTs.

Finally, as stem cell therapeutics continue to emerge in the clinic, upscaling processes must be developed to bridge the gap between microscale screening and patient demand. Toward this aim, we describe a pilot study to assess a stirred bioreactor configuration for the upscaling of 3D thermoreversible gel-encapsulated OPC production from hPSCs. Initially, we use computational modeling to predict and quantify the effect of stirred agitation on glucose concentration and shear stress profiles at a cross-section of the bioreactor vessel. Then, we use a pilot bioreactor system to measure hPSC viability, proliferation, and OPC differentiation with and without stirred agitation. Coupled together, screening and upscaling processes serve to accelerate the pace of discovery and development of much needed CRTs.

Acknowledgements

I've been so fortunate to have not one, but two very supportive PhD advisors in Dave and Doug - or as I refer to them, "DnD". The work here would not be possible without their support. Many thanks to both of them for their time, effort, guidance, feedback, sympathy, and charisma over the years! Also thanks to Henk and Sanjay for serving on my thesis committee and providing feedback as well as engaging in great conversations on the emergence of consciousness. This work was also supported by funding sources: National Science Foundation Graduate Research Fellowship Program, National Institutes of Health, and California Institute of Regenerative Medicine.

I am also very thankful to Christine, Carisa, Doris, Carlet and especially Noem for all of the administrative, logistical, and social support during my PhD. Noem, and I owe you so many drinks! No tequila, I promise.

Thank you to my peers, collaborators, undergrad mentees, and friends in the Schaffer and Clark Labs, as well as my CBE cohort, for the all shared experiences here - the good (exploring the Bay Area, Italy 2015, learning to ski and swim, ProCrops, SYIP 2017, antibodies that work) and the bad (stolen bikes, nasty exams, equipment malfunctions, gray hairs and leaky eyes). Special thanks to Sean, Maroof, Jorge S., Dawn, Anusuya, Sam, Brandon, Michelle, Efrem, Chris, Jorge M, Mary West, Eric Granlund, Henrik Wallman, George Tyson, Suzanne Sutton, and Naeem Zafar for sharing new perspectives and enjoyable interactions inside and outside of the lab - you all helped me grow in so many ways.

Also, many thanks to my fam - aunts, uncles, cousins, brothers. Those who always offered encouraging words, and those who helped me realize that I needed to improve my elevator pitch. And, of course, thanks to Mom and Dad for unwavering support, being my role models for strong will, and especially for breaking the laws of Indian Standard Time to arrive at my hooding ceremony on time.

Last, but not least, a very big thank you to Kate McKinnon - your *SNL* personalities were a reliable source of laughs to get through the lows of grad life!

Contents

List of Figures

List of Tables

List of Abbreviations

NSC ..... Neural Stem Cell

ASC ..... Adult Stem Cell

PSC ..... Pluripotent Stem Cell

OPC ..... Oligodendrocyte Progenitor Cell

FGF ..... Fibroblast Growth Factor

TGF-β ..... Transforming Growth Factor Beta

SHH ..... Sonic HedgeHog

BMP ..... Bone Morphogenetic Protein

SAG ..... Smoothened Agonist

RA ..... Retinoic Acid

GFAP ..... Glial Fibrillary Acidic Protein

TH ..... Tyrosine Hydroxylase

ECM ..... Extra-Cellular Matrix

CRT ..... Cell Replacement Therapy

DNA ..... Deoxyribonucleic Acid

2D 2-dimensional

3D 3-dimensional

PBS ..... Phosphate Buffered Saline

PFA ..... Paraformaldehyde

SLA ..... Stereolithography

DOE ..... Design of Experiments

Chapter 1

Introduction

1.1 Stem Cells in Regenerative Medicine

A stem cell is a type of biological cell within multicellular organisms that is characterized by it's capacity to self-renew and differentiate into a range of mature cell types. Generally, Adult Stem Cells (ASCs) are found in various organ systems of the adult body and have the potency to develop into cell types contained within the tissue of origin, such as adult neural stem cells (Figure 1.1) [1–4]. Pluripotent Stem Cells (PSCs), on the other hand, have a broader potency to develop into all mature cell types in the body, except germ cells, and are either found in the blastocyst of a developing embryo, termed Embryonic Stem Cells (ESCs) [5, 6], or created *in vitro* by induction of pluripotency in terminally differentiated cells, termed induced Pluripotent Stem Cells (iPSCs) [7, 8].

The potential for a stem cell to replenish itself as well as create diverse functional cell types leads to many applications in the field of regenerative medicine. For example, both ASCs and PSCs are being considered as sources of cell replacement therapy for numerous degenerative diseases [9–14]. Additionally, iPSCs from diseased patients can be differentiated into terminal cell types that can be used as disease models for fundamental biological studies or used in screening experiments for discovery of novel therapeutic agents [15–18]. Overall, many of these applications rely on clear understanding and efficient control of regulatory processes that govern expansion and differentiation of stem cells.

1.2 Regulation of Stem Cell Fate

A single stem cell can be abstracted to a unit process where the "system boundary" is the cell membrane that separates the intracellular environment from the extracellular environment. Molecular "inputs" are recieved by the cell and an "output" phenotypic response is calculated by the cell (Figure 1.2). The output response of a stem cell can be governed by both intrinsic and extrinsic regulatory mechanisms [19].

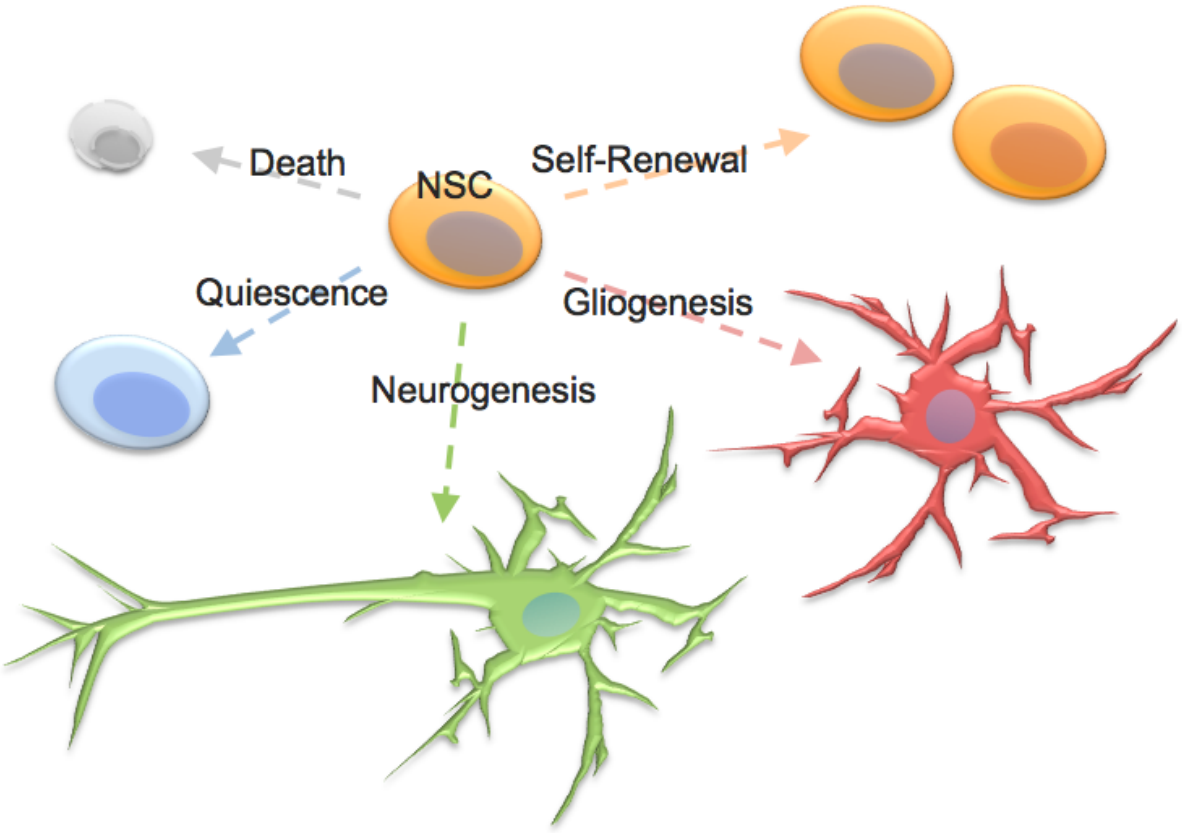

Figure 1.1: Neural stem cells from the adult hippocampus are able to remain quiescent, self renew, or differentiate into the major cell types in the adult brain - neurons and glia.

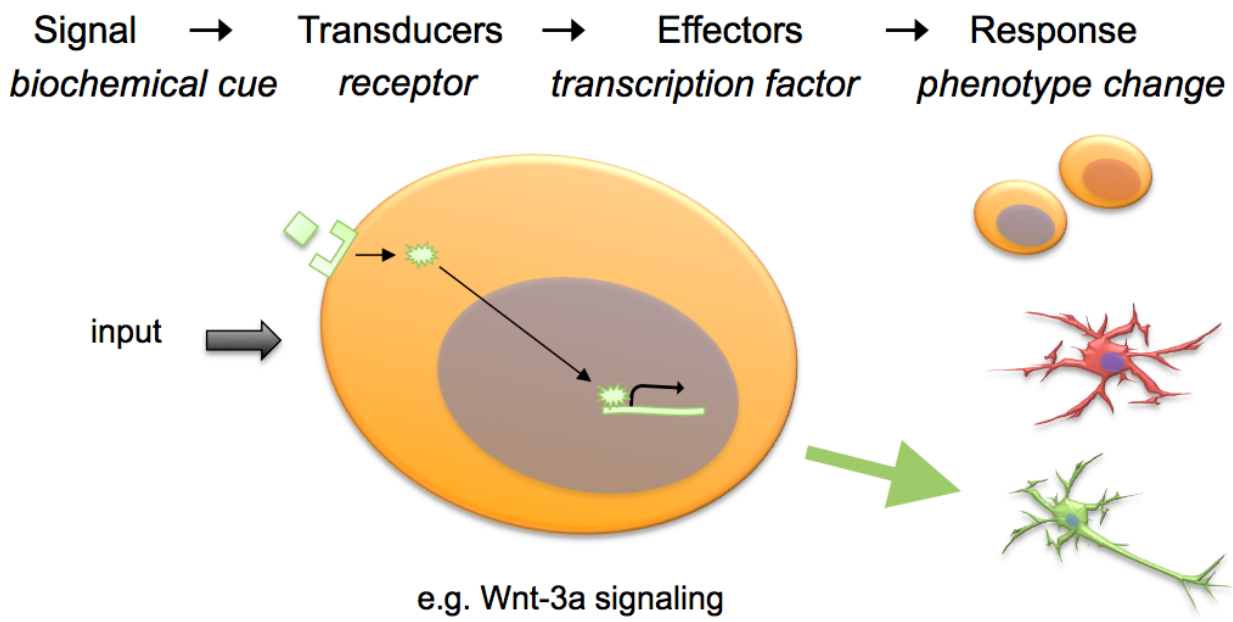

Figure 1.2: A stem cell is a unit process that recieves input signals to compute output responses, for example Wnt ligands induce neurogenesis in adult neural stem cells.

1.2.1 Intrinsic Regulation

The state of intracellular components within a stem cell confers competence to undergo various phenotypic transformations, such as a neural stem cell's capability to differentiate into a neuron [20, 21]. For example, the receptor expression profile of the cell, or the epigenetic state of the cell's DNA (altered by methylation or histone modifications) can limit a cell's competency to act on certain extracellular signals [22]. Additionally, the subcellular localization of organelles during cell division can lead to differential fate outcomes for daughter cells in the same extracellular context [23]. Intrinsic determinants of cell fate modulate the cellular response to extrinsic signals.

1.2.2 Extrinsic Regulation

Extrinsic regulation involves extracellular signals (in the form of biochemical molecules or biophysical forces) that activate specific receptors on the cell surface that relay microenvironmental information to the cell nucleus by way of intracellular signal transduction cascades. In the nucleus, transcriptional regulation is initially modulated in response to the external environment on a short timescale (minutes-hours). Cumulative changes in transcription over long time scales (hours-days) then emerge as a discrete "output" phenotypic response, such as cell cycle arrest, cell division, differentiation into a specialized cell type, or cell death [24].

In its natural environment, a stem cell resides in a complex niche that presents multiple forms of instructive or selective signals simultaneously that act as "inputs" for cellular biochemical processes [25–27]. Signals from the niche can include cell-extracellular matrix (ECM) interactions, cell-to-cell interactions with neighboring cells, and soluble cues that have been secreted from short-range or long-range distances (Figure 1.3). The extracellular matrix (ECM) of the stem cell niche is composed of a mixture of fibrous proteins, proteoglycans, glycosaminoglycans such as collagen, gelatin, heparan sulfate, laminin, and fibronectin, that contain peptide motifs which engage integrin receptors on the cell surface and activates signaling pathways in the cell [28]. Soluble cues that are secreted and diffuse from local regions or transported from distant organs through the blood stream can also activate signal tranduction cascades and phenotypic changes in stem cells, such as FGF, BMP, and TGF-β [29]. Finally, ligands that are bound to the cell surface of neighboring cells can activate signaling pathways in stem cells, such as Delta and Ephrin ligands for Notch and Eph receptors, respectively [30, 31].

1.3 Investigating Combinatorial Extrinsic Regulation of Stem Cell Fate

Interestingly, combinatorial presentation of multiple signals have reported synergistic effects that cannot be predicted from linear addition of the signals in isolation [32]. Also, variation in the temporal sequence of signals can alter cell responses [33]. *In vitro* culture systems can be harnessed as models to study the regulatory roles of extracellular signals in

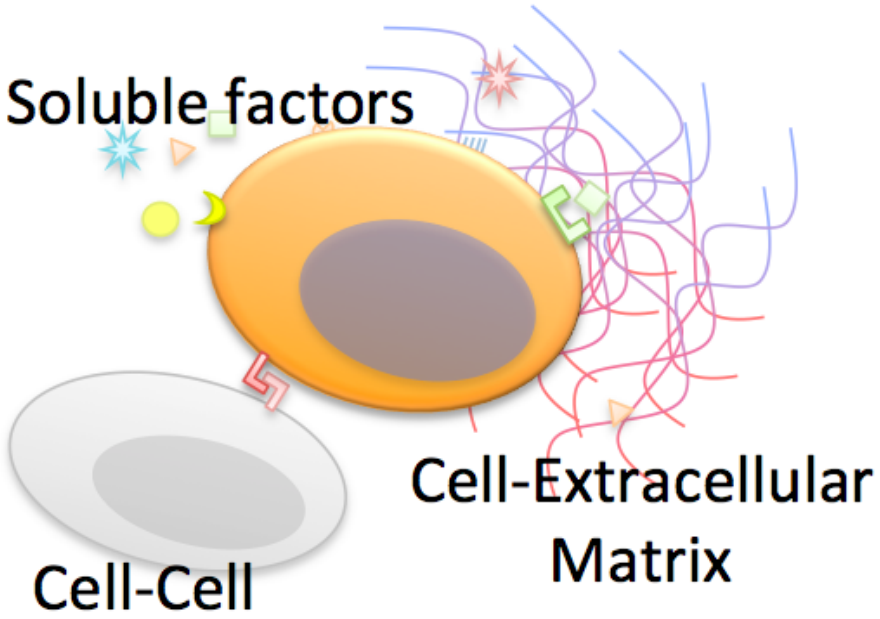

Figure 1.3: Different classes of biochemical molecules that act as extrinsic regulators of stem cell fate include soluble cues, ECM interactions, and cell-to-cell interactions.

combinations and temporal variations. These studies not only contribute to our fundamental understanding of stem cell regulation, but also can be applied toward translational endeavors such as optimization of directed differentiation protocols of cell types considered for cell replacement therapies.

1.3.1 Previous Work

Numerous studies have applied *in vitro* combinatorial screening methodologies to investigate various questions in stem cell systems and have elicited fundamental and translational insights that would not otherwise be predictable from the activity of signaling cues individually. Here we describe some recent studies that examined combinatorial effects of extracellular matrix (ECM) proteins, cell-to-cell interactions, and/or soluble cues toward the aim of recapitulating the complexity of respective stem cell niches for fundamental insights on stem cell regulation.

The patterned immobilization of proteins on a tissue culture surface has enabled controlled and systematic analysis of combinations of ECM components for better understanding the regulation of stem cells, such as for differentiation studies of embryonic neural stem cells. [34, 35] Additionally, miniaturization of the sample size is advantageous for reagents that may be cost-prohibitive, or cell types that are hard to expand *in vitro*, such as for the regulation of the endothelial-to-mesenchymal transformation. [36] Additional studies have identified combinatorial ECM compoenents that enhanced endothelial cell survival, nitric oxide production, and CD31 phenotypic expression [37] elucidated aspects of microenvironmental regulation of liver progenitors. [38]

New developments have further refined the exposure of signals to just the active peptide sequences within larger biomolecules in the cancer stem cell niche [39] or by increasing the patterning resolution of ECM proteins to the nano-scale. [40] Polymer pen lithography was applied toward studies of mesenchymal stem cell adhesion and differentiation. [41] Additionally, researchers have dramatically increased throughput of combinatorial parameter space using a bead-based signaling approach. [42]

Combinatorial studies in 3D culture systems are also emerging and enable assays that retain a more natural cellular cytoskeletal structure by avoiding the forced polarization of cells adherent to a 2D surface. These systems have provided information on combinatorial ECM influences on hESC differentiation [43] and hMSC-to-osteoblast differentiation [44]. Recently, light patterning has enabled combinatorial gradients of cell-to-cell or cell-to-ECM interactions in 3D hydrogels, which was applied to study mesenchymal stem cell biology. [45]

Many of the previously described studies that applied immobilization techniques were able to use a shared media phase across different culture conditions, as ligands of interest in their screens were not able to diffuse freely and did not risk confounding the results. For combinatorial screening of soluble cues, independant culture areas are necessary to ensure separation of different signaling conditions, as the soluble cues are free to diffuse through the media. One strategy applied here is separate microfluid chambers for full factorial analysis of soluble cues in iPSC to cardiomyocyte differentiation. [46] Alternatively, more traditional well-plate systems with robotic liquid dispensers have prevailed for long timescales in 2D [47] and for shorter timescales in 3D. [48] Further innovation in culture platforms could enable combinatorial screens of soluble cues that have been difficult to achieve in the past.

1.3.2 Proposed Work

The purpose of this work is to demonstrate the capabilities of a unique microculture methodology to investigate the effects of combinations and dynamics of soluble biochemical stimuli on neural and pluripotent stem cell fate specification, in 2D and 3D cultures, to increase our fundamental biological understanding and derive translational insights for these systems (Figure 1.4).

Aim 1 – High-Throughput Assay Development

Objective: Develop upon an existing platform to create a high-throughput, micro-scale in vitro endpoint phenotype assay for stem cells; test for cell viability and preservation of characteristic stem cell attributes. Hypothesis: Stem cell viability and characteristic attributes (proliferative and differentiative capacity) are preserved when adapting stem cells to miniaturized culture system.

Aim 2 – Characterize Effects of Combinatorial Signaling on Stem Cell Phenotype

Objective: Apply high-throughput method to measure the phenotypic endpoints of neural and pluripotent stem cell cultures in response to a large set of combinations of biochemical

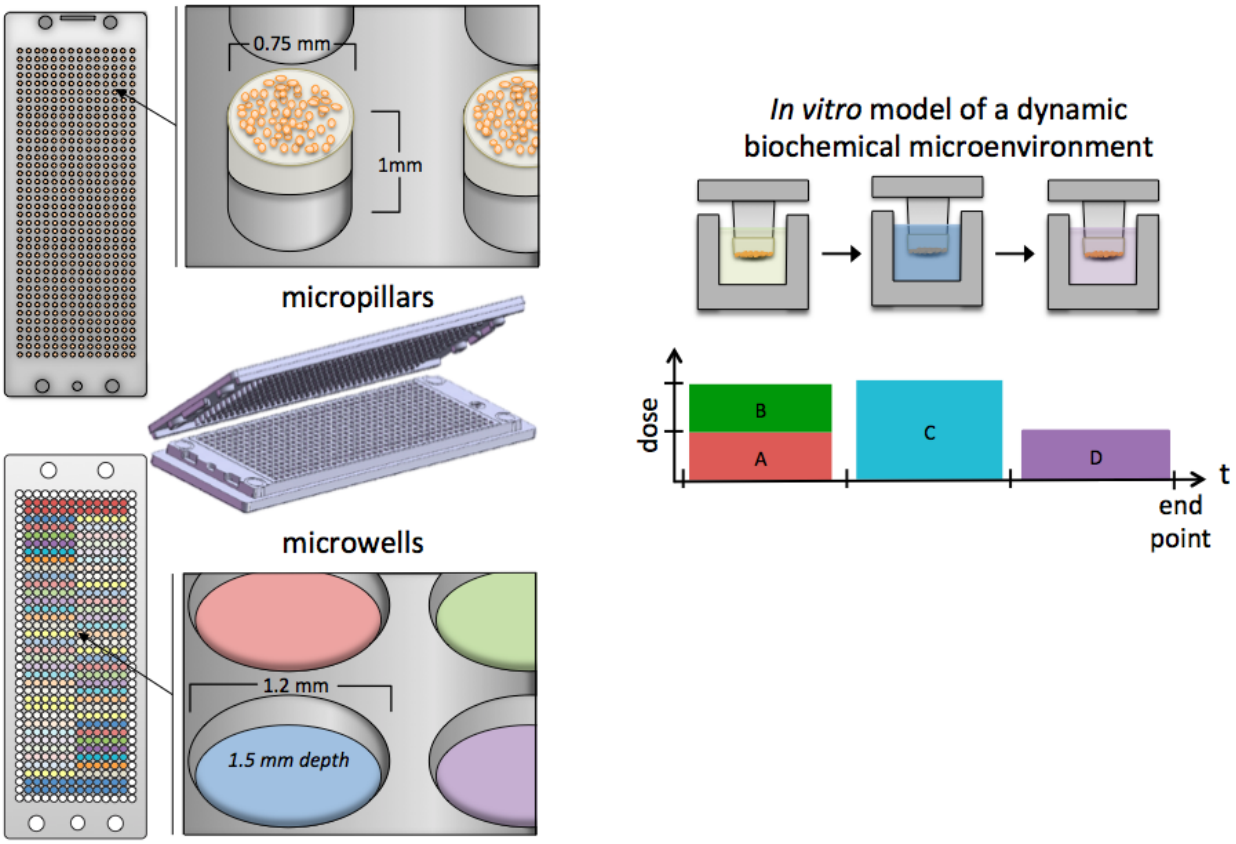

Figure 1.4: Microscale culture system for analysis of combinatorial soluble cues for stem cells in 2D and 3D. The system is composed of two halves – a chip with 532 x 750 μm wide pillars onto which cells can be deposited with a liquid dispensing system and a chip with 532 x 800 nL wells into which culture media and signaling cues can be dispensed – where placing the pillar chip into the well chip enables long term cell culture and subsequent imaging.

stimuli and apply statistical modeling approaches to elucidate trends between stimuli combinations and phenotypic response. Hypothesis: Stem cells respond to combinations of biochemical stimuli in ways that cannot be extrapolated from linear addition of the single stimuli phenotypic endpoints.

Aim 3 – Investigate Sensitivity of Dynamic Presentation on Stem Cell Phenotype

Objective: Characterize the effects of dynamic biochemical stimuli and analyze the phenotypic endpoints of neural and pluripotent stem cells. Hypothesis: Temporal modulation of stimuli can uncover potential intracellular priming relationships between endogenous biochemical cues, which enhances stem cell ability to respond more robustly to specific endogenous biochemical stimuli.

Chapter 2

Developing a System to Investigate Combinatorial Stem Cell Regulation

2.1 Introduction

The objective of this chapter was to develop upon an existing microchip technology [49, 50] to create a reliable system for the high-throughput, micro-scale in vitro endpoint phenotype assay for the study of combinatorial soluble signaling environments on stem cell proliferation and differentiation. The high-level workflow of this system can be separated into four major components (Figure 2.1).

1. Combinatorial liquid dispensing
2. Miniaturized stem cell culture
3. Fluorescence microscopy and image quantification
4. Data Handling and Visualization

The following results describe development of each sub-component to create a reliable and quality controlled system for the high-throughput study of stem cells in combinatorial signaling environments.

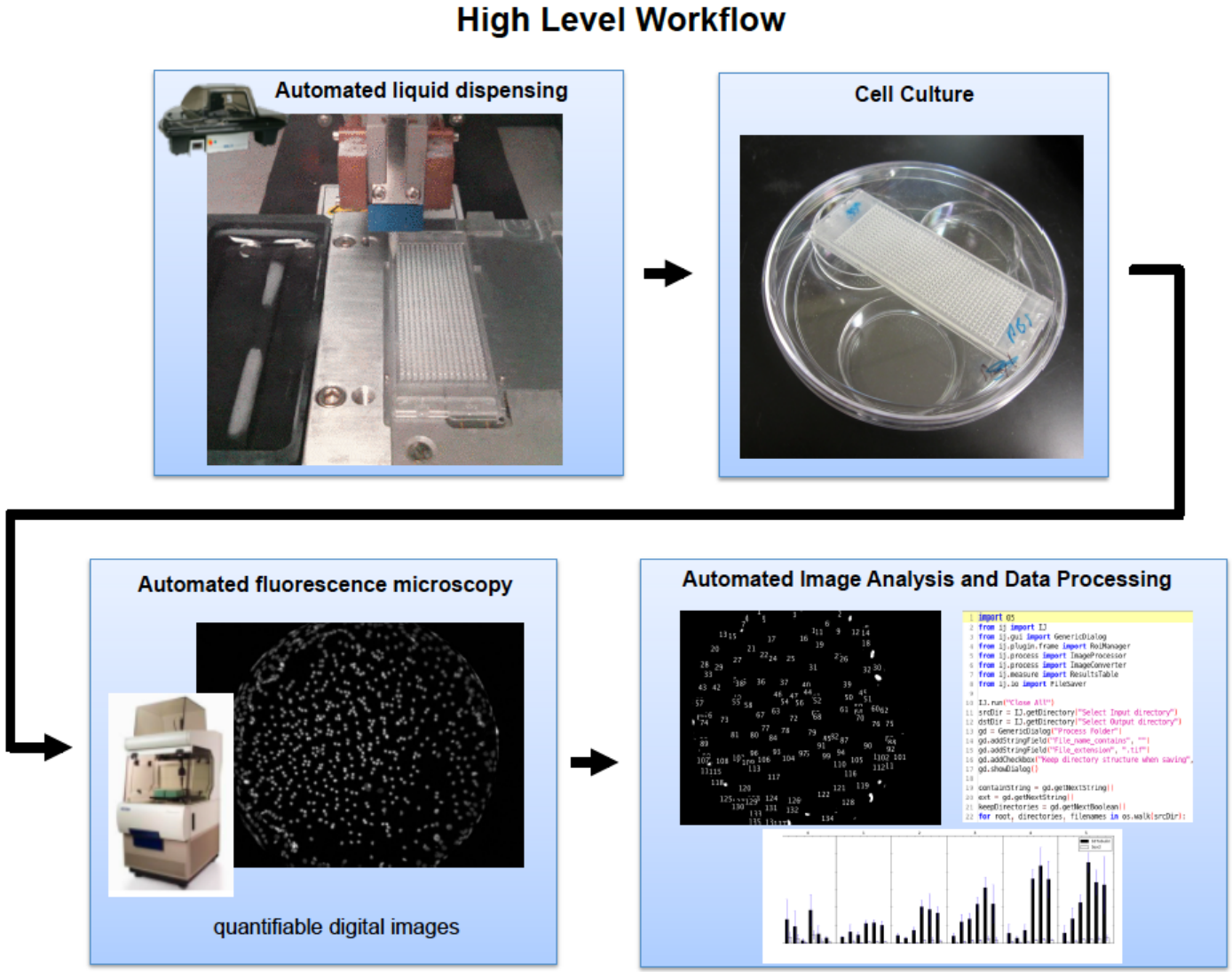

Figure 2.1: A) High-level workflow for high-throughput studies of combinatorial signaling environments. The four major components of this workflow are: combinatorial liquid dispensing, miniaturized cell culture, microscopy, and image analysis.

2.2 Experimental Procedures

2.2.1 Robotic Liquid Handling and Dispense Validation

All liquid dispensing into the microculture platform was performed with a DIGILAB Omnigrid Micro liquid handler with customized programs for deposition patterns. Colorimetric dye or fluorescent beads were used to visualize dispensing patterns.

2.2.2 Micropillar Culture

Micropillar and microwell chips (MBD Korea) made of polystyrene were manufactured by plastic injection molding as described previously. [49, 50] The micropillar culture chip was coated in laminin by placing into a microwell chip (MBD Korea) containing a solution of laminin diluted in sterile PBS overnight. Stem cells in suspensions of media or liquified hydrogel were deposited onto the micropillars and left pillar side up for at least 30 min to allow cell cultures to settle and adhere to the surface or gel. The micropillar chip was then inverted and placed into a fresh microwell chip containing cell culture media.

2.2.3 Immunocytochemistry

At the endpoint of the experiment, the micropillar chip was carefully removed from the wellchip and placed into a bath of 4% parafomaldehyde for 15 min to fix cell cultures. Then, the micropillar chip was washed twice in PBS for 5 min each and placed into a bath of 0.25% Triton-X + 5% donkey serum in PBS for 10 min to permeabilize cells. After permeabilization, the micropillar chip was washed 5 times in 5% donkey serum for 5 min each, dried, and transferred to a wellchip containing primary antibodies of interest diluted in PBS+donkey serum (dilution details in Table A.2) and stored overnight at 4°C. After primary staining, the micropillar chip was washed twice in PBS for 5 min each, dried, and then placed into a microwell chip containing the corresponding secondary antibodies (dilution details in Table A.2) and incubated at 37°C for 2 h. After secondary staining, the micropillar chip was washed twice in PBS for 5 min each, dried, and then placed into a wellchip containing PBS and individual microenvironments were imaged using automated wide-field fluorescent microscopy.

2.2.4 Automated Wide-Field Fluorescence Microscopy

Stained cultures were imaged with a 20x objective using a Molecular Devices ImageXpress Micro automated wide-field fluorescence microscope available in the Shared Stem Cell Facility at UC Berkeley. Lamp exposure time was kept constant for a fluorescence channel within an imaging set.

2.2.5 Automated Confocal Fluorescence Microscopy

Stained cultures were imaged with a 20x water objective using a Perkin Elmer Opera Phenix automated confocal fluorescence microscope available in the High-Throughput Screening Facility at UC Berkeley. Laser exposure time, gain, and laser power was kept constant for a fluorescence channel.

2.2.6 Image Analysis and Statistical Methods

Background fluorescence was removed from all images using a rolling bar radius algorithm using ImageJ. [51] Feature extraction was performed with ImageJ application NeuriteTracer [52] and custom image processing scripts or Harmony Image Analysis software (Perkin Elmer). Quantified image data was then imported into Python for statistical data analysis [53] and data visualization [54].

2.2.7 Computer Aided Drafting and 3D printing

AutoCAD software was used to design and draft custom pieces for the Chip Swapper device. Then, the .stl file of the 3D draft was uploaded into PreForm software for 3D printing on the Form2 desktop stereolithography (SLA) 3D printer using standard black resin. After 3D printing, devices were washed in isopropanol in a chemical fume hood for 20 minutes to remove non-cured resin and dried overnight to evaporate excess isopropanol.

2.3 Results

2.3.1 Creation of Liquid Dispensing Algorithms for Combinatorial Screens

Full factorial Design of Experiments (DoE) methodology was selected to explicitly quantify interaction effects between signaling cues [55]. We first employed a colorimetric dye to validate that our custom robotic liquid handling program was able to dispense all cues into the intended positions on the microwell chip to create 64 unique combinations from the six cues listed previously (Figure 2.2). We then expanded on this capability by incorporating multiple dose levels of the factors of interest totalling 90 unique culture combinations of the four different factors of interest (Figure 2.3). Finally, we designed patterns to probe the effects of gradual changes in soluble cue composition, a 3-way gradient, for applications where the total solute concentration needed to be fixed (Figure 2.4), such as optimizations of composition balance. All dispensing patterns have at least four technical replicates built in for downstream statistical analysis.

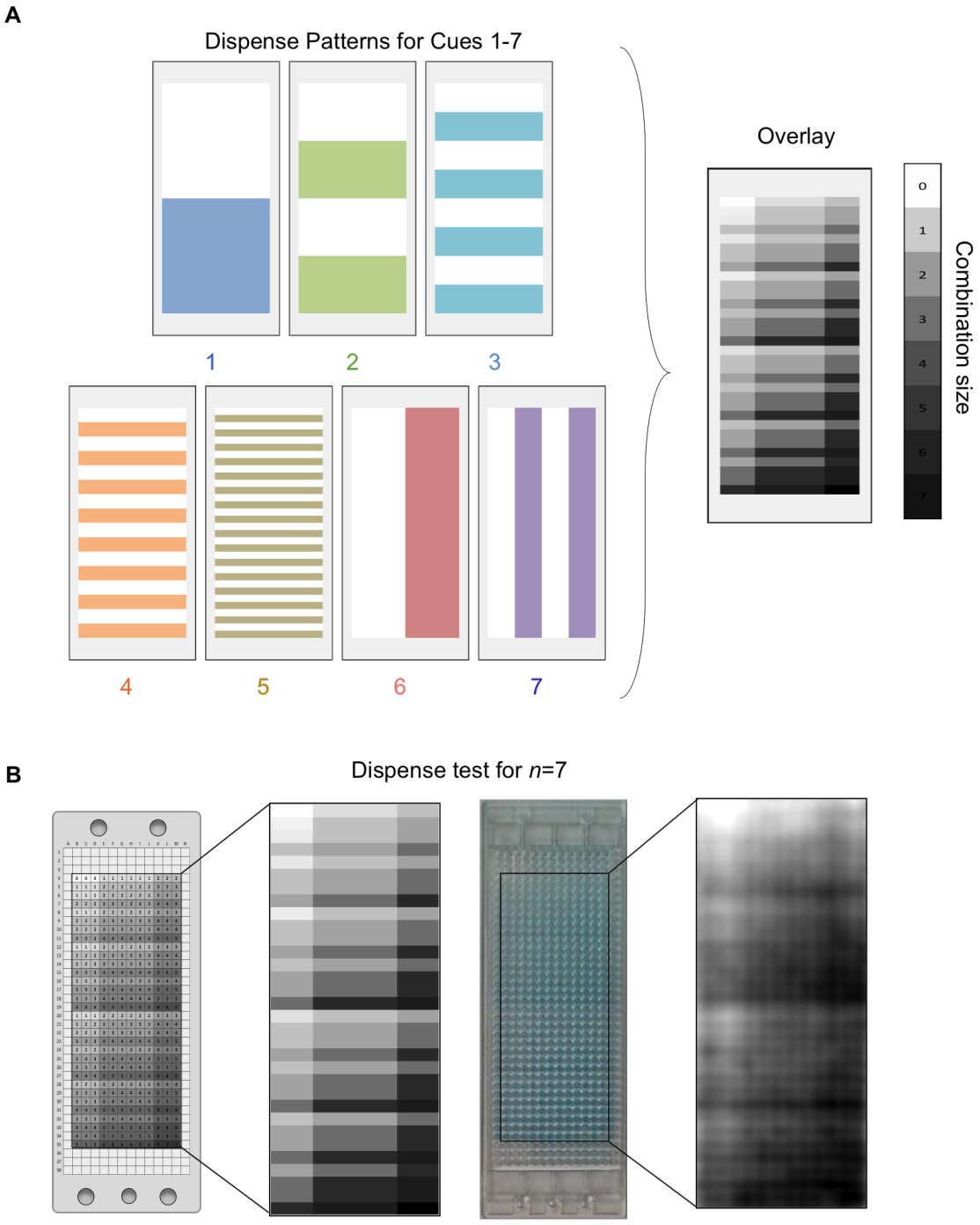

Figure 2.2: Liquid Dispensing program for 2^n Full Factorial Design for Soluble Cues in Microchip for up to n=7. A) Dispense pattern for individual cues and the overlaid result for 2^7 combinations. B) Robotic liquid dispensing validation of custom full factorial protocols using colorimetric dye and color depth comparison to intended map.

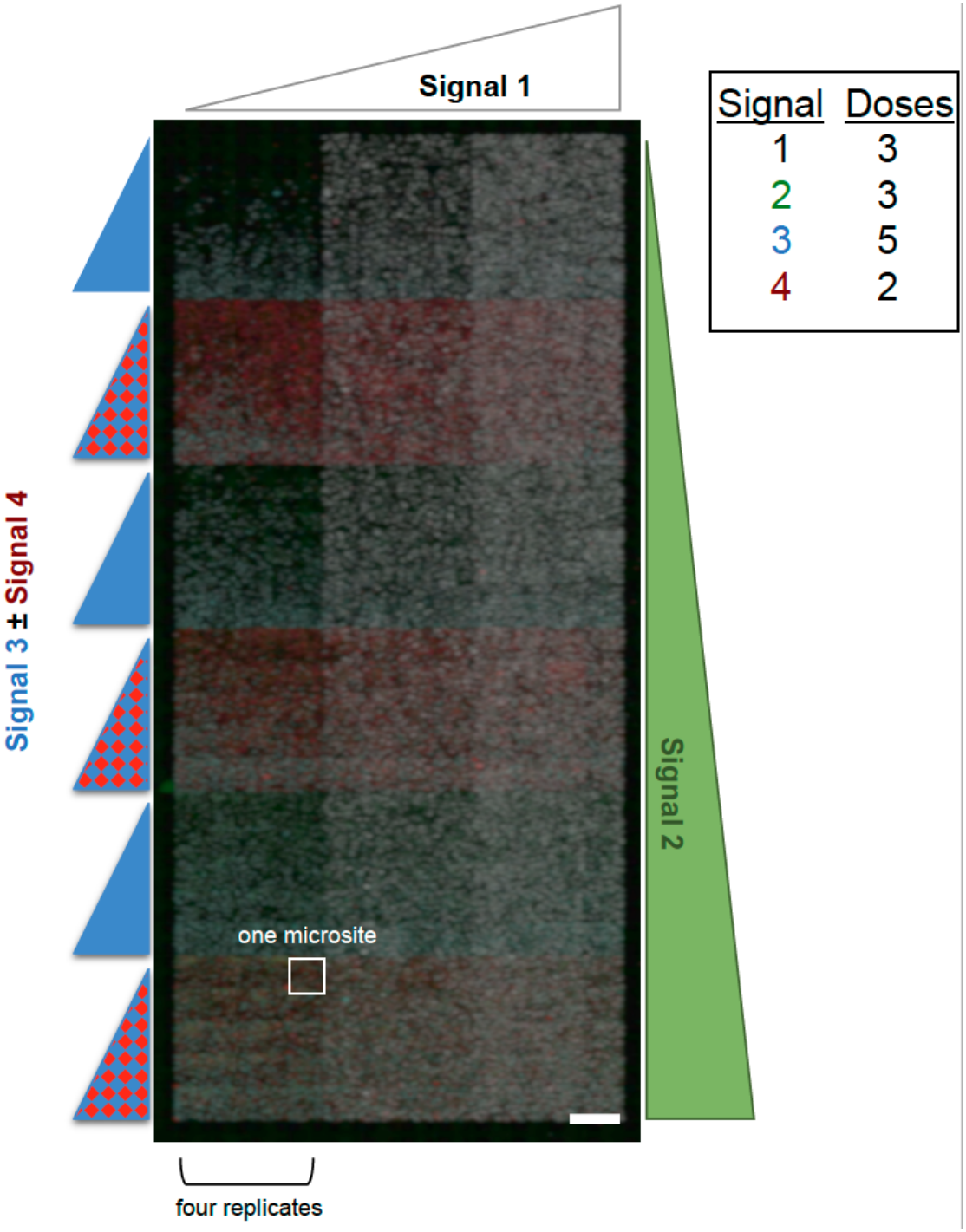

Figure 2.3: Validation of liquid dispensing layout for full factorial combinatorial study. Full factorial design with n=4 factors at a range of doses dispensed into the microwell chip validated by using fluorescent beads representing the identity and concentration of each factor. 1 chip contains 90 unique culture combinations with 4 technical replicates each, totaling 360 independent microsites. Scale bar represents 1 mm.

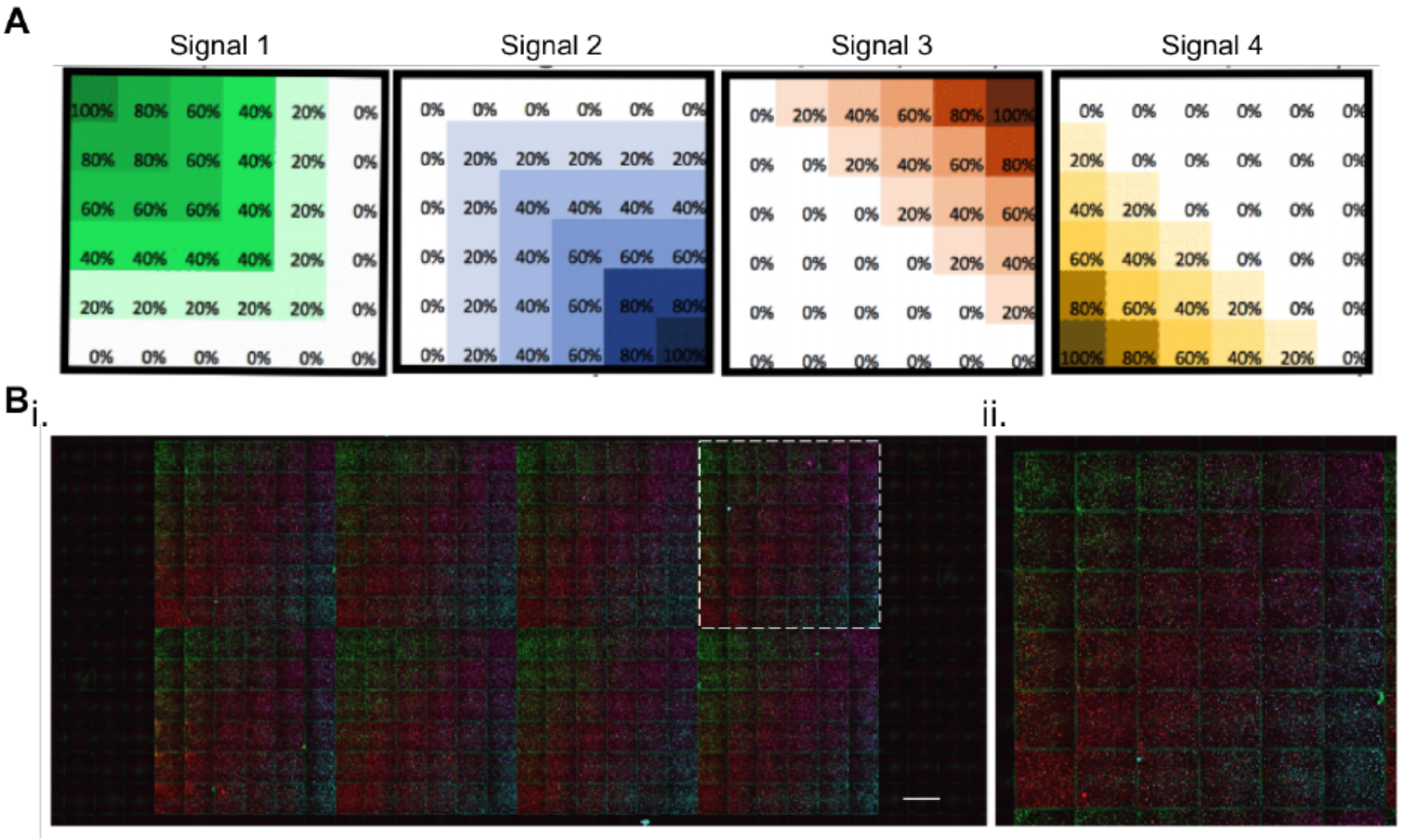

Figure 2.4: Validation of liquid dispensing layout for gradient combinatorial study. Full factorial design with n=4 factors at a range of doses dispensed into the microwell chip validated by using fluorescent beads representing the identity and concentration of each factor. 1 chip contains 36 unique culture combinations with 8 technical replicates each, totaling 288 independent microsites. Scale bar represents 1 mm.

2.3.2 Miniaturized stem cell culture

Optimization and Control of Miniaturized Stem Cell Culture

Initial optimization of stem cell culture on the micropillar chip sought to identify a laminin coating procedure that resulted in neural stem cell monolayer formation with 1) inter-pillar consistency and 2) intra-pillar uniformity for a consistent and uniform baseline. Six different concentrations of laminin diluted in sterile PBS were tested by coating micropillars overnight and then depositing a suspension of NSCs on top and inverting the pillars into NSC culture media. After 6 days of culture on the micropillars, cells were fixed and stained for nuclear marker Hoechst and imaged. A strong correlation for inter-pillar consistency was qualitatively observed with respect to laminin concentration (Figure 2.5). Further, the intra-pillar uniformity of NSC culture across the micropillar surface was quantified across the x and y dimensions of the micropillar images and plotted in histograms (Figure 2.5B). It was observed that laminin concentrations of at least 100 μg/mL were sufficient to produce the desired results. We additionally demonstrated the ability of this microculture platform to control the seeding density of initial cell cultures (Figure 2.6).

Custom Design and Fabrication of "Chip Swapper" for Consistent Microculture Handling

We created a customized device to control the reproducibility of the micropillar transfer process between microwell chips, an integral part of this micro-culture methodology (Figure 2.7). The chip swapping method consists of four steps:

1. Placement of old pillar/well chip and new well chip onto the slots of the base plate (gray)
2. Separation of the pillar chip (yellow) from the old well chip (blue) by sliding prong tool in (red)
3. Sliding the pillar chip along the guided rails to the new well chip
4. Gradual placement of the pillar chip into the new well chip by sliding prong tool out

Use of the Chip Swapper removes potential variability in handling of microcultures during the media replenishment process day to day for a single user, or user to user if multiple researchers are maintaining a single experiment.

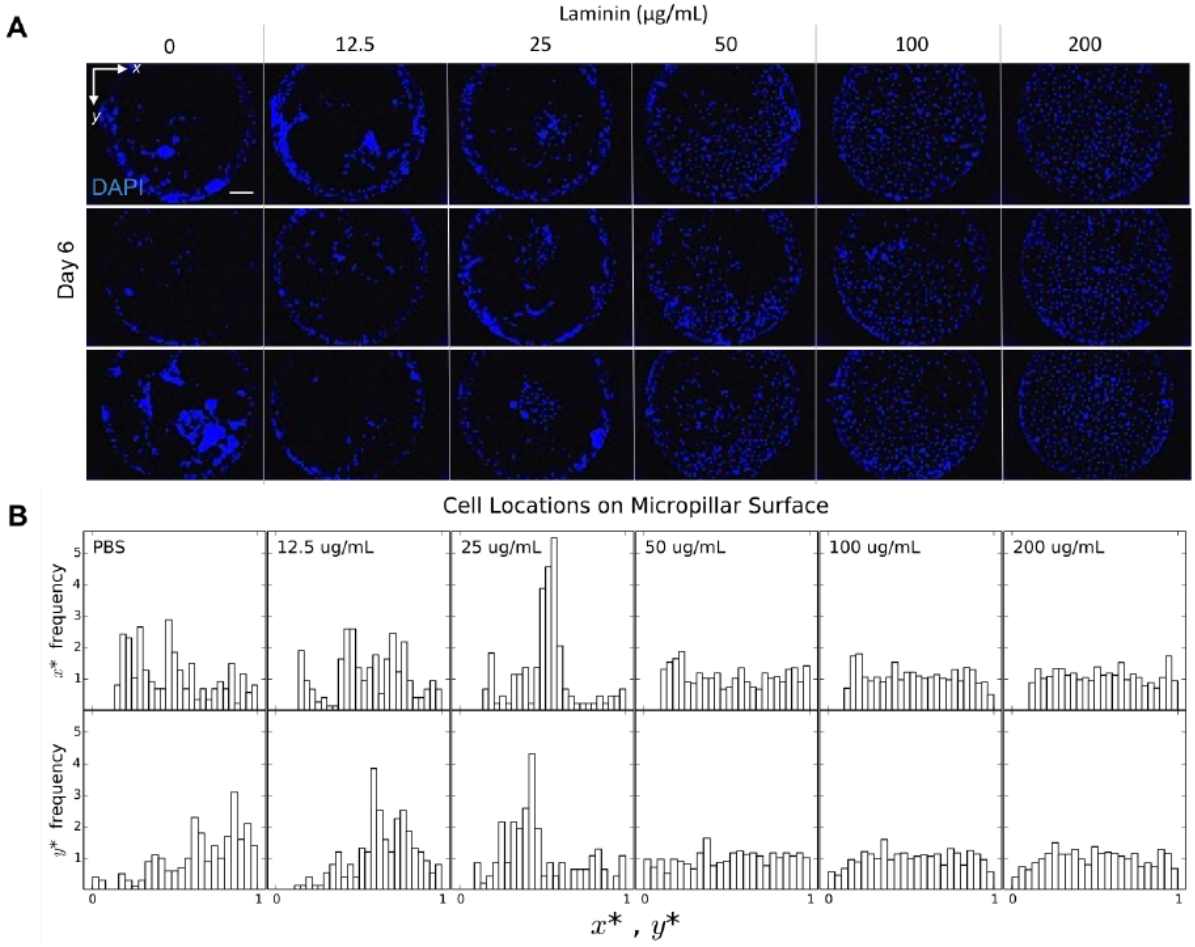

Figure 2.5: Optimization of laminin surface coating. A) Fluorescence microscopy images of Hoechst stained NSC nuclei after six days of culture on micropillars coated in a range of laminin concentrations, 3 replicates shown for each concentration; scale bar represents 100 µm. B) Distribution of cell positions in x* and y* for a representative image from each condition. Position variables are scales such that x* = x/image width, y*=y/image height, in pixels.

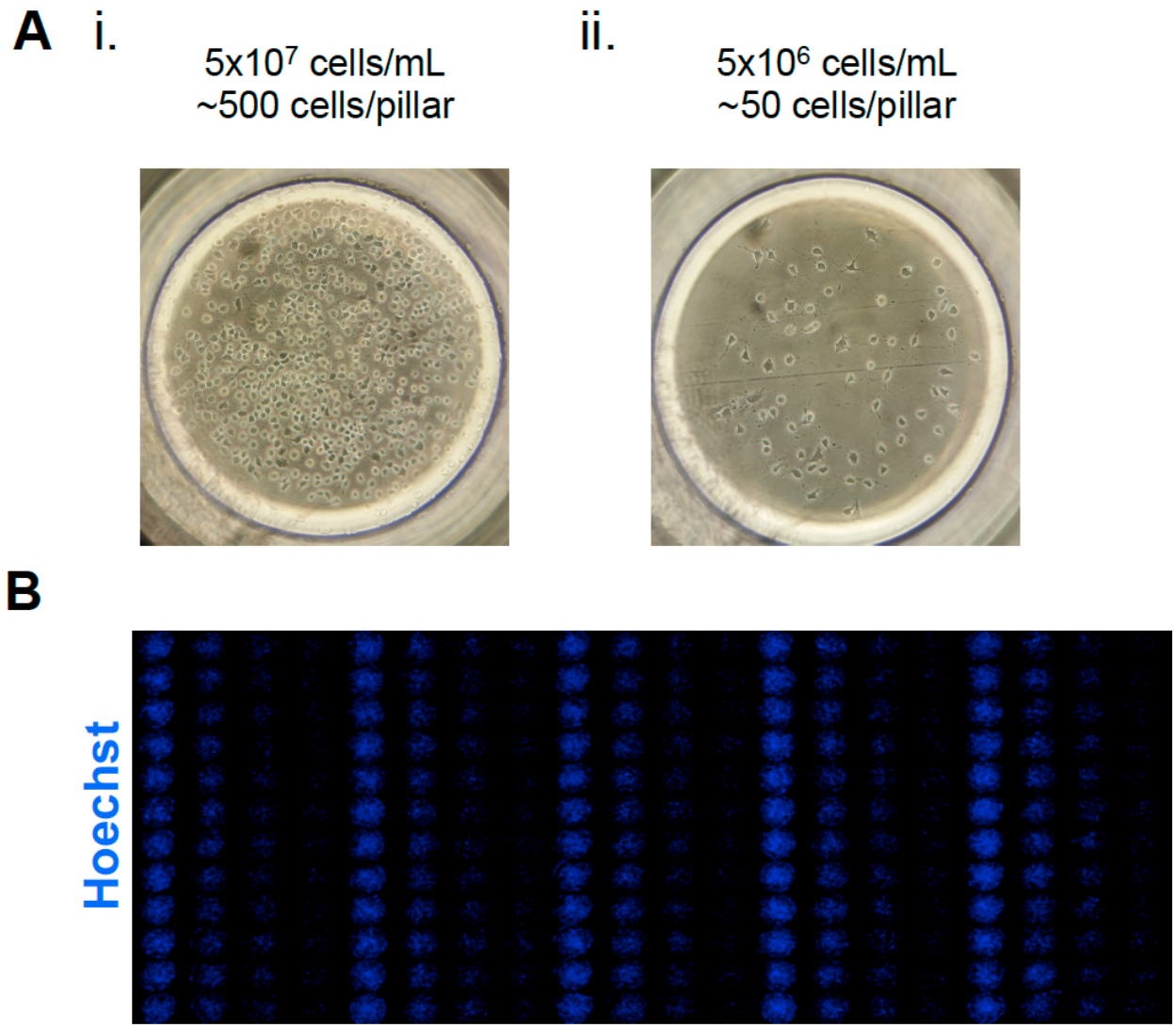

Figure 2.6: Controlled modulation of seeding density of cells onto micropillars. A) Bright field images of micropillar cultures seeded at i. $5x10^7$ cells/mL or roughly 500 cells per micropillar and ii. $5x10^6$ cells/mL or roughly 50 cells per micropillar; pillar diameter is 750 microns. B) Fluorescence microscopy of Hoechst stained cells seeded at four different densities consistent across the micropillar chip.

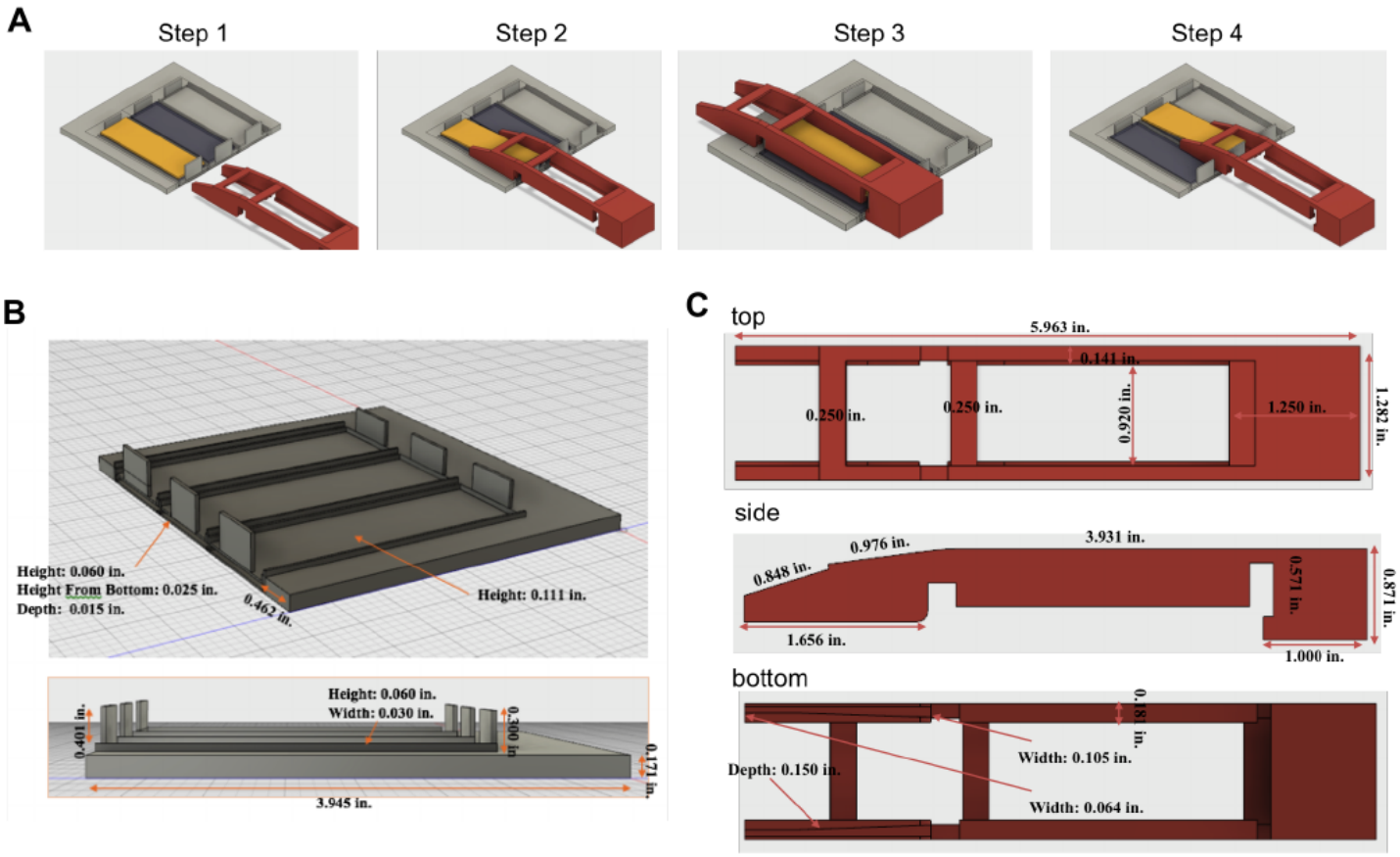

Figure 2.7: Custom Fabrication of Chip Swapper for Consistent Microchip Handling. A) The four steps involved in chip swapping. B) Dimensions of the base plate custom fit to the microwell chip. C) Dimensions of the prong tool custom fit to the micropillar chip.

2.3.3 Fluorescence Immunocytochemistry Readouts for Stem Cell Marker Expression and Morphology in 2D and 3D

Cell cultures that are in a 2D monolayer format can be stained and imaged using a wide-field fluorescence microscope [56]. Cellular markers are either contained within the nucleus, such as transcription factors, or within the cytoplasm, such as microtubules [57]. Cytoplasmic markers can be further applied toward morphometric analysis of interest, such as neurite length measurements. All cultures are counter stained with a DNA stain, such as DAPI, to be able to normalize marker expression to the total cell count. Quantification of image data for 2D cell cultures was done using custom scripting and applications in ImageJ [51,52] If positive and negative controls are available for the cellular system of interest, it is recommended to first conduct a Z-factor analysis for assessment of staining and imaging quality. [58] Here, a Z-factor analysis was applied to neural markers of interest before starting any combinatorial analyses. The Z-factors for measured variables using the appropriate positive and negative controls were calculated and were within range for an adequate screening assay (Figure 2.8).

Cell cultures that are encapsulated within 3D hydrogels require either a confocal or multi-photon microscope to clarify the cells across many microns in the z-direction enough to measure cell markers of interest [59]. Fluorescence image analysis pipelines were built for quantification of nuclear and cytoplasmic marker expression in 3D cultures (Figure 2.9). Of note, segmenting and scoring dense cell populations by expression of cellular markers localized to the cytoplasm, such as Tyrosine Hydroxylase and Tuj1, can be less straightforward than nuclear localized markers, such as Olig2 and Nkx2.2, and therefore should be considered in the design of the screening strategy. Fluorescent reporter cell lines that are a proxy for cytoplasmic markers but localize the flourescent protein to the nucleus could bypass this issue as well [60]. Quantification of image data for 3D cell cultures was performed using Harmony image analysis software from Perkin Elmer.

2.3.4 Data Aggregation, Organization, Analysis, and Visualization

In anticipation of large data sets created due to the high-throughput nature of this system (roughly 500 micro-culture sites * 4 fluorescent channels for marker readouts = 2000 datapoints per chip), it is necessary to adopt data analysis tools that can facilitate aggregation and organization of thousands of data points that are collected across many weeks to years [61].

Here, quantified image data from either ImageJ or Harmony was imported as .txt files into Python for statistical data analysis [53] and visualization using packages such as matplotlib or seaborn [54]. For comparisons between data sets acquired across different experimental sessions, raw data was scaled and centered by z-score, and descriptive statistics were calculated from at least 4 technical replicates. Error bars represent 95% confidence intervals unless otherwise specified. If comparisons across more than three conditions are conduction, appropiate corrections for false positives should be applied, such as a Benjamini - Hochberg False Discovery Rate correction [62].

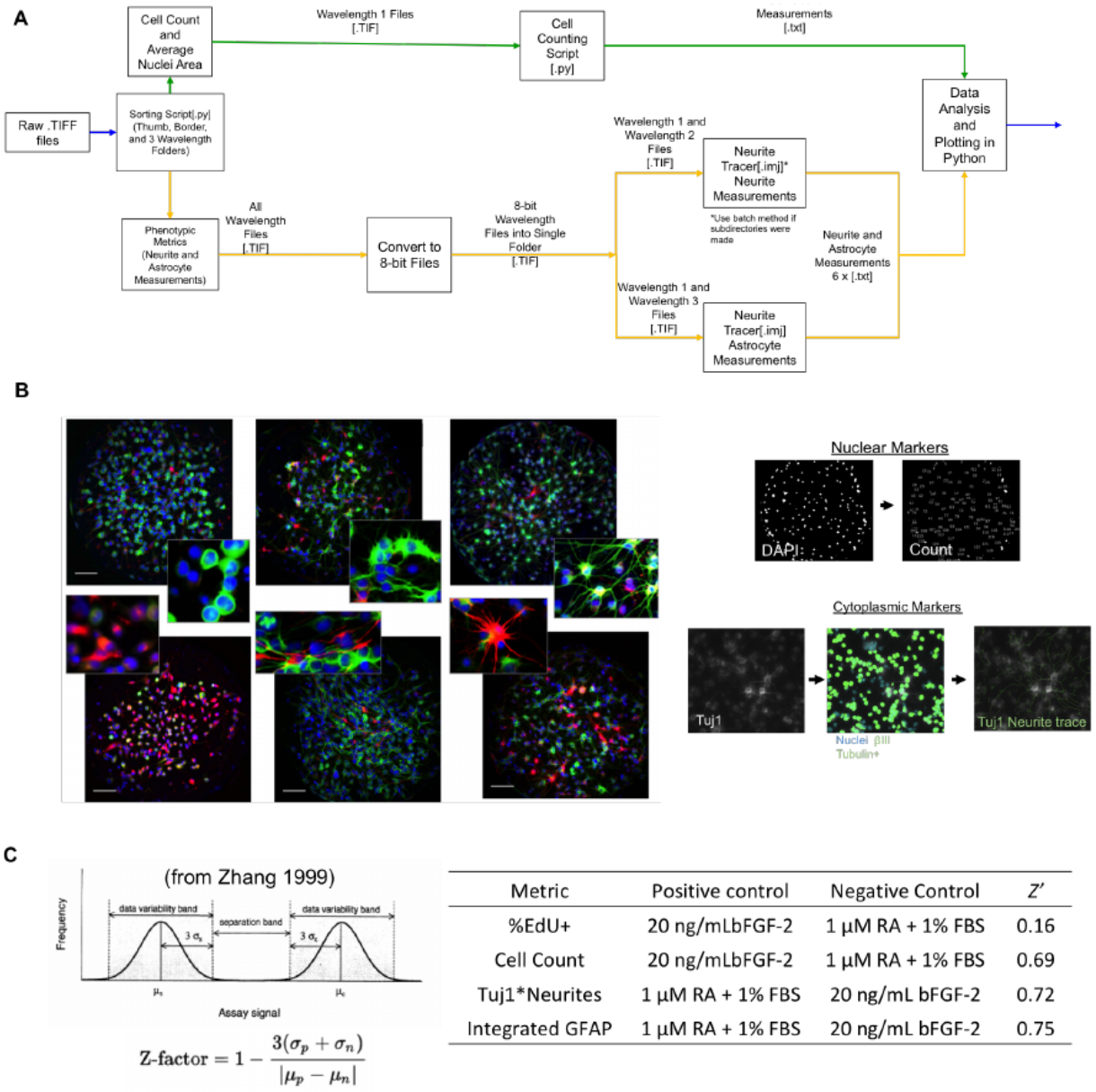

Metric	Positive control	Negative Control	Z'
%EdU+	20 ng/mLbFGF-2	1 µM RA + 1% FBS	0.16
Cell Count	20 ng/mLbFGF-2	1 µM RA + 1% FBS	0.69
Tuj1*Neurites	1 µM RA + 1% FBS	20 ng/mL bFGF-2	0.72
Integrated GFAP	1 µM RA + 1% FBS	20 ng/mL bFGF-2	0.75

Figure 2.8: Image Processing and Analysis. A) Phenotype quantification from raw image data. B) Example feature extraction from high-content fluorescence microscopy images; nuclei are represented in blue, GFAP is in red, and βIII-Tubulin is in green. C) Z-factor analysis with positive and negative controls for each metric.

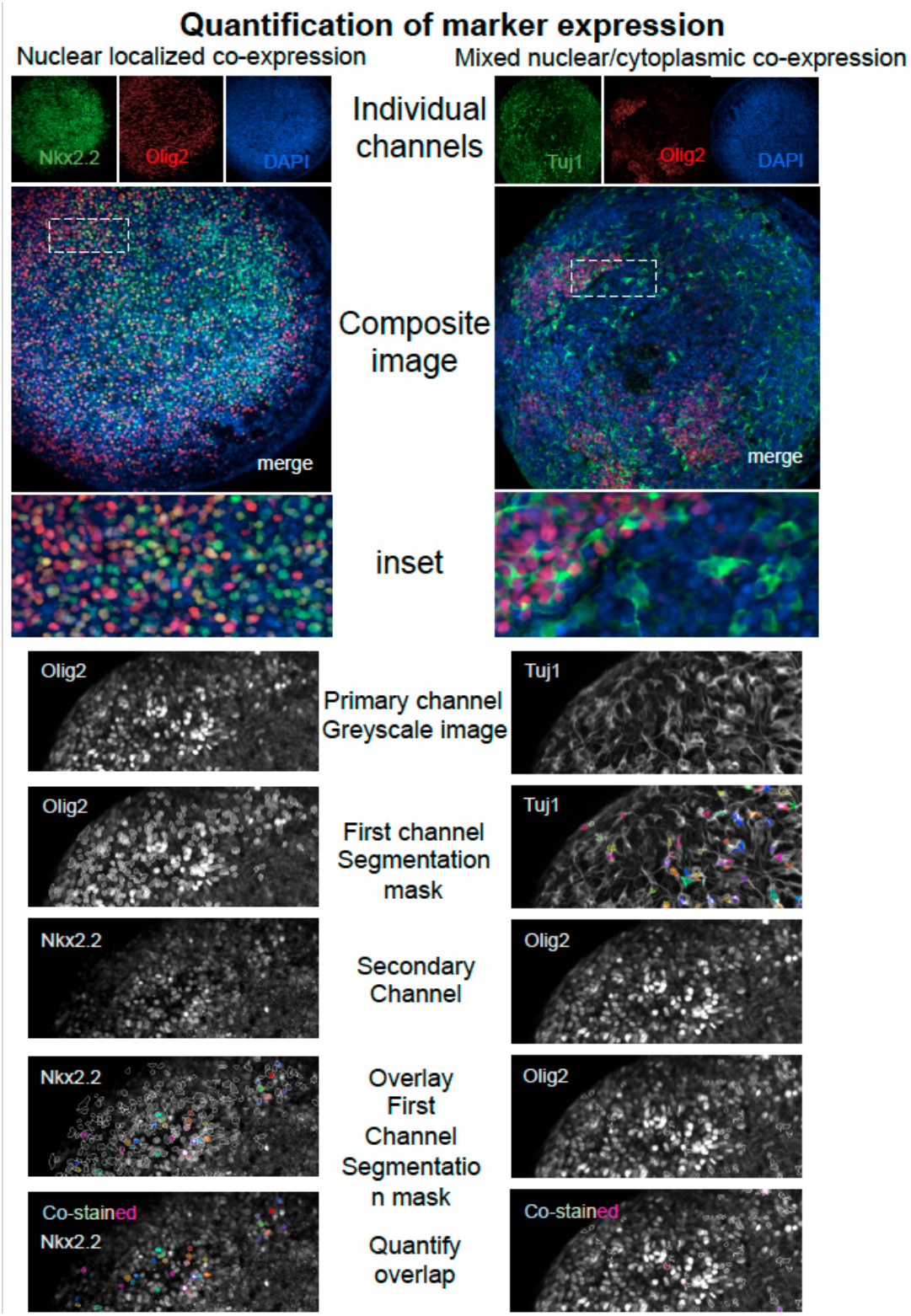

Figure 2.9: Image analysis pipeline for quantification of nuclear and cytoplasmic cellular markers and co-expression.

2.4 Conclusion

These data collectively demonstrate the integration of four main components (combinatorial liquid dispensing, miniaturized stem cell culture, fluoresence microscopy, and programmatic data handling) to create a system that facilitates high-throughput phenotypic screening of stem cell proliferation and differentiation, in both 2D and 3D formats, while maintaining rigorous quality control measures for fundamental studies or translational applications of key questions in stem cell biology.

Chapter 3

Combinatorial Screening Reveals Interactions Between Signaling Molecules that Regulate Adult Neural Stem Cell Fate

3.1 Abstract

Advancing our knowledge of how neural stem cell (NSC) behavior in the adult hippocampus is regulated has implications for elucidating basic mechanisms of learning and memory as well as for neurodegenerative disease therapy. To date, numerous biochemical cues from the endogenous hippocampal NSC niche have been identified as modulators of NSC quiescence, proliferation, and differentiation; however, the complex repertoire of signaling factors within stem cell niches raises the question of how cues act in combination with one another to influence NSC physiology. To help overcome experimental bottlenecks in studying this question, we adapted a high-throughput microculture system, with over 500 distinct microenvironments, to conduct a systematic combinatorial screen of key signaling cues and collect high-content phenotype data on endpoint NSC populations. This novel application of the platform consumed only 0.2% of reagent volumes used in conventional 96-well plates, and resulted in the discovery of numerous statistically significant interactions among key endogenous signals. Antagonistic relationships between FGF-2, TGF-β, and Wnt-3a were found to impact NSC proliferation and differentiation, whereas a synergistic relationship between Wnt-3a and Ephrin-B2 on neuronal differentiation and maturation was found. Furthermore, TGF-βand BMP-4 combined with Wnt-3a and Ephrin-B2 resulted in a coordinated effect on neuronal differentiation and maturation. Overall, this study offers candidates for further elucidation of significant mechanisms guiding NSC fate choice and contributes strategies for enhancing control over stem cell based therapies for neurodegenerative diseases.

3.2 Introduction

Stem cells, defined as immature cells capable of self-renewal and differentiation into a range of mature cell types, play fundamental roles in tissue formation and maintenance, and have broad applications for in vitro disease modeling, drug screening, and in vivo tissue regeneration. [63–67]. Neural stem cells (NSCs) in the hippocampus of the adult brain are of particular interest because of their potential to proliferate and differentiate into new neurons and glia throughout adulthood. [68] These tightly regulated NSC processes have impact on learning and memory, as well as implications for the treatment of neurodegenerative disorders such as Alzheimer's disease. [69]

Adult hippocampal NSCs reside within the dentate gyrus of the subgranular zone – a complex and intricate niche that presents various forms of instructive regulatory stimuli. Numerous studies have identified a range of individual endogenous signaling molecules that regulate NSC quiescence, proliferation, and/or differentiation. For example, early studies on primary NSCs isolated from the adult rodent hippocampus established a proliferative effect of FGF-2, [70, 71] and SHH was subsequently found to promote proliferation in vitro and in vivo. [72, 73] Furthermore, Wnt-3a and Ephrin-B2 ligands within the NSC niche were discovered to regulate neurogenesis, [31, 74] whereas BMP-4 and most recently TGF-β signals have been associated with quiescence of adult hippocampal NSCs. [75–79]

While such reductionist studies have greatly advanced our knowledge of NSC regulators, these cells are likely exposed to multiple cues simultaneously within the niche (Figure A.1), [80] and the potential effects of their combinatorial presentation within the hippocampal NSC niche have not yet been examined. Unfortunately, experimental capabilities to examine such interactions using conventional well-plate platforms are constrained by reagent costs and feasibility as the parameter space for unbiased and systematic combinatorial studies grows exponentially; for example, 2^n possible combinations can be formed from n different factors.

To overcome these limitations, many researchers have adopted novel miniaturized cell culture platforms for dissecting analogous cell niches, [34, 81–86] and in some cases these studies have revealed non-intuitive cell behavior that would be difficult to detect without an unbiased screen. [36, 46] Accordingly, here we have adapted and demonstrated the utility of a high-throughput micro-culture platform (Figure 3.1, previously applied toward toxicological assays [49, 50, 87] enabling independent preparation and control of media and cell substrates, simultaneous media replenishment of over 500 microcultures, and higher exposure to microcultures for immunocytochemistry. After platform optimization and characterization, we employed a full factorial design to systematically expose NSCs to combinatorial niche signals and collected high-content image data [88] of NSC proliferation, neuronal/glial differentiation, and morphology (Figure 3.1B,C). We discovered that antagonistic relationships among FGF-2, TGF-β, and Wnt-3a impact NSC proliferation and differentiation, and that a synergistic relationship between Wnt-3a and Ephrin-B2 promotes neuronal differentiation and maturation. Furthermore, we observed that TGF-β and BMP-4 in combination with Wnt-3a and Ephrin-B2 exhibited a coordinated effect on neuronal differentiation and maturation. Finally, we arranged conditions based on

similarity in the direction and extent of phenotypic responses to identify broader trends across combinatorial signaling environments.

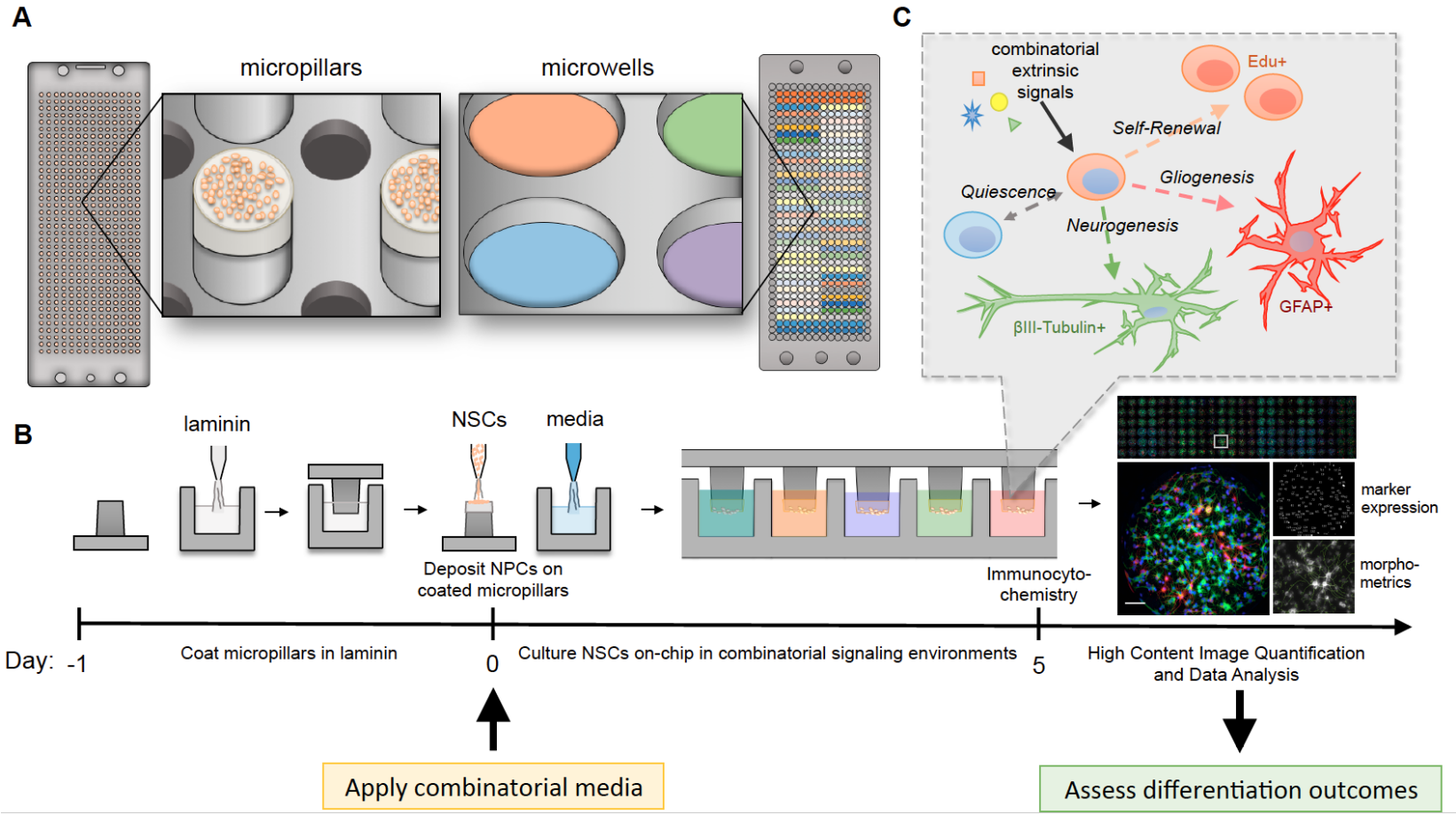

Figure 3.1: High-throughput micropillar and microwell culture system for high-content screening of stem cell proliferation and differentiation. A) The high-throughput cell culture array consists of complementary micropillars and microwells that combine to form 532 independent cell culture environments. B) NSCs in a 60 nL suspension were deposited on the surface micropillars, and cell culture media containing select chemical signaling cues were dispensed into the microwells. C) NSCs were exposed to systematic combinations of soluble cues to recapitulate the complexity of the in vivo hippocampal niche where combinatorial extrinsic signals guide phenotypic processes including self-renewal, gliogenesis, neurogenesis, quiescence, and death.

3.3 Experimental Procedures

3.3.1 Primary adult hippocampal neural stem cell culture

Adult rodent NSCs were cultures as described previously. [24] NSCs were subcultured in DMEM-F12 + N2 supplement and 20 ng/mL FGF-2 on laminin-coated polystyrene dishes. NSCs were dissociated with Accutase for replating upon confluency and seeding into conventional plate and microculture experiments.

3.3.2 Synthesis of Multivalent Ephrin-B2

An EphB4 binding peptide TNYLFSPNGPIARAW [89] with a 70 nM Kd, previously identified by phage display was conjugated to a 1500 kDa hyaluronic acid (HA) chain to generate a multivalent ligand. A bi-functional molecule N-E-maleimidocaproic acid hydrazide (EMCH) was utilized to bridge HA and the peptide of interest, where it was first reacted with the carboxylic acid functional group on HA to generate an amide, and subsequently reacted with the thiol group on the EphB4 binding peptide. The valency of the multivalent peptide conjugate is 40, which was calculated as the molar ratios of HA to ligand, as determined by the BCA assay, a method that was previously confirmed by size exclusion chromatography coupled with multi-angle static light scattering measurement. [90]

3.3.3 NSC micro-culture on Pillar/Well Chip System

Micropillar and microwell chips (MBD Korea) made of polystyrene were manufactured by plastic injection molding as described previously. [49, 50] The micropillar culture chip was coated in laminin by placing into a microwell chip (MBD Korea) containing a solution of laminin diluted in sterile PBS overnight. NSCs in suspension were deposited onto the laminin-coated micropillar and left pillar side up for at least 30 min to allow NSCs to settle and adhere to the surface. The micropillar chip was then inverted and placed into a fresh microwell chip containing cell culture media. All liquid dispensing into the microculture platform was performed with a DIGILAB Omnigrid Micro liquid handler with customized programs for deposition patterns. Media was changed daily by transferring the micropillar chip into a microwell chip containing fresh media every other day using a custom made mechanical "Chip Swapper" for consistent transfer. Technical replicates included two different dispensing patterns to average out positional effects across the microchip.

3.3.4 On-chip Viability Assay

At the endpoint of the experiment, the micropillar chip was carefully removed from the wellchip and placed in new wellchip containing Calcein AM, Ethidium Homodimer, and Hoechst diluted in sterile PBS (dilution details in Table A.2). The chip was incubated for 20 min and then transferred to a new wellchip containing PBS and individual microenvironments were imaged using fluorescent microscopy.

3.3.5 On-Chip Immunofluorescence and Proliferation Assays

At the endpoint of the experiment, the micropillar chip was carefully removed from the wellchip and placed into a bath of 4% parafomaldehyde for 15 min to fix cell cultures. Then, the micropillar chip was washed twice in PBS for 5 min each and placed into a bath of 0.25% Triton-X + 5% donkey serum in PBS for 10 min to permeabilize cells. After permeabilization, the micropillar chip was washed 5 times in 5% donkey serum for 5 min each, dried, and transferred to a wellchip containing primary antibodies of interest diluted in PBS+donkey serum (dilution details in Table A.2) and stored overnight at 4°C. After primary staining, the micropillar chip was washed twice in PBS for 5 min each, dried, and then placed into a microwell chip containing the corresponding secondary antibodies (dilution details in Table A.2) and incubated at 37°C for 2 h. After secondary staining, the micropillar chip was washed twice in PBS for 5 min each, dried, and then placed into a wellchip containing PBS and individual microenvironments were imaged using automated wide-field fluorescent microscopy.

3.3.6 Well-plate NSC culture and Immunocytochemistry

Individual wells in a tissue culture treated uClear 96-well plate (Greiner Bio-One, 655090) were coated with laminin by incubating overnight in a solution of laminin diluted in sterile PBS. On Day 0, NSCs were seeded at a uniform concentration of 2.2E5 cells/mL per well (roughly 40,000 cells/well, or 1.4E3 cells/mm2). Culture media containing individual and combined signaling cues (dosage details in Table S1) was applied on Day 0 and replaced every other day. On Day 5, cells were fixed in 4% parafomaldehyde for 15 min. Then, cultures were washed twice in PBS for 5 min each and placed permeabilized in 0.25% Triton-X + 5% donkey serum in PBS for 10 min. After permeabilization, the wells were washed 5 times in 5% donkey serum for 5 min each and incubated in primary antibodies of interest diluted in PBS+donkey serum (dilution details in Table A.2) and stored overnight at 4°C. After primary staining, wells were washed twice in PBS for 5 min each and then incubated in the corresponding secondary antibodies (dilution details in Table A.2) at 37°C for 2 h. After secondary staining, wells were washed twice in PBS for 5 min each. Individual sites within each well were imaged using automated confocal microscopy.

3.3.7 Automated Wide-Field Fluorescence Microscopy

Stained micropillar chips were sealed with a polypropylene film (GeneMate T-2452-1) and imaged with a 20x objective using a Molecular Devices ImageXpress Micro automated wide-field fluorescence microscope available in the Shared Stem Cell Facility at UC Berkeley. Lamp exposure time was kept constant for a fluorescence channel within an imaging set.

3.3.8 Automated Confocal Fluorescence Microscopy

28 sites within each stained well of a 96-well plate were imaged with a 40x water objective using a Perkin Elmer Opera Phenix automated confocal fluorescence microscope available in the High-Throughput Screening Facility at UC Berkeley. Laser exposure time, gain, and

laser power was kept constant for a fluorescence channel.

3.3.9 Image Processing, Data Analysis, and Statistical Methods

Background fluorescence was removed from all images using a rolling bar radius algorithm using ImageJ. [51] Feature extraction was performed with ImageJ application NeuriteTracer [52] and custom image processing scripts. Quantified image data was then imported into Python for statistical data analysis [53] and data visualization. In brief, raw data was scaled and centered by z-score, and descriptive statistics were calculated from four replicates at the chip-level and six replicates within each chip. Error bars represent 95% confidence intervals unless otherwise specified. A factorial ANOVA was used to calculate statistical significance from a group of conditions. Non-significant terms were removed to create the OLS model; beta parameters were calculated for all significant terms as a simplified measure of their relative contribution to the extent of neurogenesis observed in a population of NSCs. For the hierarchical cluster model, the Euclidean distance was used to measure pairwise distance between each observation and the UPGMA algorithm was used to calculate the linkage pattern. Code available upon request. For validation studies in 96-well plate format, Harmony image analysis software (Perkin Elmer) was used to quantify neurite morphological features. A gamma correction of 2.0 was applied to highlight morphological features of select images for clarity in visualization only; quantification of image features was performed with the original images. A Student's T-test or Welch's T-test was applied to well-averaged data for equal and unequal sample sizes, respectively, with at least n=3 replicates.

3.4 Results

3.4.1 Miniaturization and Increased Throughput of Primary NSC Culture for Phenotypic Screening

Our system is composed of two halves – a chip with 532 x 750 μm wide pillars onto which cells can be deposited with a liquid dispensing system and a chip with 532 x 800 nL wells into which culture media and signaling cues can be dispensed – where placing the pillar chip into the well chip enables long term cell culture and subsequent imaging (Figure 3.1). NSCs derived from the adult rodent hippocampus are typically propagated in vitro on substrates coated with extracellular matrix protein laminin, [24] so initial optimization was performed to identify a coating procedure for laminin that could enable NSC monolayer formation with 1) inter-pillar consistency and 2) intra-pillar uniformity (Figure 2.5). Subsequently, coating parameters were kept constant for all studies to ensure a consistent and uniform initial condition across all 532 micropillar environments (Figure 3.2A).

Next, we assessed the capacity of the micropillar chip system to maintain NSC viability and reproduce proliferation and differentiation in response to well-characterized cues. A live/dead assay several hours after initial seeding showed a high proportion, >80%, of viable cells across all 532 microenvironments (Figure 3.2B,C), comparable to seeding into a standard well plate. Additionally, we observed uniform seeding across the entire micropillar

chip (3.2D) for an even baseline. Next, to assess whether NSC cultures retained the capacities for proliferation and differentiation into neurons and glia, we applied known proliferation-inducing and differentiation-inducing media conditions. Media was replenished by transferring the micropillar chip into a new microwell chip with fresh media every other day. After 5 days, proliferation was measured using an EdU assay, and differentiation into neurons and glia was marked with immunocytochemistry of βIII-Tubulin and GFAP, respectively. Anticipated increases in proliferation and differentiation were observed (3.2E). Additionally, the Z-factors for these and additional measured variables using the appropriate positive and negative controls were calculated and are within range for an adequate screening assay [58] (Figure 2.8). Finally, we created a customized device to control the reproducibility of the micropillar transfer process between microwell chips, an integral part of this micro-culture methodology. These data collectively demonstrate the ability to miniaturize NSC culture while maintaining rigorous quality control measures to enable high-throughput phenotypic screening of NSC proliferation and differentiation.

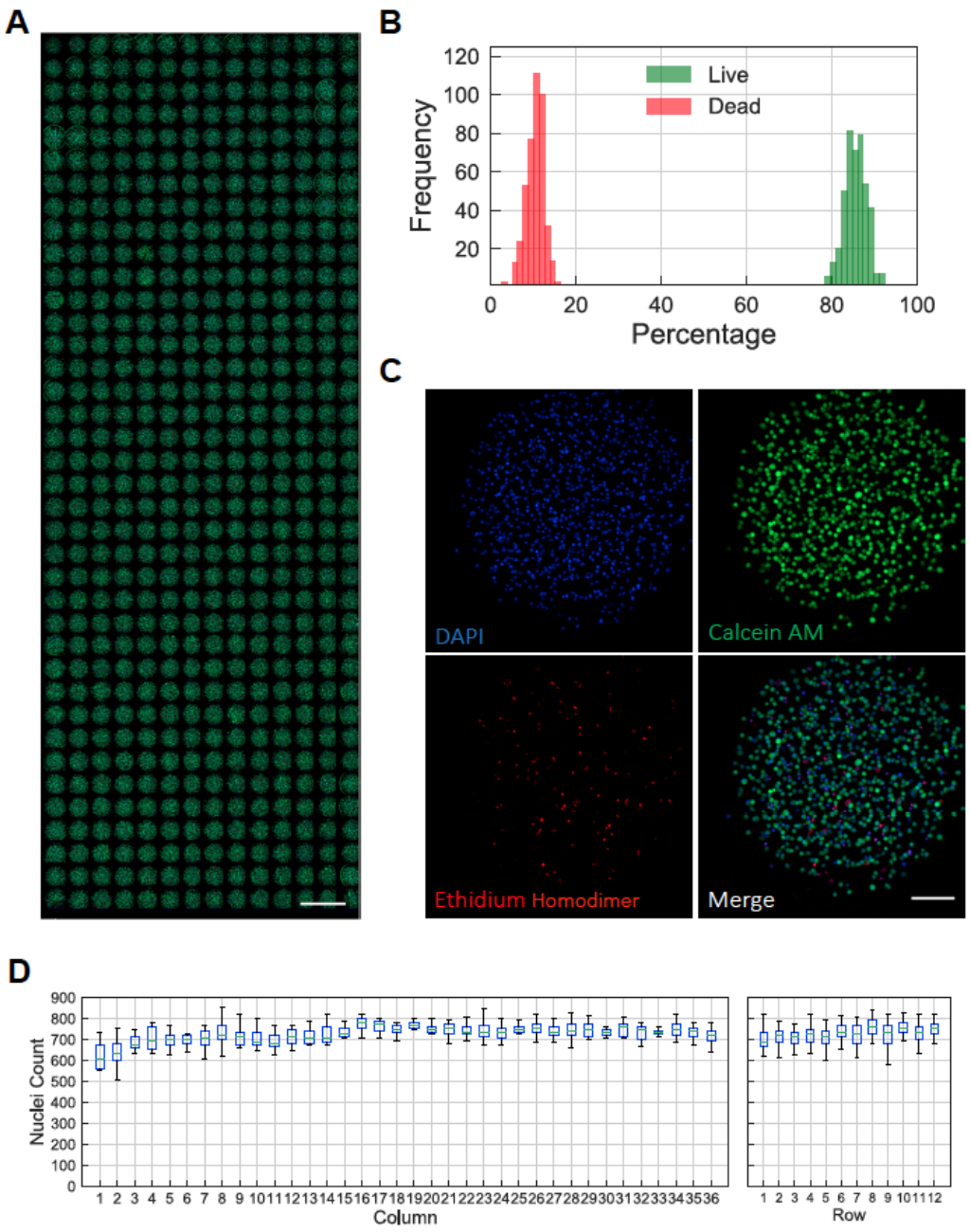

Figure 3.2: Primary NSC cultures on micropillars demonstrated uniform initial seeding and retain viability, proliferation, and differentiation potential. A) Day zero montage of NPCs seeded onto 532 microenvironments and stained for calcein AM (green), ethidium homodimer (red), and Hoechst (blue); scale bar represents 2 mm. B) Histograms of % live and dead cells across 532 microcultures. C) 20x magnification of stained micropillar culture showing individual fluorescence channels and merge; scale bar represents 100 μm. D) Quantification of micropillar total cell count by column and by row.

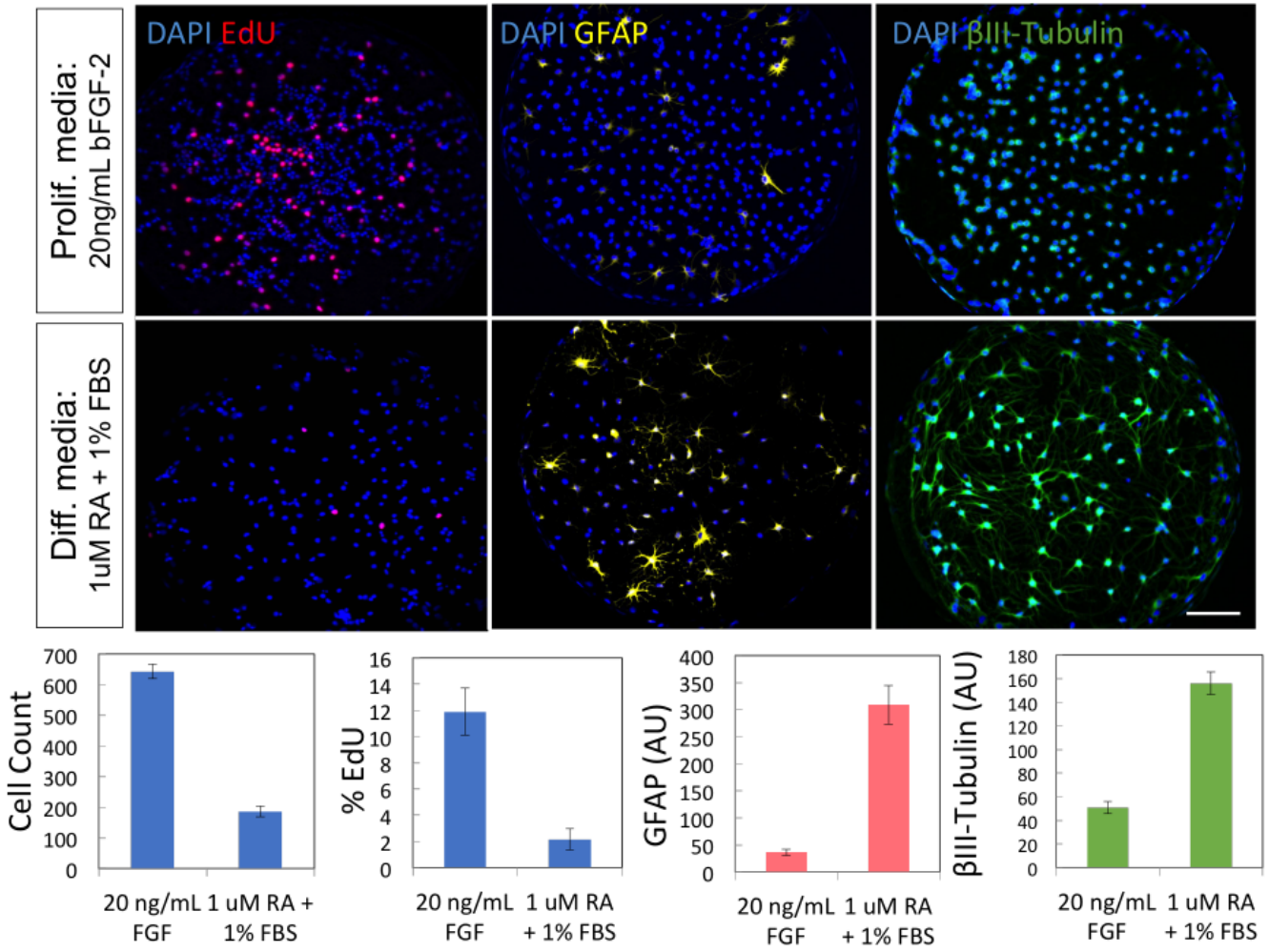

Figure 3.3: Induced proliferation or differentiation on micropillar/microwell culture platform with 20 ng/mL FGF-2 or 1 μM retinoic acid + 1% FBS, respectively. Immunocytochemistry was conducted after 5 days for EdU incorporation or GFAP and β-III Tubulin expression; scale bar represents 100 μm. Error bars represent standard deviation of 24 replicates.

3.4.2 Implementation of Combinatorial Signaling Screen in the Microchip System

We designated six endogenous signaling cues (FGF-2, SHH, Wnt-3a, Ephrin-B2, BMP-4, and TGF-β) from the adult hippocampal niche to be of particular interest for this combinatorial study because of their prominent roles in NSC regulation, their opposing effects on the NSC behavior as described above, and the lack of quantitative information on the potential interactions these cues may have with one another when simultaneously present in the niche. Therefore, a full factorial Design of Experiments (DoE) methodology was employed to explicitly quantify interaction effects between signaling cues [55]. We first employed a colorimetric dye to validate that our custom robotic liquid handling program was able to dispense all cues into the intended positions on the microwell chip to create 64 unique combinations from the six cues listed previously (Figure 2.2). Then, each cue was dispensed into the microwell chip at the EC_{50} dosage (Table A.1). The complementary micropillar chip with NSCs was stamped into the microwell chip with media replenishment every other day. After five days in culture with combinatorial stimuli, quantitative population average measurements of multiple metrics were obtained, including the total cell count and the EdU+ for a measure of proliferative activity, βIII-Tubulin expression and neurite extension as a measure of neurogenicity, and GFAP expression as a measure of gliogenicity (Figure 3.3Aii).

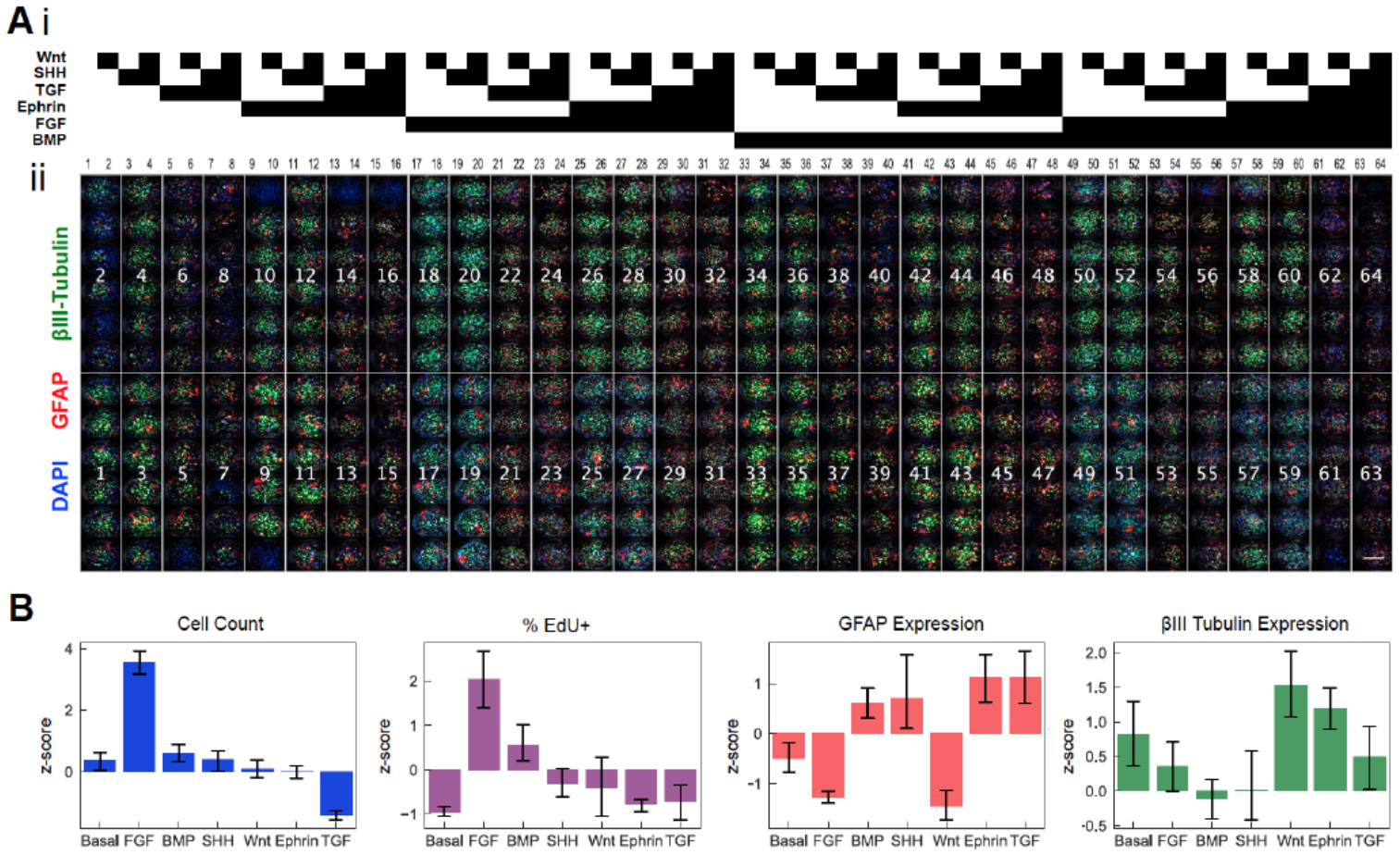

Figure 3.4: Full factorial combinatorial screen of endogenous signaling cues. A) i. Design matrix of full factorial experimental conditions involving Wnt-3a, TGF-β, Ephrin-B2, BMP-4, FGF-2, and SHH-N. ii. Montage of immunocytochemistry for 384 microcultures after exposure to full a factorial set of combinations for 5 days. Replicates are grouped within boxes and labelled by condition in i; scale bar represents 500 microns. B) Quantified population level responses from each microculture after 5 days of exposure to each of six signaling cues. Data were scaled and non-dimensionalized using z-score method. Error bars represent a 95% confidence interval.

3.4.3 Baseline Activity of Individual Signals on NSC Phenotype

To test the efficacy of each signaling cue to induce NSC response on-chip in accordance with previous literature, we examined the normalized endpoint phenotypes of NSC cultures exposed to each cue individually and compared them to the basal media condition of minimal FGF-2, which was chosen to maintain survival but not promote proliferation (Figure 3.4B). The basal media condition exhibited low levels of βIII-Tubulin expression, likely due to spontaneous differentiation upon decreased FGF-2. Importantly, Wnt-3a or Ephrin-B2 increased βIII-Tubulin expression consistent with reported literature [31, 74]; FGF-2 induced proliferation [70, 71]; and TGF-β suppressed proliferation and differentiation of NSCs [76, 79]. Unexpectedly, we observed increased GFAP expression in response to BMP-4, TGF-β, or Ephrin-B2 relative to the basal media condition. Finally, SHH showed increased but non-statistical proliferative activity relative to the basal medium condition, potentially due to a less potent recombinant form of the molecule used here. [91] Overall, FGF-2, Wnt-3a, Ephrin-B2, and TGF-β induced NSC phenotypic responses in accordance with the literature, while BMP-4, TGF-β, and Ephrin-B2 were also found to increase GFAP expression – a trend not previously reported for adult hippocampal NSCs.

3.4.4 Pairs of Signaling Cues Exhibit Additive, Antagonistic, and Synergistic Relationships

Pairwise interactions were analyzed by examining how the extent of a specific NSC response induced by each signaling cue may be modulated by the presence of another potent signaling cue in the cellular microenvironment. A marginal means calculation was used to quantitatively discern the main effect of an individual cue from the interaction effect between two cues on the endpoint phenotypes measured. [55] Furthermore, the marginal means plots characterized the type of interaction between two signaling cues – pairs of cues with parallel lines in the interaction plot were classified to have an additive relationship, while any deviation from parallel was classified as non-additive [55] and pointed to a pair of cues that act either antagonistically or synergistically to impact NSC proliferation or differentiation (Figures 3.5, A.2, A.3, and A.4).

Many cues functioned additively, and thus did not point to statistical evidence of a potential biological interaction between the cues; however, non-additive interactions occurred in several cases. The proliferative activity of FGF-2 on NSCs was found to be antagonistically modulated by the presence TGF-β or Wnt-3a (representative images of FGF-2 and TGF-β micro-cultures are depicted in Figure 3.5i). TGF-β also affected the activity of Wnt-3a and Ephrin-B2 to decrease the extent of NSC proliferation. The most apparent trend for glial differentiation was the antagonistic activity of FGF-2 with all other cues, shown by a decrease of GFAP expression across all conditions with FGF-2 present. For neuronal differentiation, a single case of synergy was evident between Wnt-3a and Ephrin-B2 in the expression of βIII-Tubulin and dendritic extensions. In summary, these data provide new information on how the activity of one endogenous cue may be modulated by the presence of just one additional signaling cue in the NSC

microenvironment to impact NSC fate, and significantly narrows the field for interesting interactions to investigate further in vivo.

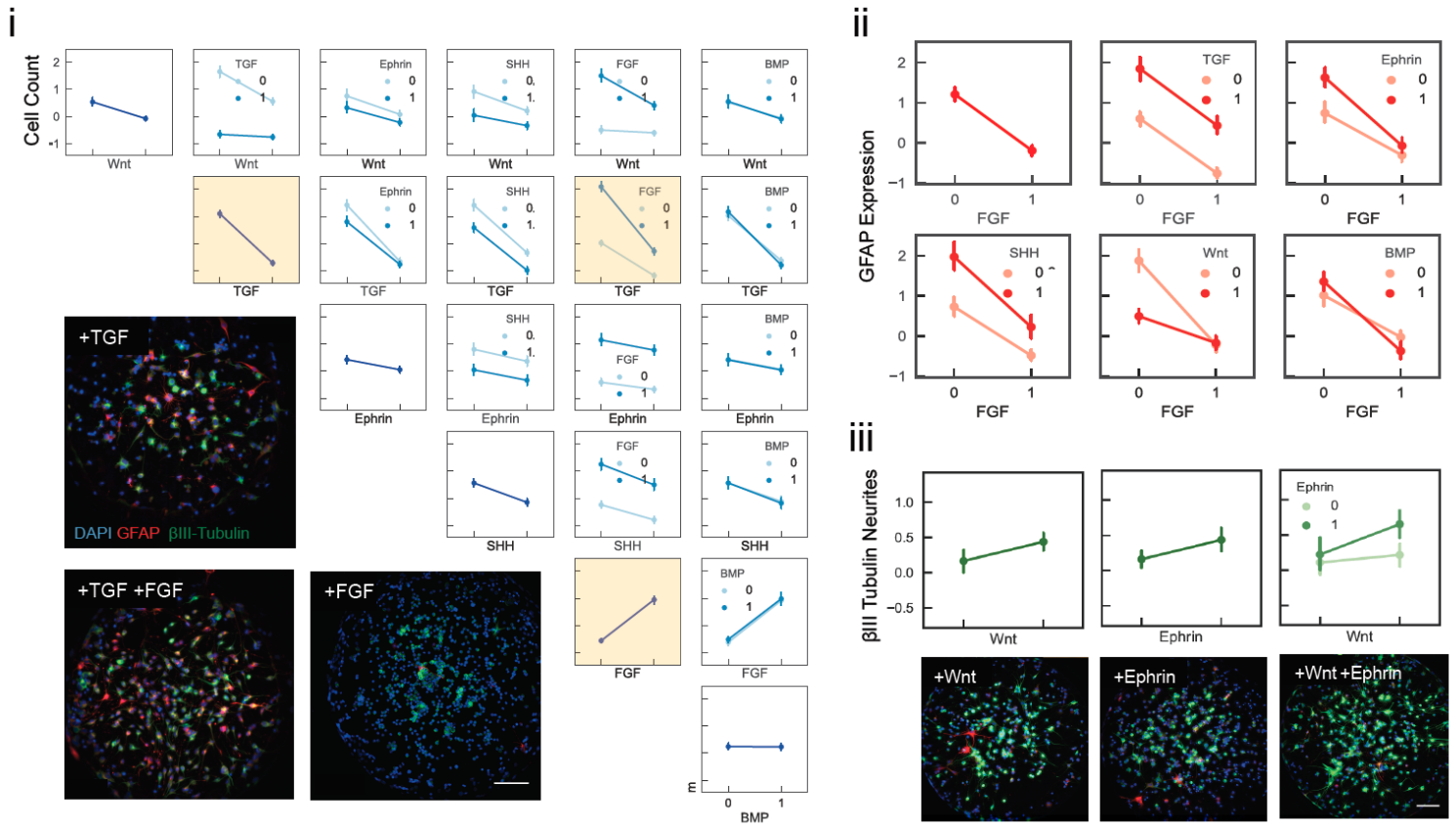

Figure 3.5: Marginal means analysis for main and pair-wise interaction effects among all soluble cues for proliferative activity. FGF-2 and TGF-β interaction is highlighted with corresponding immunocytochemistry images of micro-cultures; scale bar represents 100 microns. ii. Marginal means interaction plots for glial response of FGF-2 in the presence of all other cues. iii. Marginal means plots for β-III Tubulin and neurite extensions of Wnt-3a and Ephrin-B2 with corresponding immunocytochemistry images of micro-cultures; scale bar represents 100 microns. Data were scaled and non-dimensionalized using z-score method. Error bars represent a 95% confidence interval.

3.4.5 Cooperative Action by Tertiary and Quaternary Signal Combinations Influences Neuronal Differentiation

Subsequently, we examined whether higher order combinations of signaling cues (e.g., interactions among three or more factors) in a microenvironment may interact uniquely to impact NSC behavior. We first used a factorial ANOVA to quantify the significance levels of all individual cues (main effect) and groups of cues (interaction effect) on NSC proliferation, glial differentiation, and/or neuronal differentiation, relative to the absence of that cue or group (Figures 3.7A, A.5, and A.6) subject to a false-discovery rate correction. [62] Then, we took the top 10 rank ordered combinations and created an Ordinary Least Squares (OLS) model to represent the relative impact of each signaling environment to the extent of proliferation or differentiation observed. One 4th order combination was identified to have significant contributions to the extent of neurogenesis in a population, specifically Wnt-3a + BMP-4 + Ephrin-B2 + TGF-β was found to drive neuronal differentiation to an extent greater than any of these components individually (Figure 4B). Interestingly, the main effect of Ephrin-B2 on βIII-Tubulin expression and neurite extension was lesser in magnitude than the combined factors listed above (Figure 3.7B), yet simply replacing Ephrin-B2 with SHH in the previous combination switched the outcome from a strong promotion to the strongest suppression of neurogenesis. These results point to a group of cues that act in a cooperative manner to impact the level of neurogenesis in adult NSCs. To examine if the microculture methodology might contain inherent confounding variables in this study, we conducted validation studies in an independent culture format.

Validation of select findings in conventional culture format We conducted a set of validation experiments using a more standard well-plate culture format to examine whether the microculture platform contained inherent attributes that would confound the main findings of this study. Two cases of antagonism were tested: a slight case of antagonism between FGF:Ephrin on the EdU response (microculture data in Figure A.2) and a dramatic case of antagonism between FGF:TGF on the cell count response (microculture data in Figure 3.5) for which we found the trends to hold in the well-plate format (Figure 3.6A,B).

We also tested a set of conditions that displayed a synergistic relationship for the βIII-Tubulin/neurite extensions response: Wnt:Ephrin and Wnt:Ephrin:TGF:BMP (microculture data in Figure 3.7). In a well-plate format, the combination of Wnt:Ephrin :TGF:BMP was observed to have a statistically higher neurite quantity than the cues individually. Immunocytochemistry images showed differences in neuronal morphology between the conditions and by utilizing a new and more powerful microscope and analysis software, we took this one step further by quantifying the number of neurite roots across all conditions to hypothesize a potential mechanism of action for the combined signals in promoting emergence of new neurite branches, rather than extension of existing branches. Although we observed an increase in neurite roots for the combined Wnt:Ephrin:TGF:BMP case, it was not statistically significant from the individual factors (Figure 3.6C) To interpret this, we think that the combined action of Wnt:Ephrin:TGF:BMP may increase

the quantity of neurite roots, which contributes to the increase in total neurite quantity, however, neurite root increase is not the main driver of increased neurite growth and there may be additional sub-components of neurite growth that are influenced by the combined action of Wnt:Ephrin:TGF:BMP as well to explain the overall increase in neurite quantity.

Finally, the Wnt:Ephrin combination was greater, yet not statistically significant, in the neurite quantity compared to Wnt or Ephrin individually. Of note, we did observe lower than expected bioactivity of Ephrin in this experiment. Multivalent Ephrin used in this study is synthesized in batches manually by experts within our lab and we used a different batch than the microculture experiments performed previously that may have had a lower EC_{50}. It's additionally possible that cells exposed to TGF:BMP are sensitized to Ephrin such that the dose level used in this experiment was sufficient for measurable activity in the Wnt:Ephrin:TGF:BMP case.

3.4.6 Global Analysis of Extrinsic Signaling and Phenotype Relationship for NSC Populations

To reveal additional trends within the multi-dimensional dataset, we described each signaling combination as a vector of the endpoint proliferation, neuronal differentiation, and glial differentiation and employed a hierarchical clustering technique to arrange them into categories based on similarity in the direction and extent of the endpoint phenotypes observed (Figure 3.8A).

The conditions with the most proliferation and least differentiation, marked as Category 1, all share the presence of FGF-2 and had a lower order combination of signals, i.e., there was an average of only two signaling cues in the microenvironment. Category 4 also shared the presence of FGF-2 in most microenvironments, yet exhibited low proliferation and low differentiation. Ten out of the 13 conditions in Category 4 also had TGF-β and/or Wnt-3a present, which apparently antagonized the mitogenic activity of FGF-2 such that the combination showed very modest cell expansion. The remaining conditions in low proliferation and differentiation Category 4 contained combinations of BMP-4, SHH, and Ephrin-B2, where the average number of signaling cues per microenvironment was above three. Two categories contained low proliferation and high differentiation responses into either neural or glial lineages, but not both. The most neurogenic category, Category 5, had conditions that all shared the presence of Wnt-3a. In contrast, the highest GFAP expressing category, marked as Category 3, had conditions that all shared the absence of FGF-2. Finally, the last two categories straddled the line between two phenotype directions: Category 2 contained low neural and low glial differentiation while Category 6 contained low proliferation and low neuronal differentiation. Interestingly, no categories were found that contained proliferation and glial differentiation together.

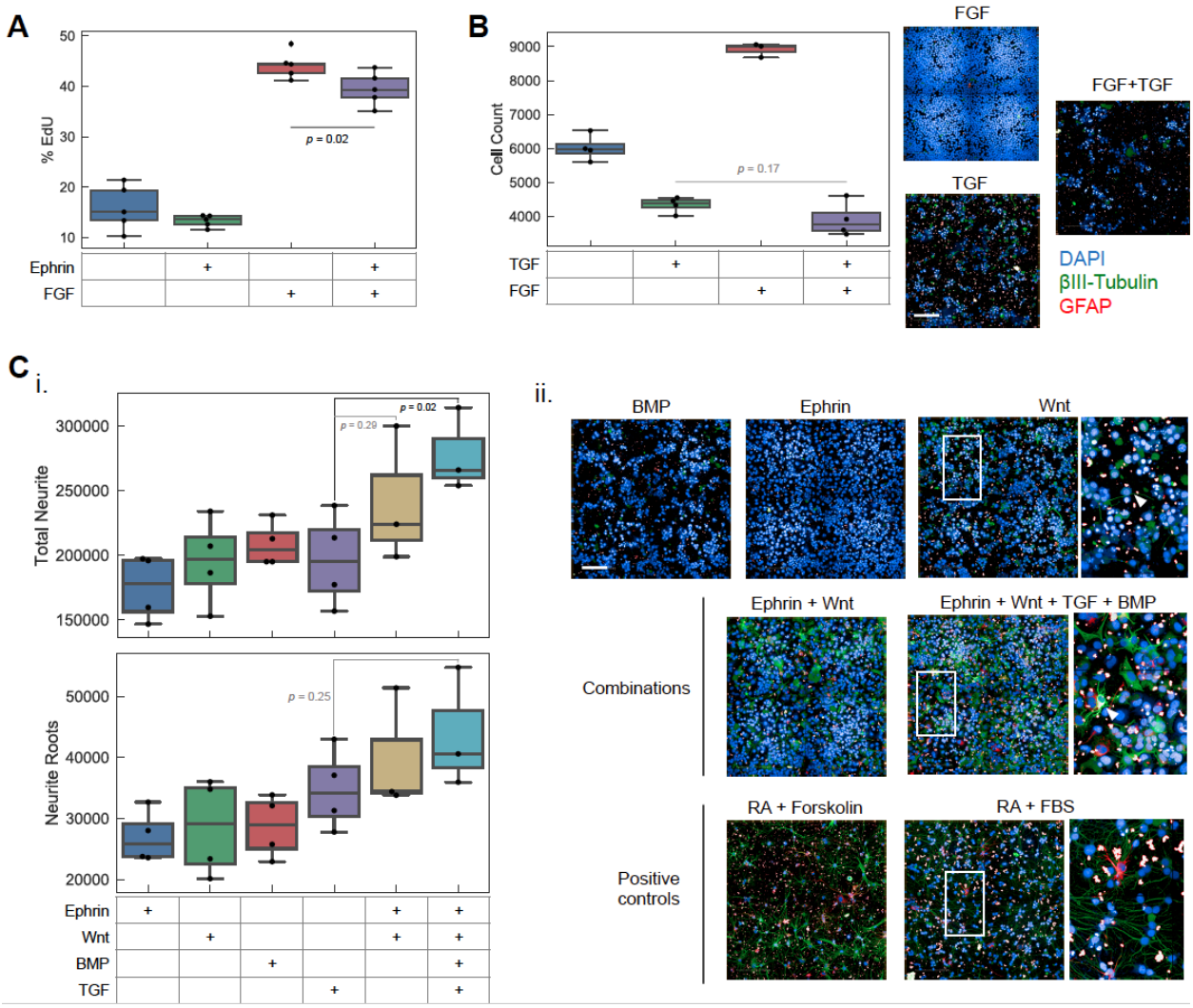

Figure 3.6: Validation of findings in conventional 96-well plate culture format. A) Slight antagonistic relationship between FGF and Ephrin in EdU response of NPCs. B) Dramatic antagonistic relationship between FGF and TGF with corresponding immunocytochemistry images of NPC cultures; scale bar represents 100 microns. C) i. Quantification of neurite trace and neurite roots per well from 6 different culture conditions. ii. Immunocytochemistry images from cultures in individual signaling cues (top row), combinations of signaling cues (middle row), and positive differentiation controls for NPCs (bottom row); scale bar represents 100 microns, white arrows point to representative differences in morphological features.

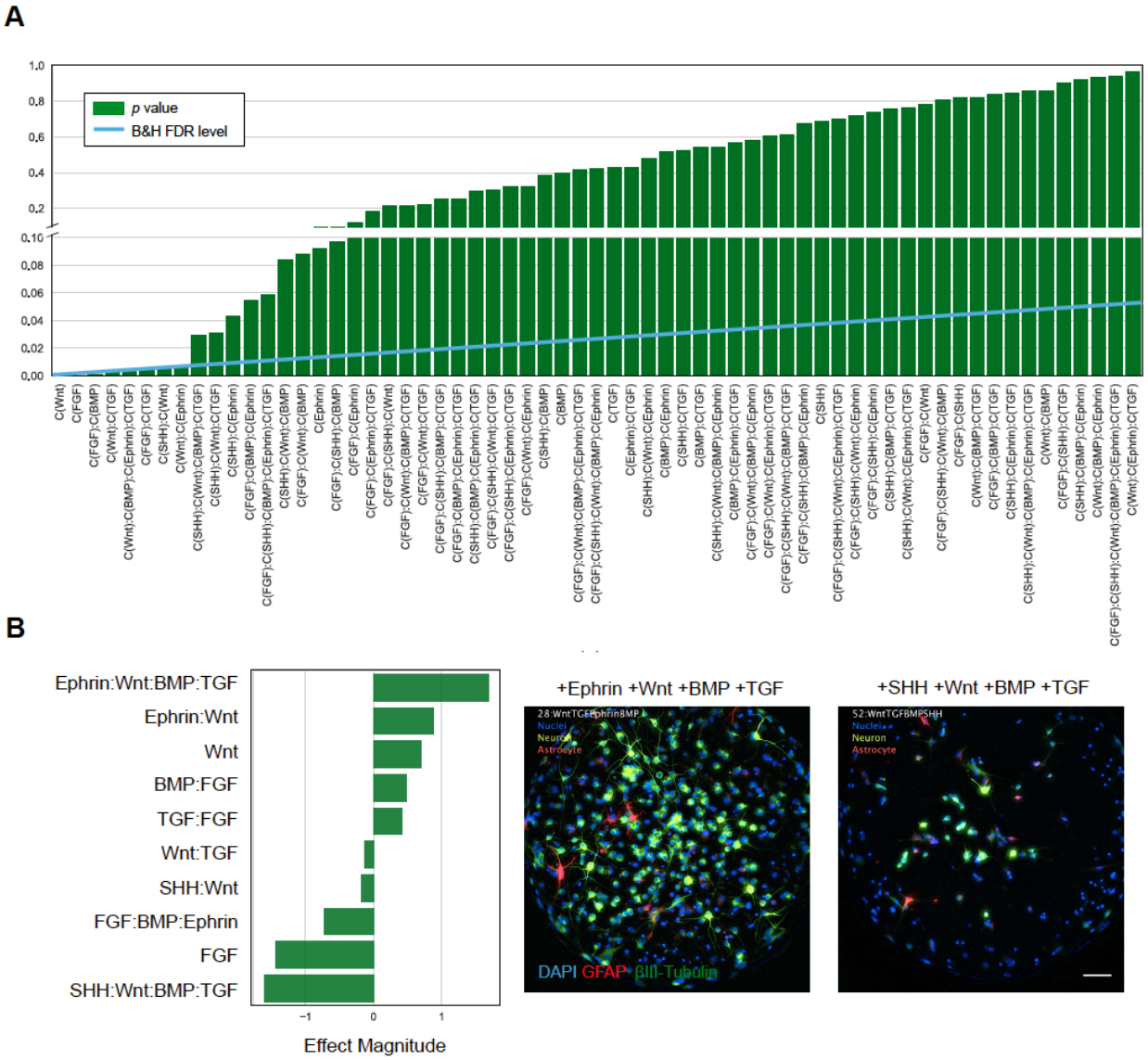

Figure 3.7: Factorial ANOVA model for βIII-Tubulin expression and neurite extensions. A) p-values of main and interaction effects for all signaling environments and the Benjamini - Hochberg threshold for multiple comparisons at a significance level of 0.05. B) Pareto plot of fitted OLS model parameters for top 10 responses and corresponding immunocytochemistry images for the most positive (top) and most negative (bottom) contributions to βIII-Tubulin expression and neurite extensions; scale bar represents 100 microns.

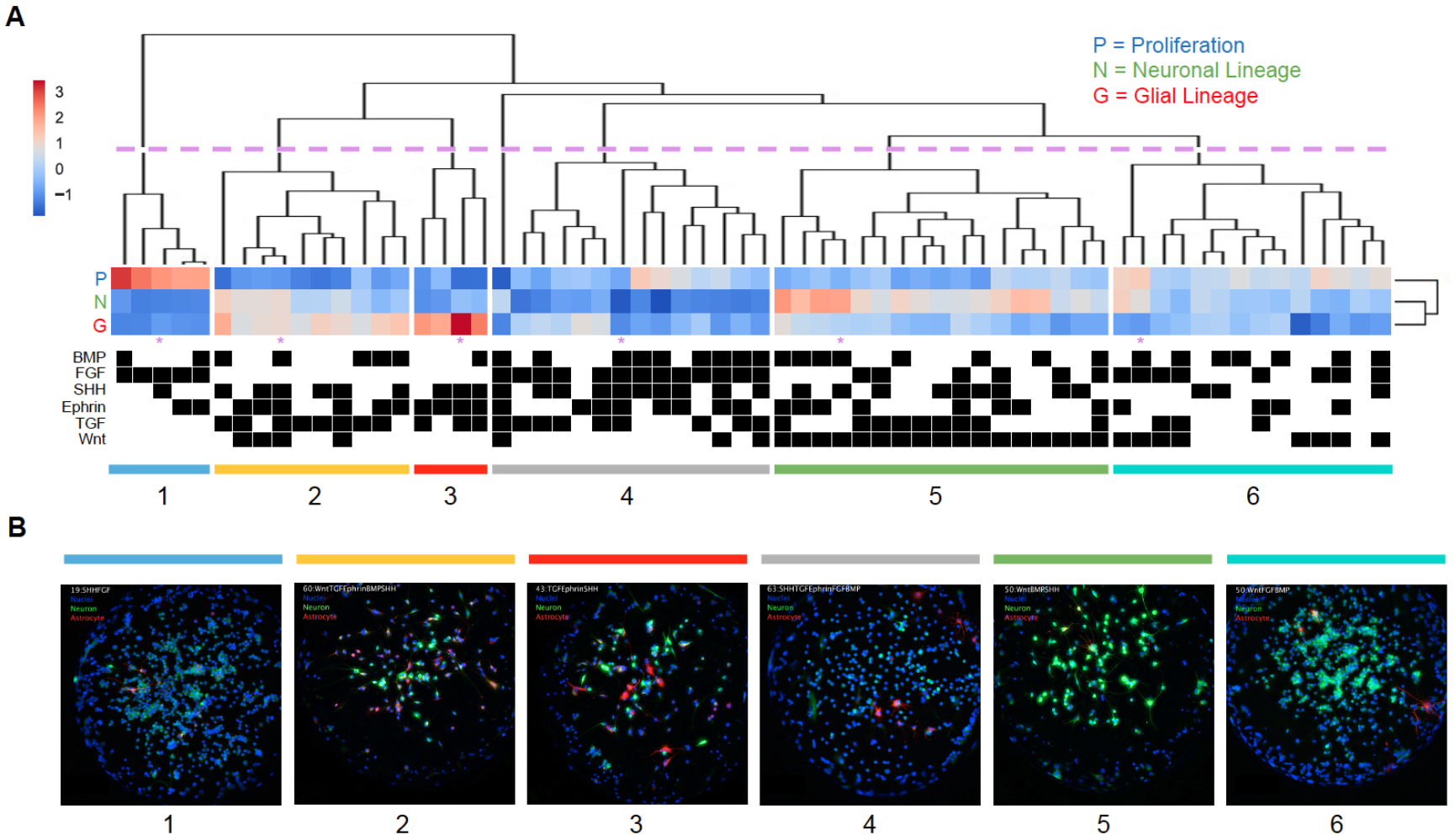

Figure 3.8: Multivariate analysis of phenotypic response from combinatorial signaling environments. A) Hierarchical cluster dendogram of main NSC phenotypes with corresponding signals present at each condition and six main classifications are identified by phenotype similarity; data are standardized by z-score for each measurement variable (row). B) Corresponding immunocytochemistry images of microenvironments with asterisks in A).

3.5 Discussion

3.5.1 Combinatorial Screening to Accelerate Understanding of the Adult Hippocampal Neural Stem Cell Niche

Numerous insights have been gathered from miniaturization and high-throughput studies of stem cell niche components. [46, 81, 84, 86] Here we provide a demonstration of the micropillar/microwell platform to expand beyond toxicology screening [49, 50, 87] and probe fundamental questions regarding how primary NSCs respond to combinatorial signals from the endogenous adult hippocampal niche. In doing so, we were able to simultaneously assay over 500 independent soluble microenvironments and acquire high-content images of NSC proliferation, differentiation, and morphological responses while consuming only 0.2% of the reagent volumes for conventional 96-well plates. Not only is this a favorable system for high-cost reagents, such as recombinant protein growth factors, but also for cell types that are difficult to expand. Furthermore, the parallel processing of 500 independent samples enabled a highly controlled and systematic study to probe phenotypic variations between signaling cue combinations while eliminating confounding variables such as cell passage number of primary NSCs, batch-to-batch variability and degradability of reagents, day-to-day variation in equipment parameters, or even person-to-person variations in technique. We further discuss numerous results from the dataset below and provide a feasible parameter space for investigation in vivo.

3.5.2 New Phenotypes in Response to BMP-4, TGF-β Signals

To our knowledge, this is the first report of BMP-4, TGF-β, or Ephrin-B2 signals increasing expression of GFAP in a population of adult hippocampal neural stem cells. [31, 75, 77–79, 90] In vivo, GFAP is expressed in Type I radial glial cells that are quiescent in the adult hippocampus as well as in lineage-committed astrocytes. Here, we observed two distinct morphologies of GFAP+ cells: one with multiple prominent extensions protruding from the cell body that resemble a characteristic example of an astrocyte, and the other with minor extensions from the cell body (Figure 2.8B). It is conceivable that the latter GFAP+ cell type is closer in identity to the Type I radial glial cell since BMP-4 and TGF-β are known to play a role in the regulation of quiescence of adult hippocampal NSCs. To further investigate a potential role for BMP-4 or TGF-β as a cue to revert Type II neural progenitor towards Type I radial glial cells, future work could examine the effect of BMP-4 or TGF-β exposure on the population of Type I radial glial cells, identified by co-expression of GFAP and neural stem cell markers such as Nestin or Sox2.

3.5.3 Convergence to an Outcome by the Integration of Simultaneous Signals

At the signal transduction level, the numerous extrinsic signaling molecules, and combinations thereof, that exist within the stem cell niche to influence cell fate are ultimately translated to relatively few phenotypes, pointing to the existence of integration

mechanisms within the cell that converge inputs to reach an outcome. For adult hippocampal NSCs, this concept has been discussed previously by Schwarz et al. with Notch signaling proposed as a central node of convergence for BMP-4, TGF-β, SHH, and FGF-2 signals. [92] Here, we uncover additional interactions involving cues discussed by Schwarz et al. as well as Wnt-3a and Ephrin-B2 that influence the phenotypic outcome of NSCs. The molecular basis of these interactions is likely unique for each pair or combination and could assume multiple forms including an extracellular interaction between ligands, such as the mechanism described for the antagonistic relationship between Noggin and BMP signaling cues. [93] Additional hypotheses for intracellular mechanisms could include signal pathway crosstalk at the level of phosphorylation cascade or transcription factor, or priming by translocation of key intermediates by one pathway for the other.

The unique case of synergy we observed between Wnt-3a and Ephrin-B2 to increase β-III Tubulin expression and neurite extensions is of particular interest to investigate further. Previous studies showed that Ephrin-B2 can activate the co-activator β-catenin, pointing to a possible node of convergence between the two pathways. [31] Additionally, a link between the Ephrin and Wnt signaling pathways has been established in the analogous adult stem cell system of the intestinal crypt, where canonical Wnt signaling through β-catenin was found to up-regulate the expression of EphB2/EphB3 receptors. [94] Given that many aspects of signal transduction are conserved across various cell types, it is conceivable that a similar signaling network layout is present here in adult hippocampal neural stem cells.

The majority of higher order combinations of signals probed in other differentiated cell types have exhibited negligible synergy at the level of intracellular signaling cascades, as reviewed previously by Janes et al. [95] Our results from the factorial ANOVA and OLS modeling indicate that this paradigm can potentially be extended to neural stem cell population level responses to combinatorial stimuli as well (Figures 3.7A, A.5, and A.6). However, as described in the next section, even a single case of higher order combinatorial interactions can provide a fruitful area of further investigation to understand combinatorial complexity in stem cell niches, and therefore including them in systematic screening efforts early on might be worthwhile for stem cell differentiation in particular, as their developmental outcome might by more flexible and sensitive to higher-order combinations of signals than terminally differentiated cell types.

3.5.4 Niche Zones that Display the Clearest "Instructions" for a Specific Phenotypic Response

At the niche level, it is conceivable that there is heterogeneity in signal presentation across local NSC microenvironments that contributes to the range of fate outcomes for NSCs within the dentate gyrus. [96, 97] The results in this study point to details of extrinsic signaling combinations that might shift NSC fate outcome toward proliferation, quiescence, or differentiation.

The most proliferative NSC response in microenvironments occurred with FGF-2 alone.

The presence of additional cues either had negligible effect (BMP-4) or acted antagonistically (Ephrin-B2, TGF-β, Wnt-3a). Therefore, it is possible that NSCs undergoing the most proliferation and potentially self-renewal are located in zones of FGF-2 exposure, with minimum conflicting signals. In contrast, there is a shift toward quiescence in zones that present numerous conflicting signals, such as FGF-2, Wnt-3a, and TGF-β together. Additionally, these observations point to a dual role for FGF-2 as mainly proliferative in simple (i.e., one or two cues) signaling environments, and mainly repressive of differentiation in more complex signaling environments.

The higher order combination of Wnt-3a + Ephrin-B2 + BMP-4 + TGF-β could provide a neurogenic and neuronal maturation niche. The contrasting role of TGF-β in this combination versus in isolation is noteworthy. Previous reports have provided evidence for dual roles of BMP-4 and TGF-β as quiescence factors for NSCs and maturation factors for committed neuroblasts, [76, 98] which could explain the results observed here. It is conceivable that the initial exposure of NSCs to Wnt-3a + Ephrin-B2 to induce neuroblast commitment while the simultaneous presence of Wnt-3a + Ephrin-B2 with BMP-4 + TGF-β in a niche could induce neuroblast commitment and accelerate the maturation process. In vivo, migration of neuroblasts away from the subgranular zone during maturation may alternatively offer a mechanism where the presence of BMP-4 + TGF-β is in a spatially distinct zone, to enable sequential exposure to different signals as cells progress down a neuronal lineage. Either way, the signals appear to cooperate to influence neuronal differentiation and maturation.

3.5.5 Context Dependence of NSC Fate

Overall, the various cases of signaling interactions identified here and their implications in NSC signal transduction and for the NSC niche share a larger theme of context dependence, where the activity of multiple signaling cues is modulated by the presence of additional cues in the microenvironment of an NSC. These studies quantitatively demonstrate that a highly intricate and sensitive balance of multiple cues guides the endpoint phenotype of NSC populations and these in vitro results are potentially representative of NSC fate within the adult hippocampal niche. Disruption of precise balances between molecular cues could contribute to the cell and tissue degeneration in the hippocampus during aging [29] or by disease, having consequences for learning and memory throughout adulthood.

3.6 Conclusion

The novel application of a high-throughput micropillar/microwell methodology enabled careful and systematic dissection of the combinatorial signaling niche. Interactions between key endogenous cues can play a large role in the regulation of neural stem cell phenotypes, and the quantitative analyses presented here identify numerous cases of signaling context-dependence. These data also provide promising leads for an in vivo investigation of the implications of combinatorial signals, such as the antagonism between FGF-2 and TGF-β, or the synergistic neurogenesis from Wnt-3a + Ephrin-B2 + BMP-4 + TGF-β .

Overall, this study contributes to further understanding of the intricate and complex mechanisms guiding NSC fate choice, and provides insight that may enhance control over stem cell based therapies for neurodegenerative diseases.

Acknowledgements Thank you to Dr. Mary West for microscopy resources through the Shared Stem Cell Facility (SSCF) and High-Throughput Screening Facility (HTSF); the College of Chemistry Machine Shop and Eric Granlund for machining custom equipment; and Prof. Henk Roelink, Prof. Sanjay Kumar, and the members in the NSC sub group, for insightful discussions. This research was supported by an NSF Graduate Research Fellowship (to R.J.M) and the National Institutes of Health (R01 ES020903) and Instrumentation Grant (S10OD021828) that provided the Perkin Elmer Opera Phenix microscope.

Chapter 4

3D Microculture Platform Enables Advanced, High-Throughput Differentiation Screening of hPSC-derived Therapies

4.1 Abstract

The promising outlook for hPSC-derived cell therapies leads many to consider the development of manufacturing processes to meet the patient demand for such therapeutics. Toward this aim, 3D culture systems for hPSC differentiation are emerging because of their potential for higher expansion and yield of target cell types compared to 2D culture systems. Therefore, the ability to screen through a multifactorial parameter space of exogenous chemical cues for 3D hPSC cultures would greatly accelerate the pace of discovery and development of efficient in vitro differentiation protocols for target cell types of interest. Here, we demonstrate the advanced capabilities of a 3D micro-culture platform that we employ to screen through more than 1000 unique combinations of 12 independent 3D culture parameters to derive Olig2+Nkx2.2+ oligodendrocyte progenitor cells (OPCs) from hPSCs with 0.2% of the reagent volumes used in 96-well plates. We leverage novel fluorescent hPSC reporter cell lines to live-monitor proliferation and differentiation for over 80 days in the 3D micro-culture system. The robust data set enabled statistical modeling of the OPC differentiation process to uncover interactions and differential sensitivities to culture parameters such as hPSC seeding density, Retinoic Acid dose, Wnt pathway agonist CHIR dose and duration, SHH pathway agonist SAG dynamics, and combinations thereof. To show the generalizability of the platform, we then applied it to simultaneously assay 90 unique differentiation protocols to derive TH+ midbrain dopaminergic neurons from hPSCs. Overall, we demonstrate a strong methodology for upstream microscale screening/optimization to inform downstream scale-up processes to improve 3D production strategies of hPSC-derived CRTs.

4.2 Introduction

Stem cells – including adult and pluripotent subtypes – offer tremendous clinical promise for the treatment of a variety of degenerative diseases, whereby a single stem cell has the capacity to self-renew indefinitely as well as mature into functional cell types and serve as a source of cell replacement therapies (CRT). Human pluripotent stem cells (hPSCs) are of increasing interest for development of CRTs because of their capacity to differentiate into wide range of mature cell types for which adult tissue specific stem cells may not exist. [99–103] A leading example of this is the derivation of oligodendrocyte progenitor cells (OPCs) from hPSCs for the treatment of Spinal Cord Injury (SCI) [104] for which hPSC-OPCs have recently advanced to Phase II clinical trials [105, 106] and are even being considered for additional disease targets in the Central Nervous System (CNS), such as Multiple Sclerosis (MS). [107]

The promising outlook for hPSC-OPCs so far leads many to consider the development of manufacturing processes to meet the patient demand for such hPSC-derived therapeutics. For example, roughly 250,000 patients in the U.S. suffer by some form of SCI, with the total growing annually by an estimated 15,000 new patients. [108] Clinical trials of hPSC-OPCs in humans were recently dosed at 20 million cells per patient, [105] amounting to over 1 trillion OPCs required to meet the total patient demand today. It is therefore imperative to develop systems that enable discovery of efficient and scalable differentiation protocols for these therapies.

Differentiation protocols to direct hPSCs into functional OPCs have developed by recapitulating the signaling environment within the developing spinal cord in vivo where exists a complex intersection of growth factor and morphogen gradients that vary across time as the embryo develops. [109, 110] In vitro, this requires optimization of a large combinatorial parameter space of signaling agonists and their doses, durations, dynamics, and combinations over many weeks to achieve efficient yield of the target cell type (Figure 4.1), measured by expression cellular markers present in OPCs, such as transcription factors Olig2 and Nkx2.2 [111]. Derivation strategies for hPSCs to OPCs have seen great, yet slow, improvement since the original protocol [112] with increases in efficiently deriving the target cell type. [113]

More recently, adoption of 3D culture systems has demonstrated strong potential for larger scale and higher yield [114] of hPSC expansion and differentiation processes than 2D counterparts, as well as compliance with Good Manufacturing Practice (GMP). [115–117] It is apparent, however, that a bottleneck exists in the optimization of 3D differentiation protocols for OPCs and other hPSC-derived cell therapies. Current high-throughput experimental systems are better suited to screening 2D cultures [47, 118, 119] where there is less risk for a robotic dispensing nozzle to disrupt the culture during media replenishment. For 3D cultures, however, this problem has limited the use of robotic systems in dense well plates, such as 96- or 384- well plates, to where the length of assay is limited to a few days. [120]

Here, we demonstrate the versatile capabilities of a uniquely structured microculture

platform, previously applied toward toxicology assays [49, 50, 87], for 3D differentiation screening and optimization of hPSC-derived cell therapies (Figure 4.2). The independent control of gel-encapsulated cells (on pillar chip) and media (in well chip) removes the risk of gel disruption during robotic dispensing of over 500 independent wells of media. We employ custom hPSC reporter cell lines [60] to enable live-imaging of differentiation and proliferation for over 80 days on the microculture chip. Over 1000 culture conditions that varied signal dose, duration, dynamics, and combinations were screened utilizing 0.2% of the reagent volumes of a standard 96-well plate format. Further, the robust dataset enabled statistical modeling for empirical optimization of the differentiation to identify differential sensitivities of differentiation efficiency to certain culture parameters across time. Finally, we demonstrate the generalizability of the platform by applying it toward a screen for differentiation of Tyrosine Hydroxylase+ midbrain dopaminergic neurons from hPSCs.

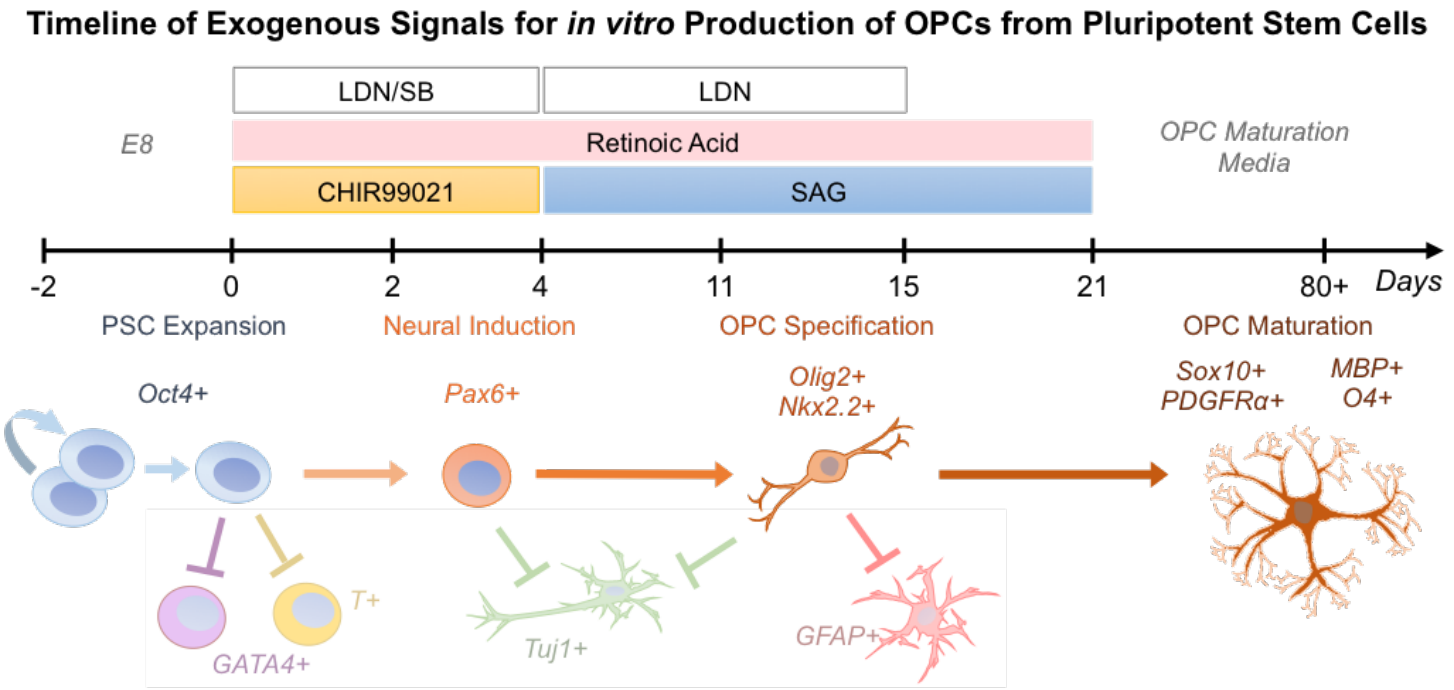

Figure 4.1: Timeline of exogenous signals for in vitro OPC differentiation from human pluripotent stem cells and expected cellular marker expression along various differentiation stages.

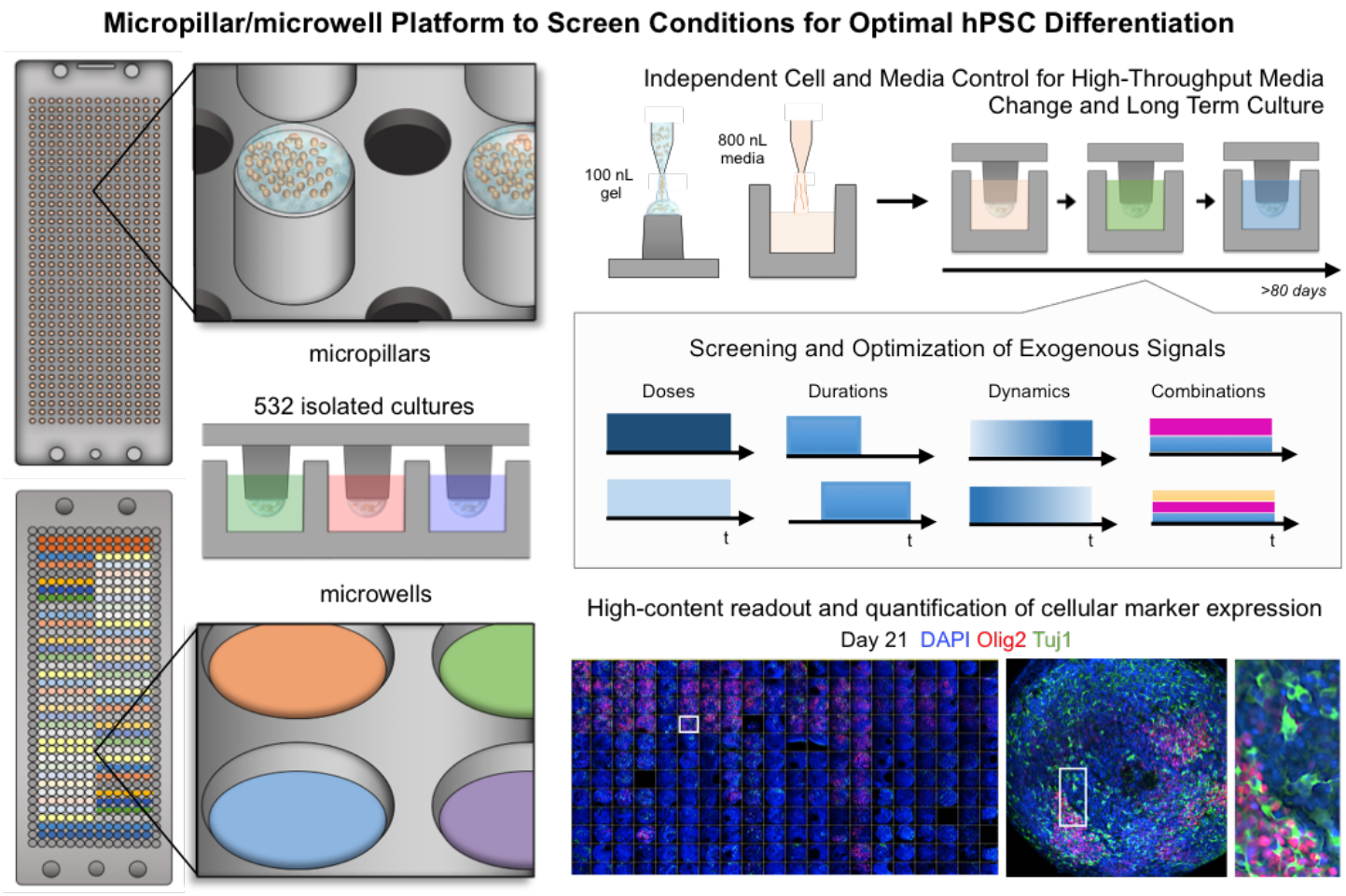

Figure 4.2: Micropillar and Microwell High-Throughput Culture System. A micropillar chip with cells suspended in a 3D hydrogel is stamped to a complementary microwell chip containing isolated media conditions to make 532 independent microenvironments. 100 nL of hPSCs suspended in a hydrogel is automatically dispensed onto the micropillars, and 800 nL of media is automatically dispensed into the microwells by a robotic liquid handling robot programmed to dispense in custom patterns. The independent substrate for cells and media enables screens of combinations of soluble cues at various dosages and timings.; scale bar represents 1 mm.

4.3 Experimental Methods

4.3.1 Human Pluripotent Stem Cell Culture

Human embryonic stem cells (H9s, NIH Stem Cell Registry 0062) were subcultured in monolayer format on a layer of 1% Matrigel and maintained in Essential 8 medium during expansion. At 80% confluency, H9s were passaged using Versene solution and replated at a 1:8 split.

4.3.2 3D PSC microculture on Pillar/Well Chip System

Micropillar and microwell chips (MBD Korea) made of polystyrene were manufactured by plastic injection molding as described previously [49,50]. H9s were dissociated into single cells using Accutase solution and resuspended in Essential 8 medium containing 10 μM Y-27632 (Rock Inhibitor). H9s were counted and resuspended at defined densities in 50% Matrigel solution on ice. While chilled, 100 nL of H9s in 50% Matrigel solution were deposited onto the micropillars using a custom robotic liquid handling program and then incubated at 37°C for 20 minutes to promote gelation of 3D cultures. The micropillar chip was then inverted and placed into a fresh microwell chip containing cell culture media (Table B.1). All liquid dispensing into the microculture platform was performed with a DIGILAB Omnigrid Micro liquid handler with customized programs for deposition patterns. Media was changed daily by transferring the micropillar chip into a microwell chip containing fresh media every other day using a custom made mechanical "Chip Swapper" for consistent transfer. Technical replicates included two different dispensing patterns to average out positional effects across the microchip.

4.3.3 On-chip Viability Assay

At the endpoint of the experiment, the micropillar chip was carefully removed from the wellchip and placed in new wellchip containing Calcein AM, Ethidium Homodimer, and Hoechst diluted in sterile PBS (dilution details in Table B.2). The chip was incubated for 20 minutes and then transferred to a new wellchip containing PBS and individual microenvironments were imaged using fluorescent microscopy.

4.3.4 On-Chip Immunofluorescence Assays

At the endpoint of the experiment, the micropillar chip was carefully removed from the wellchip and placed into a bath of 4% parafomaldehyde for 15 minutes to fix cell cultures. Then, the micropillar chip was washed twice in PBS for 5 minutes each and placed into a bath of 0.25% Triton-X + 5% donkey serum in PBS for 10 minutes to permeabilize cells. After permeabilization, the micropillar chip was washed 5 times in 5% donkey serum for 5 minutes each, dried and transferred to a wellchip containing primary antibodies of interest diluted in PBS+donkey serum (dilution details in Table B.2) and stored overnight at 4°C. After primary staining, the micropillar chip was washed twice in PBS for 5 minutes each, dried,

and then placed into a microwell chip containing the corresponding secondary antibodies (dilution details in Table B.2) and incubted at 37°C for 2 hours. After secondary staining, the micropillar chip was washed twice in PBS for 5 minutes each, dried, and then placed into a wellchip containing PBS and individual microenvironments were imaged using fluorescent confocal microscopy.

4.3.5 High-Throughput Fluorescence Microscopy

Stained micropillar chips were sealed with a polypropylene film (GeneMate T-2452-1) and imaged with a 20x objective using a Perkin Elmer Opera Phenix automated confocal fluorescence microscope available in the High-Throughput Screening Facility at UC Berkeley. Laser exposure time and power was kept constant for a fluorescence channel within an imaging set.

4.3.6 Image Processing, Data Analysis, and Statistical Methods

Images are scored for marker expression depending on nuclear or cytoplasmic localization (Figure 2.9). Quantified image data was then imported into Python for statistical data analysis [53] and visualization. For comparisons between data sets acquired across different experimental sessions, raw data was scaled and centered by z-score, and descriptive statistics were calculated from 4 technical replicates. Error bars represent 95% confidence intervals unless otherwise specified. For the hierarchical cluster model, the Euclidean distance was used to measure pairwise distance between each observation and the UPGMA algorithm was used to calculate the linkage pattern. A Benjamini - Hochberg False Discovery Rate correction [62] was applied as needed to correct for multiple comparisons. Code available upon request.

4.4 Results and Discussion

4.4.1 Miniaturization and increased throughput of 3D hPSC culture for differentiation screening

Initially, we assessed the ability to deposit hPSCs uniformly and with high viability onto the micro culture platform to determine if any aspects of the microculture methodology should be identified as confounding variables in the study. Quantification of total, live, and dead cell counts across the microchip indicates uniform dispensing and culture seeding and high levels (>70%) of cell viability at the start of an experiment (Figure 4.3A). We then employed a custom-made reporter cell line 25 to longitudinally monitor proliferation and differentiation of hPSCs to Nkx2.2+ oligodendrocyte progenitors in 3D on the microchip platform. A small range of culture conditions from previously published protocols of OPC differentiation was selected for a pilot differentiation experiment and the GFP expression was quantified at later stages of differentiation. Cellular morphological changes from neural lineage commitment and maturation were clearly observable at later stages in the

differentiation (Figure 4.4) as cultures were maintained and monitored for more than 80 days on the microchip. We further built fluorescence image analysis pipelines for quantification of nuclear and cytoplasmic marker expression via immunocytochemistry for endpoint analyses (Figure 2.9). Together, these results support the robust and long-term culture potential and cellular marker expression readout of this miniaturization methodology for hPSC differentiation screening.

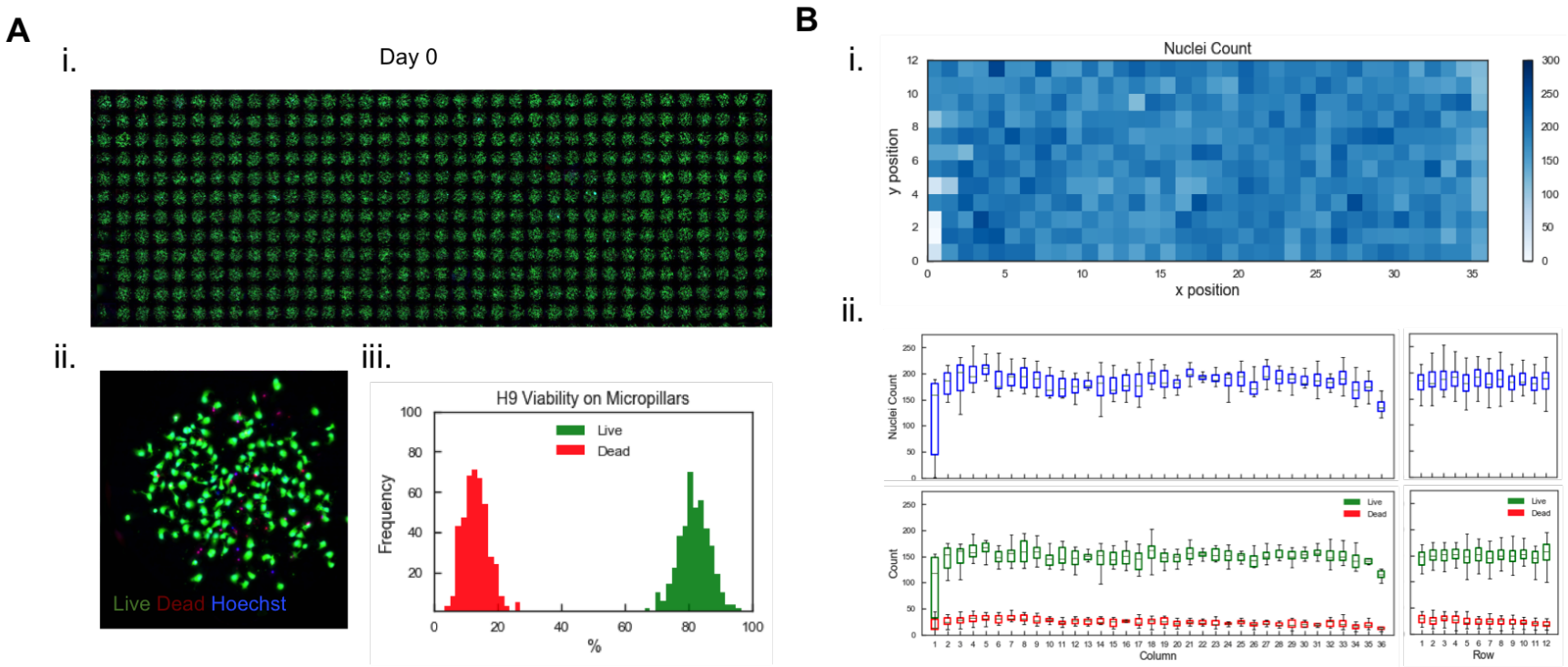

Figure 4.3: H9 seeding and viability across the micropillar culture chip. A) i. Montage of 432 micropillar H9 culture environments stained with Hoechst (blue), calcein AM (green) and ethidium homodimer (red) to assess viability; scale bar represents 1 mm. ii. Image of a single microenvironment; scale bar represents 100 microns. iii. Histograms of percentage live and dead cells across the micropillar culture chip. B) i. Heatmap of total cell count across all positions on the micropillar culture chip. ii. Boxplots of i. total and ii. live/dead cell counts across every column and row of the micropillar chip.

4.4.2 Olig2 expression is substantially modulated by tuning early 3D culture parameters

hPSC Seeding Density

We first focused on parameters within the early stages of 3D differentiation of hPSCs into OPC (Figure 4.5A). The existence of autocrine and paracrine signaling mechanisms in many cells led us to hypothesize that the density of cells at the start of differentiation would impact the early neural induction efficiency and consequently the efficiency of differentiation into OPCs. We therefore demonstrated the ability of this microculture platform to test a range of initial hPSC seeding densities on Day -2 (Figure 2.6) and tested the effect of seeding density on Olig2 expression. We observed notable differences in levels of cell-to-cell adhesion in hPSC cultures by Day 0, only two days after initial seeding. Then, after 15 days of differentiation, we observed a broad trend that lower hPSC seeding density increases OPC specification, and that lower cell seeding densities have a higher sensitivity to dosing of key patterning cues, in this case SAG (Figure 4.5B). In a bio-manufacturing context, lower initial densities will additionally benefit from less input material required to achieve a similar output, increasing the overall yield (defined as output OPCs per input hPSCs). Additionally, the risk of overcrowding and nutrient depletion is mitigated with lower initial seeding densities and in culture vessels that are not amenable to intermittent cell passaging, or where intermittent cell passaging is undesirable such as for bioreactor scale processes, a lower seeding density on the order of 1E5 cells/mL appears optimal.

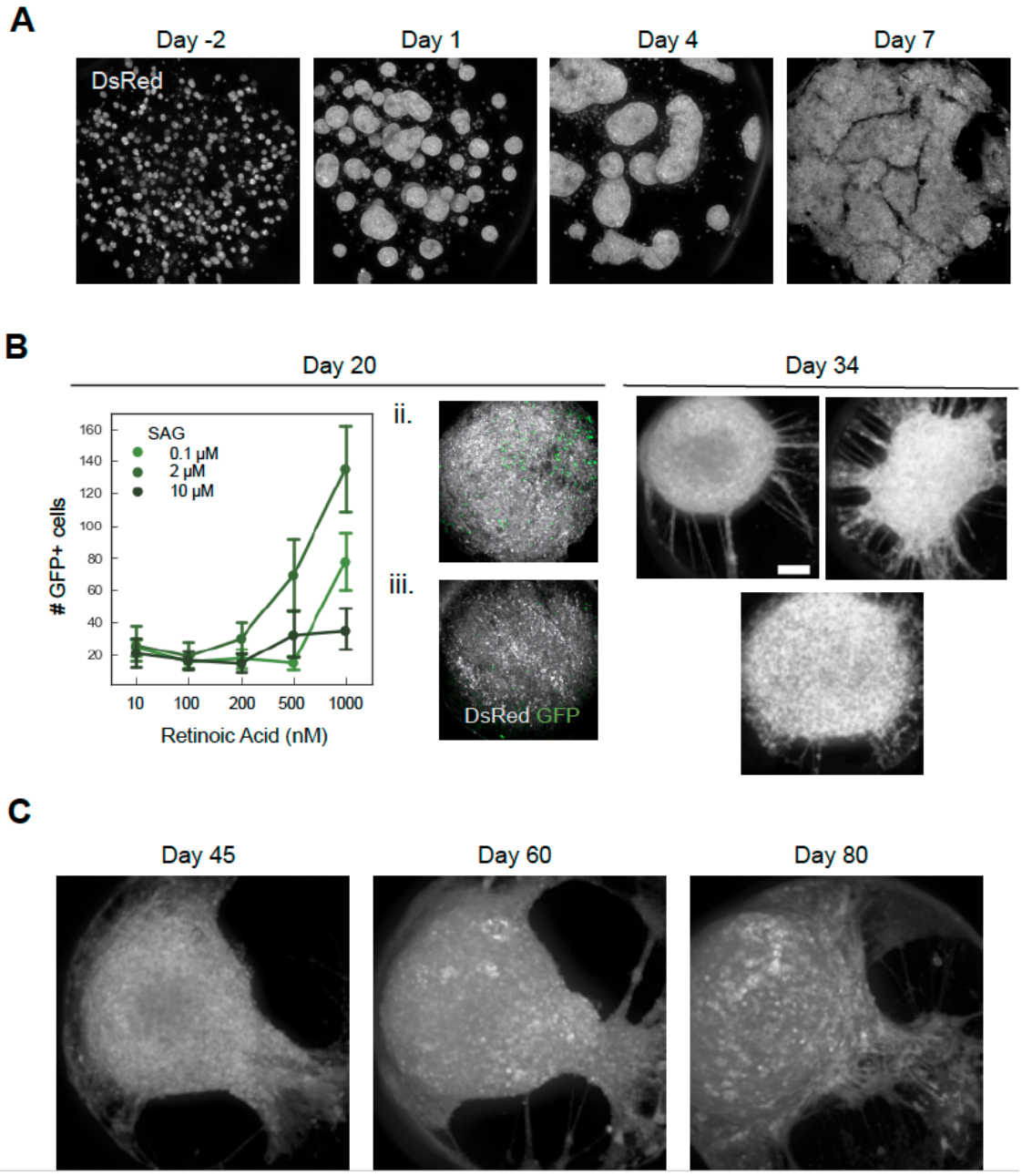

Figure 4.4: Longitudinal study of proliferation and differentiation on micropillar platform. A) Fluorescent confocal images of DsRed fluorescence from H9s cultured in 3D Matrigel from Day -2 to Day 7. B) Quantification of GFP+ cells after 20 days of differentiation in 15 different combinations of RA and SAG concentrations with fluorescent confocal images of dsRed (gray) and GFP (green) at ii. 2 μM SAG + 1000 nM RA and iii. 10 μM RA + 1000 nM RA conditions. Error bars represent 90% confidence interval from 4 technical replicates. Morphological changes are visible on Day 34. C) Fluorescent confocal images of dsRed between Day 45 and Day 80 of differentiation.

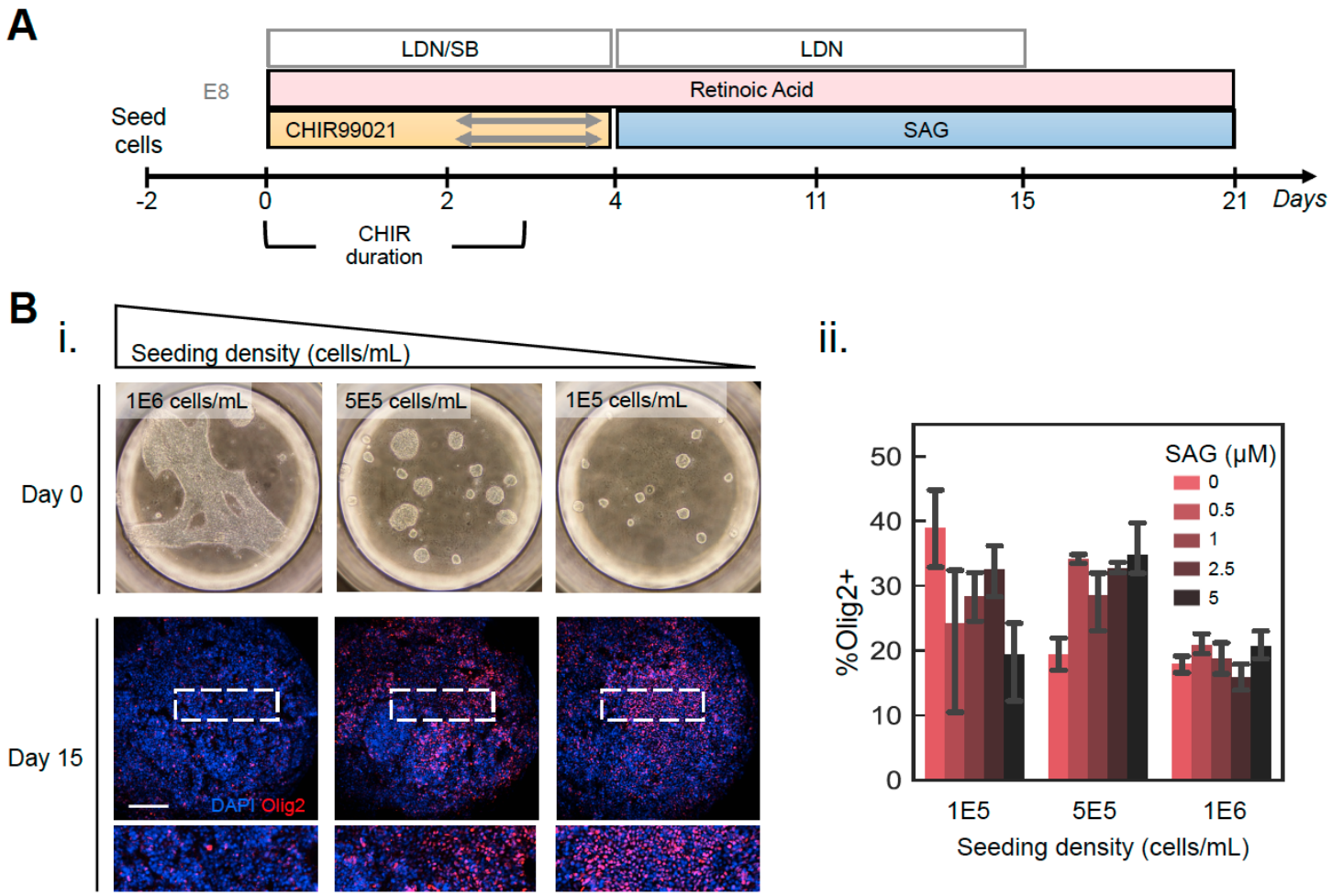

Figure 4.5: Early culture parameters play a large role in OPC differentiation efficiency. A) Timeline of key parameters in the early phase of OPC differentiation. B) i. Bright field images of 3D H9 microculture sites at Day 0 seeded with varying cell densities and the immunocytochemistry images of Olig2 (red) expression at Day 15; scale bar represents 100 microns. ii. Quantification of Day 15 Olig2 expression with respect to seeding density and SAG dose.

Duration of Neural Induction period

We then hypothesized that the differentiation efficiency of hPSCs to OPCs would be sensitive to the duration of the neural induction phase, based on the in vivo timeline of embryonic neural tube formation. In vitro, we induced neural induction of hPSCs by inhibition of BMP-4 signaling using the dual SMAD inhibition approach [121] with LDN193189 and SB431542 and tested a range of neural induction durations before agonists for additional key developmental signaling pathways, such as Wnt, Retinoic Acid (RA), and SHH, were introduced. We observed a strong trend between neural induction time and OPC specification such that shorter neural induction duration resulted in higher Olig2 expression (Figure B.1). These data also suggest a limited window of opportunity, roughly 2 days after the start of neural induction, for maximal cell competence to the subsequent patterning cues Wnt, RA, and SHH.

Dose and Duration of Key Signaling Agonists

After neural induction, we examined the combinatorial and temporal effects of three signaling cues that play a large role in the specification of the neural tube domain from which oligodendrocyte progenitors arise: Wnt-3a (activated by CHIR99021, hereafter referred to as CHIR), RA, and SHH (activated by Smoothened Agonist hereafter referred to as SAG). It's conceivable that to best recapitulate the signaling context from this domain, one would fine-tune the in vitro culture doses of these cues and, therefore, we assessed the Olig2 expression resulting from a full factorial combinatorial screen of these cues (Figure 2.3). Most notably, we observed significant trends in Olig2 expression with respect to RA dose and the duration of CHIR exposure at the beginning of differentiation (Figure 4.6). These 3D results follow similar trends observed in an independent study of 2D OPC differentiation [47] that can be interpreted as evidence for this microculture platform's ability to be representative of differentiation outcomes in larger scale formats. Further, we observed a bi-phasic relationship with respect to CHIR dosing such that 6 μM resulted in the maximum proportion of cells co-expressing Olig2, potentially due to toxicity of high CHIR doses because of the proportionally high DMSO content which was used as the solvent for the CHIR solution (Figure B.1). This observation alludes to a larger technical limitation in these assays – the use of DMSO as a solvent for numerous small molecule signaling agonists could constrain the upper limit of dosing assays, especially combinatorial assays, as previous reports have identified toxicity of hPSCs to DMSO above 0.5% [122]. To somewhat mitigate this confounding effect, it's possible to concentrate stock solutions of all small molecules as high as the solubility limit will allow.

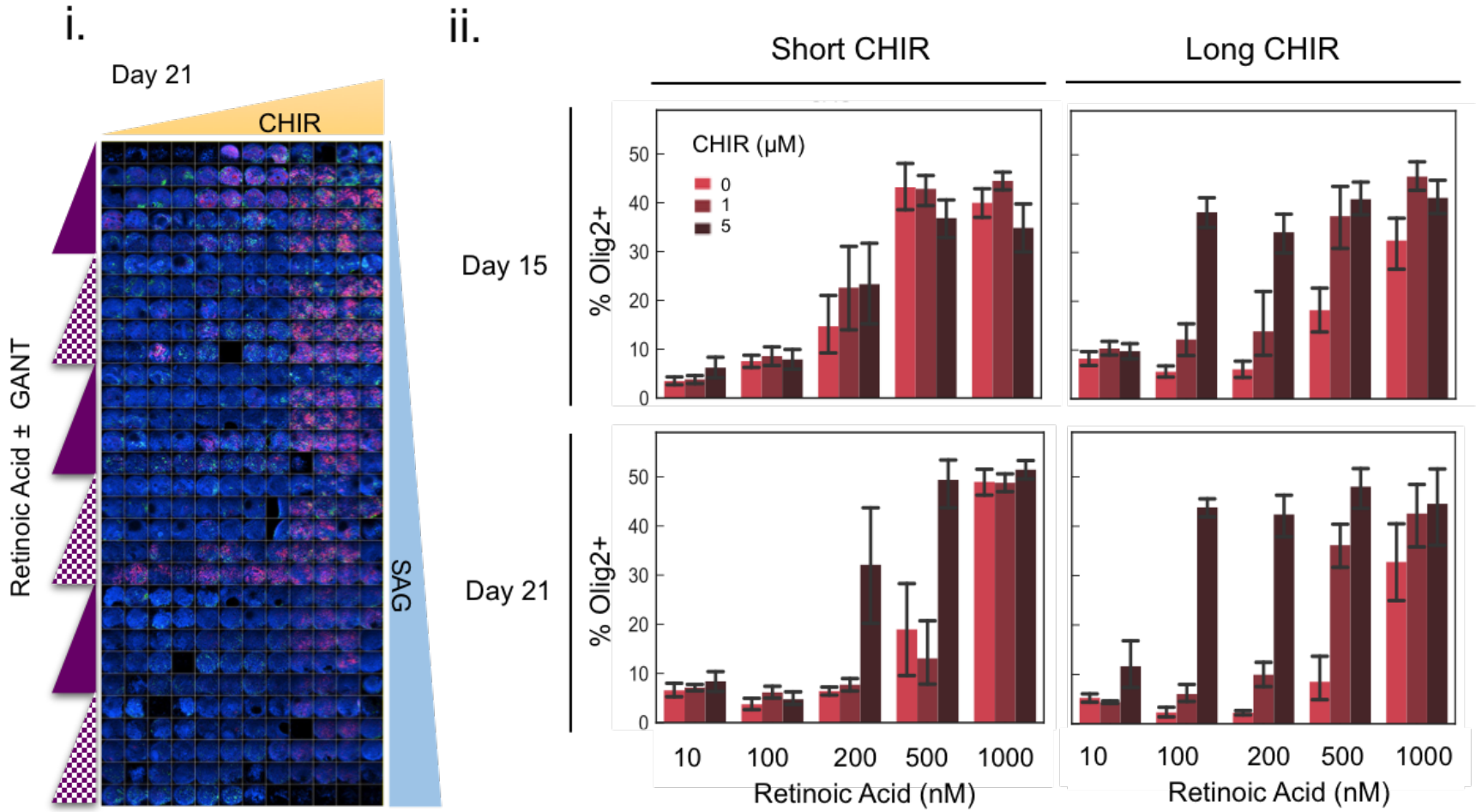

Figure 4.6: Interaction between RA dose and CHIR duration. i. Montage of 360 fluorescent confocal images representing 90 unique differentiation timelines on a single microchip stained for Hoechst (blue), Olig2 (red) after 21 days of differentiation. ii. Trends in Olig2 expression at Day 15 and Day 21 in various CHIR and RA concentrations and durations.

4.4.3 Strategic addition of signaling antagonists to modulate OPC specification

The absence of certain signaling cues perhaps plays equal importance to the presence of other signaling cues in the development of a target cell type; therefore we hypothesized that by supplementing antagonists of signaling pathways strategically at strategic time intervals, we could further enhance differentiation efficiency into OPCs. We identified three signaling antagonists to apply toward this aim: GANTT61 is an antagonist of the SHH pathway, IWP-2 is an antagonist of the Wnt pathway, and DAPT is an antagonist of the Notch pathway. These molecules were added to inhibit basal signaling levels when the opposing agonist was not present. We employed a full factorial analysis of these cues to also probe for combinatorial interactions between the antagonists.

To further refine the measurement for OPC specification, we measured Nkx2.2 expression in addition to Olig2 expression and quantified the proportion of cells co-expressing both OPC markers. Most notably, a significant decrease in Olig2 was observed in response to DAPT across all conditions tested. Interestingly, the same trend was not observed with respect to Nkx2.2. This could point to a role for Notch signaling in maintaining or promoting specification of Olig2+ progenitors – a hypothesis not previously examined to our knowledge – and serves as preliminary evidence to test Notch agonists such as DLL-4, in follow-up studies of OPC optimization. Then, we observed a slight increase in Olig2+ cells with respect to IWP-2 dose when no GANTT61 was present, and a slight increase in Nkx2.2+ cells with respect to IWP-2 and GANTT61 dose, pointing to a potential interaction between the two cues in inducing Nkx2.2 expression. The highest proportion of co-expressed cells was observed at the highest IWP-2 and GANTT61 doses, and was not influenced by DAPT exposure, however, the absolute number of co-expressed cells would be much higher in the absence of DAPT if there is a higher proportion of Olig2+ cells in that population (Figure 4.7), and therefore might be the highest performing culture condition for the specification of Olig2+Nkx2.2+ progenitors.

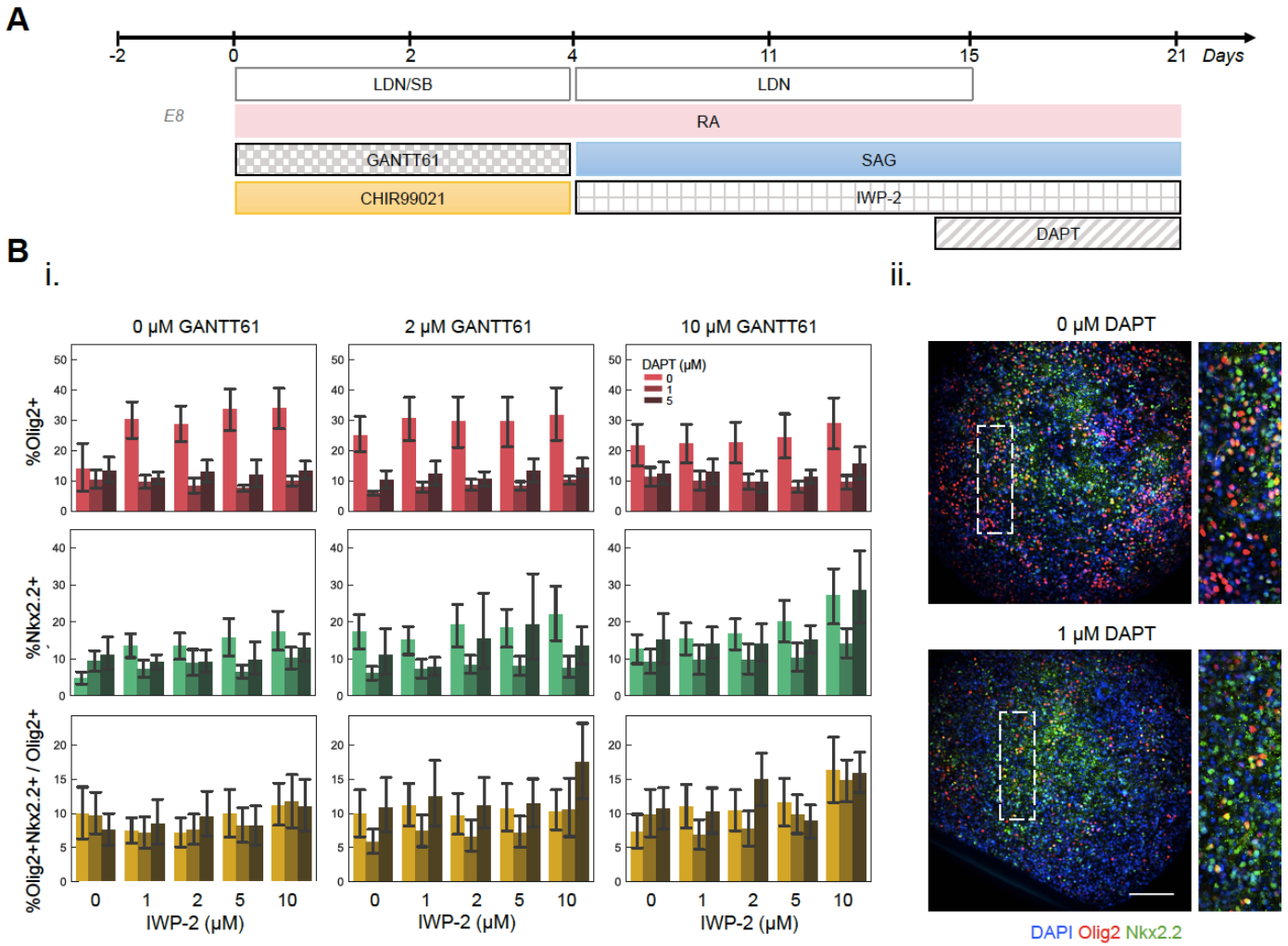

Figure 4.7: Strategic addition of signaling antagonists to modulate OPC specification. A) Timing of addition for 3 novel signaling cues GANTT61, IWP-2, and DAPT in the OPC differentiation protocol. B) i. Olig2, Nkx2.2, proportion of Nkx2.2+ Olig2+ cells in total Olig2+ at Day 21 in response to full factorial combinations of selected novel signaling antagonists. ii. Immunocytochemistry images of co-stained Olig2 (red) and Nkx2.2 (green) cells; scale bar represents 100 microns.

4.4.4 Temporal sensitivity of OPC specification revealed by varying the signal dose over time

Based on the limited efficiency of coupling together agonists and antagonists for an abrupt transition from activation to inhibition of signal, we hypothesized that a middle ground where a gradual change in the delivery of a signal might lead to additional insights for optimizing OPC production. Traditionally, dose levels of signaling cues have remained constant throughout differentiation protocols, however, it's conceivable that a dynamic dose level could better recapitulate the natural developmental environment of certain target cell types, for example, temporal changes in signal magnitude are observed in neurodevelopmental biology of neural tube formation where the SHH gradient along the dorso-ventral axis was mathematically modeled to reveal dynamic magnitude during the weeks of pMN patterning. [123] Based on this, we applied the micropillar/microwell chip to screen through numerous temporal profiles of SAG, as well as RA due to its analogous role along the rostro-caudal axis during spinal cord development, by dividing the signal window into "Early" and "Late" stages that were dosed independently to form constant, increasing, and decreasing dose profiles over time (Figure 4.8A). Additionally, to further specify our OPC measurement strategy, we measured Tuj1 expression and calculated the proportion of Olig2+ cells that co-expressed Tuj1 to potentially identify any modulators of the balance between Olig2+ cells that proceed down a motor neuron fate (also Tuj1+) versus an oligodendrocyte fate (also Nkx2.2+).

To consider all measured phenotypes simultaneously, we applied a hierarchical cluster analysis from which we were able to identify some patterns. As evident from the cluster analysis, a wide range of endpoint phenotype proportions were found from varying the temporal dosing of only two signaling cues, pointing to a very fine sensitivity to temporal changes in signal exposure in these populations. We then created four categories of endpoint marker expression profile that to further interpret the cluster analysis. Category 1, composed of phenotypes ranking low on OPC progenitor fate (low Olig2 and/or Nkx2.2 expression), all shared the low dosing of Retinoid Acid at 0.1 μM throughout the duration of the experiment, further emphasizing the high impact of RA in OPC yield. In contrast, Category 3, composed of highest Olig2 and Nkx2.2 expression as well as Olig2+Nkx2.2+ proportion, and the subset of conditions within Category 3 that exhibited the highest Olig2 expression correlated with the highest dose of "Early SAG", however had negligible differences across doses of "Late SAG", perhaps pointing to a limited window of competence to SAG signals in the early OPC differentiation phase. From a manufacturing point of view, especially relevant for larger scale production scenarios, this insight could reduce the necessary quantity of SAG by more than 50% to achieve maximal OPC differentiation. Then, Category 4 points to a bi-phasic relationship between RA and Nkx2.2 expression, in that high doses of RA of 1 μM in the Late stage of differentiation resulted in lower Nkx2.2 expression (Figure 4.8B, B.2) compared to a consistent dosing of RA at 0.5 μM throughout the entire differentiation. It appears that Olig2 and Nkx2.2 are maximal at different RA dosage levels (Figure 4.6C), and using the measurement of co-expressing Olig2+Nkx2.2+ to find an optimum might be logical here.

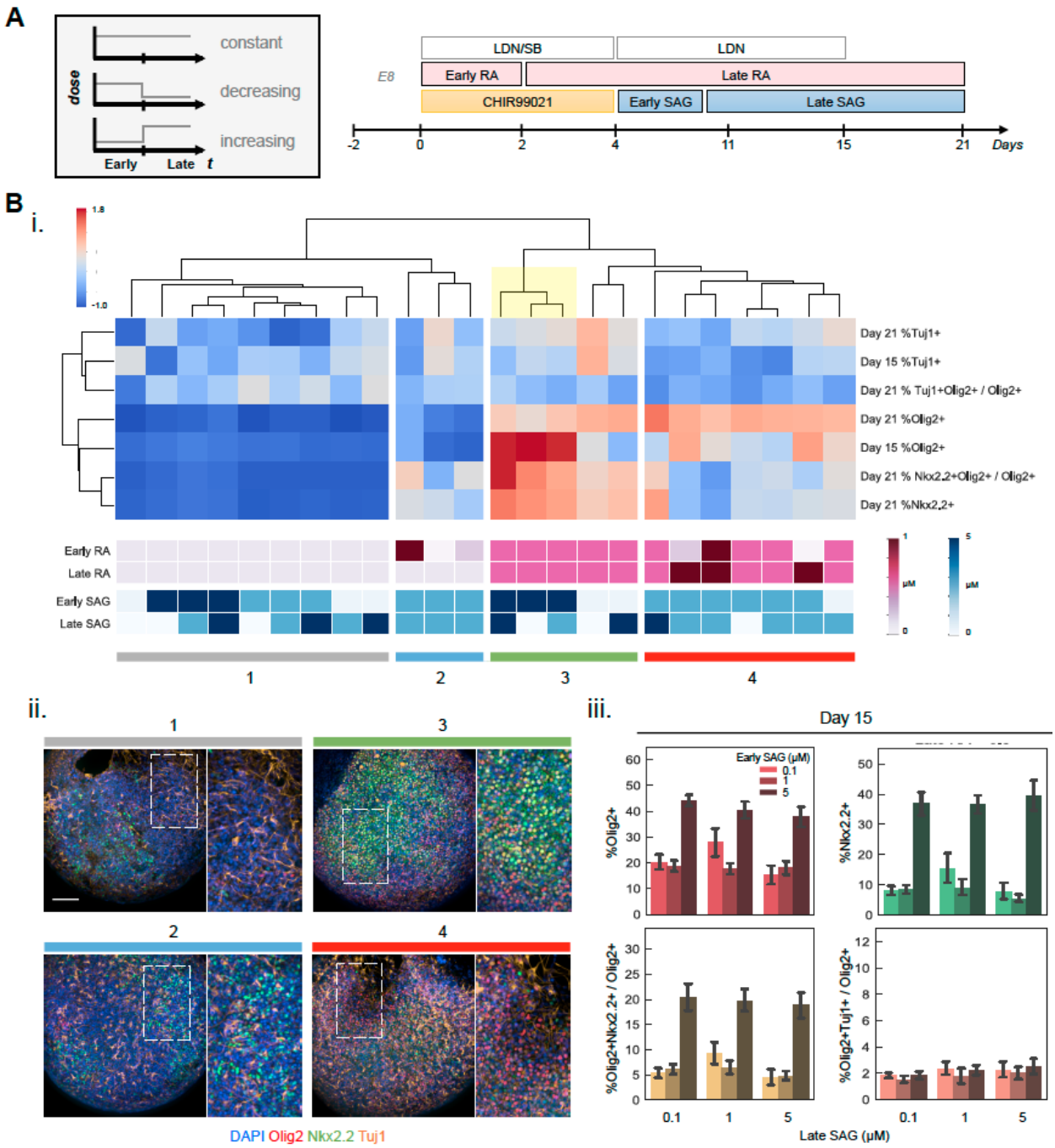

Figure 4.8: Fine tuning temporal profiles of RA and SAG to influence OPC specification. A) Timeline of early and late windows for RA and SAG exposure. B) i. Hierarchical cluster analysis of multiple endpoint phenotypes in response to temporal changes in RA and SAG dose during OPC differentiation. ii. Representative immunocytochemistry images of each major category of endpoint population phenotype mix; scale bar represents 100 microns. iii. Marker expression at Day 15 in response to time-varying doses of SAG.

4.4.5 Holistic analysis and prioritization of key parameters to influence OPC specification

We sought a comprehensive, yet concise, analysis to describe individual and combinatorial effects of all 12 culture parameters and 1000 unique differentiation conditions involved in this study. Therefore, we fit generalized linear models for the expression and co-expression of Olig2 and Nxk2.2 to single and pairwise interaction effects of all 12 independent variables. First, we identified significant parameters of interest for each phenotype measured using a factorial ANOVA (Figure 4.9, B.3). After applying a Benjamini - Hochberg False Discovery Rate correction for multiple comparisons [62], we fit an ordinary least squares model of the statistically significant terms to the phenotype of interest. The parameter coefficients were analyzed as a measure of relative influence on the expression of a certain endpoint phenotype, such as Olig2+Nkx2.2+ cells, and could be interpreted as a sensitivity analysis of key parameters on the OPC specification process (Figure 4.10). We also propose that this be used as a set of parameters to prioritize in tuning future production scenarios as they are observed to have the highest impact in marker expression.

The dose of Wnt signaling antagonist IWP-2 and the duration of Wnt signaling agnonist CHIR were two culture parameters that had a statistically significant positive correlation with all three phenotypes of interest. Taken together, it appears that the role of Wnt signaling changes during the 21-day differentiation window of hPSCs to OPCs in that initially (Days 0-3) it promotes OPC differentiation and shifts to possibly inhibitory at later stages (Days 4-21). Then, RA was among the most impactful parameters in this study. As described in the previous section, we observed different expression maxima between Olig2 and Nkx2.2 with respect to the dose of RA in the "Late RA" stage of the experiment. As revealed by the model, a dose of Early RA positively correlated with higher co-expression of Olig2 and Nkx2.2. Synthesizing these observations, a high dose of RA (1 μM) early in the differentiation (Day 0-1) coupled with a medium dose of RA (0.5 μM) for the later stages (Days 2-21) appears to maximize co-expression of Olig2 and Nkx2.2. Along the same lines, the dosing of SAG during Days 4-10 of differentiation, termed "Early SAG", was identified to be among the most significant variables to the promote Olig2+Nkx2.2+ differentiation, whereas the dosing of SAG during Days 11-21 of differentiation, termed "Late SAG", has a negligible effect. Overall, it's evident that there's much room to improve in the area of temporal dosing of key signaling cues whereby independently tuning the dose exposure at select time windows of differentiation could benefit the process by either increasing expression of target markers of interest or identifying negligible contributions to simplify a protocol and reduce resources needed to achieve the same outcome.

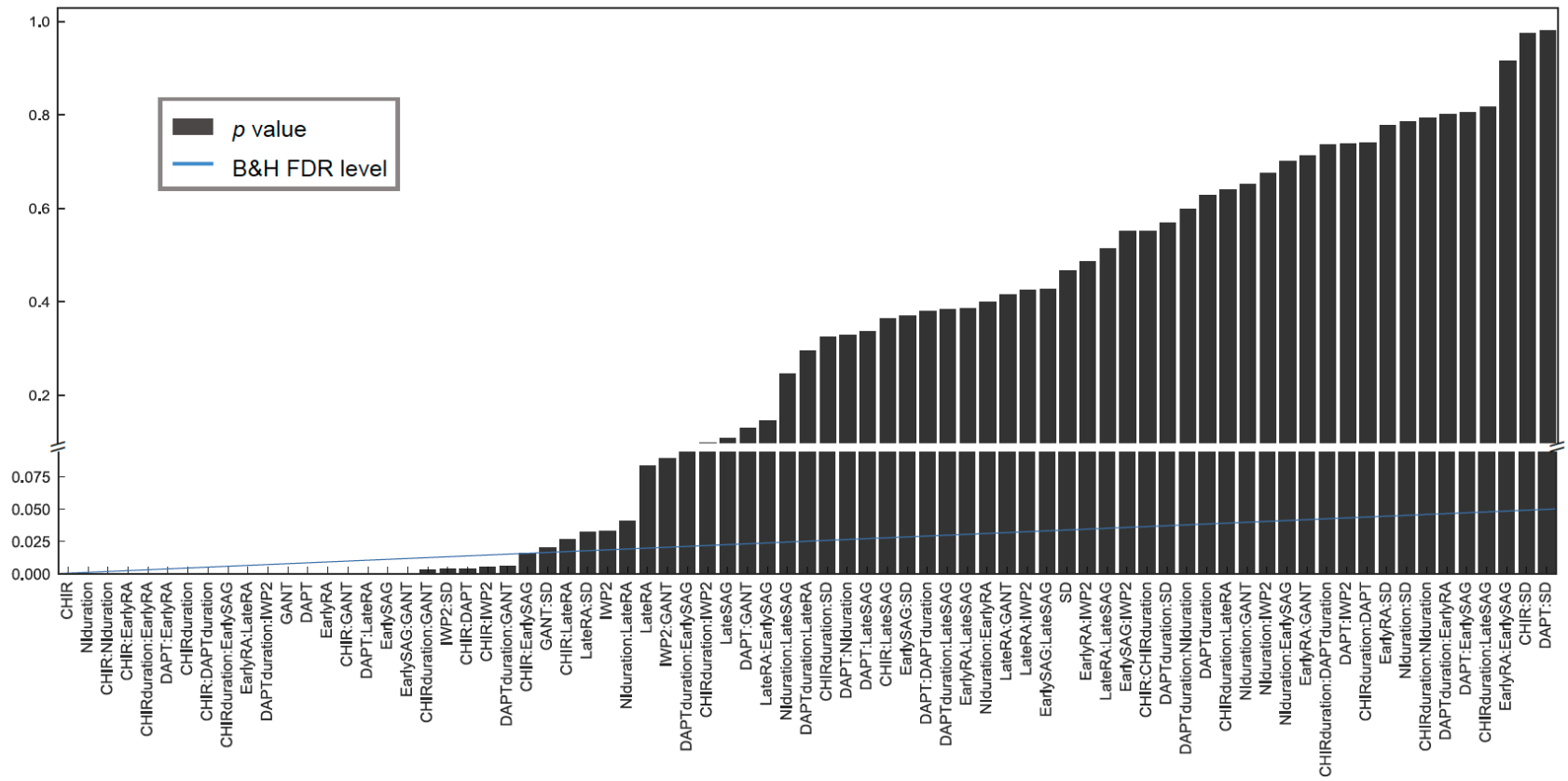

Figure 4.9: Factorial ANOVA model of individual and combinatorial effects of 12 culture parameters on expression of key markers in OPC specification. A) Identification of statistically significant culture parameters using a Factorial ANOVA of all single and pairwise effects on Nkx2.2 expression subject to the Benjamini - Hofsberg False Discovery Rate correction.

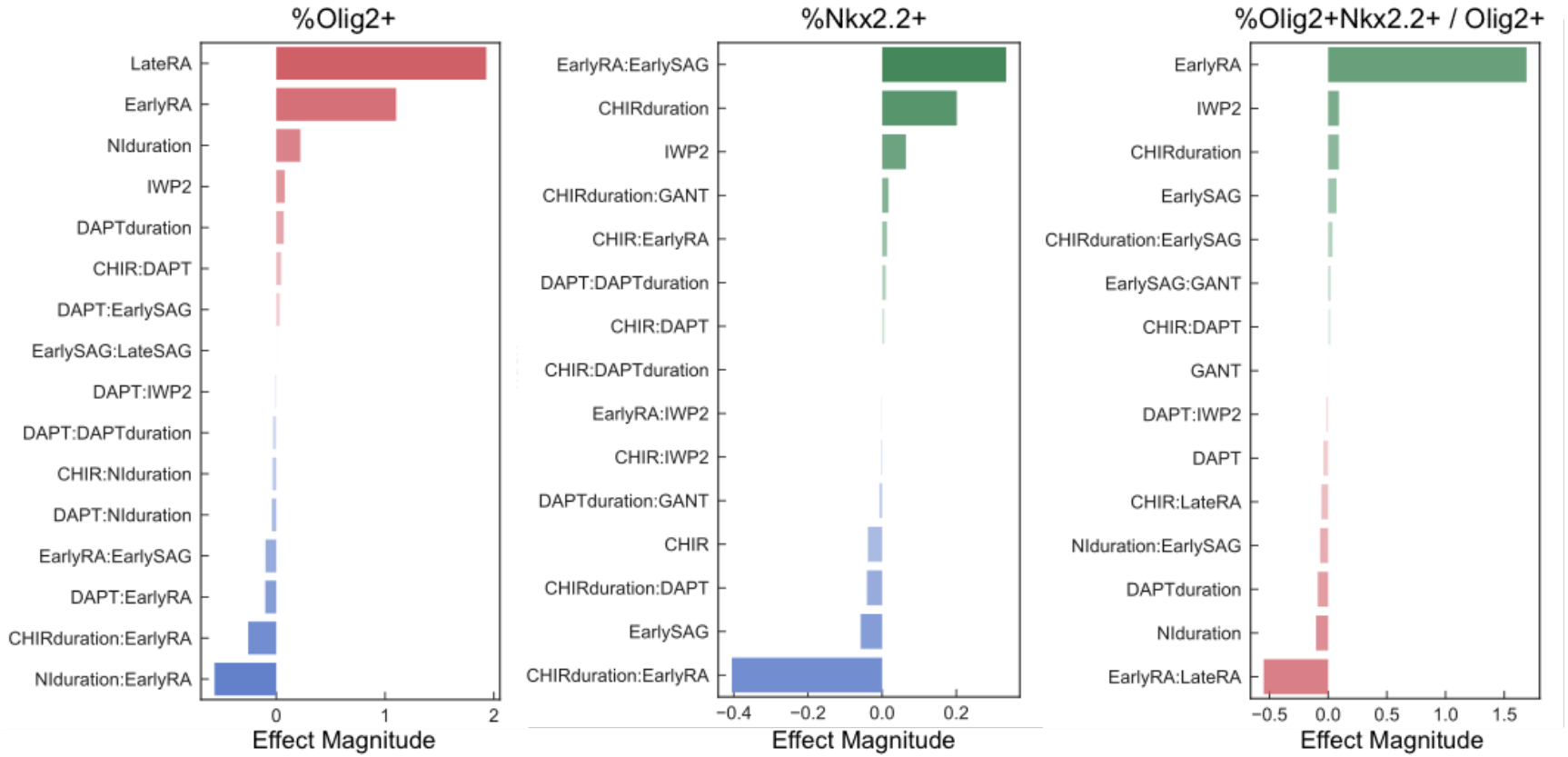

Figure 4.10: Sensitivity Analysis of individual and combined culture parameters. Effect magnitude of significant culture parameters for expression of Olig2, Nkx2.2, and co-expression Olig2 and Nkx2.2

4.4.6 Microculture chip can be applied to multiple types of 3D hPSC differentiation screens

We then applied the system to screen through 90 unique hPSC differentiation timelines for Tyrosine Hydroxylase+ midbrain dopaminergic (mDA) neurons [117] to demonstrate the generalizability of this methodology platform (Figure 4.11). Here, exposure of CHIR was divided into three periods (early, middle, late) and dosage for each period was varied independently. This screening strategy uncovered a key window of CHIR competence between Days 3-7, a negligible effect of CHIR between Days 8-11 and an inhibitory effect of CHIR between Days 12-25 of mDA differentiation. Of note, the immunofluorescence microscopy readout used in this methodology is in the form of image data, and therefore segmenting and scoring dense cell populations by expression of cellular markers localized to the cytoplasm, such as Tyrosine Hydroxylase and Tuj1, can be less straightforward than nuclear localized markers, such as Olig2 and Nkx2.2, and therefore should be considered in the design of the screening strategy.

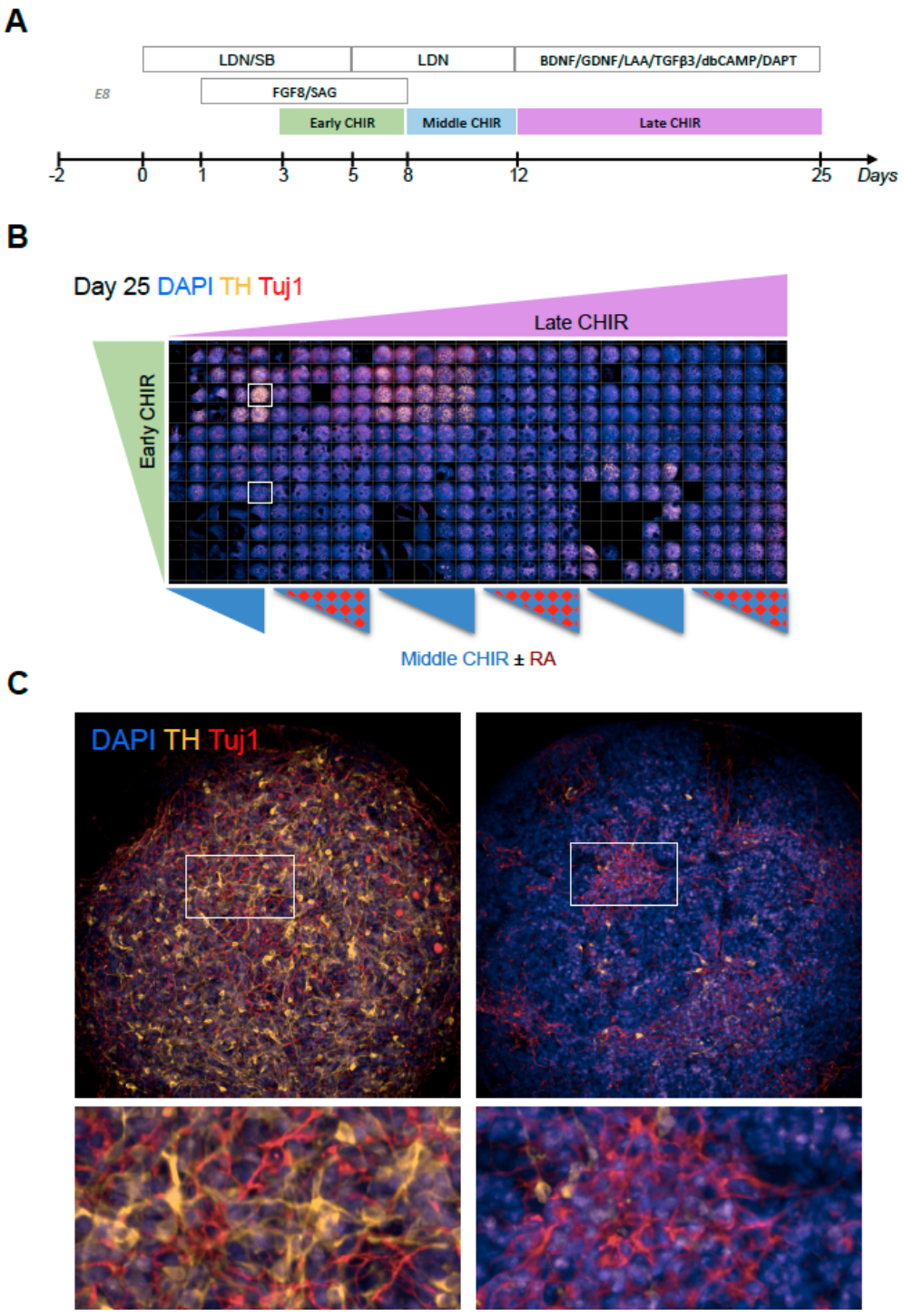

Figure 4.11: A generalizable platform for screening parameters for optimization of CRT differentiation. A) Timeline of small molecule addition for differentiation of dopaminergic neurons from human pluripotent stem cells. B) Montage of 90 unique differentiation timeline to test temporal profiles of CHIR dose. C) Immunocytochemistry images of high and low proportions of tyrosine hydroxylase+ (yellow) neurons (red).

4.5 Conclusion

We demonstrate the versatile capabilities of a unique microculture platform for 3D differentiation screening and optimization of hPSC-derived cell therapies whereby over 1000 unique OPC differentiation timelines, corresponding to roughly 2000 GB of fluorescence confocal microscopy data, were sampled utilizing 0.2% of the reagent volumes of a standard 96-well plate format. The statistical modeling with the robust dataset enabled empirical optimization and identified differential sensitivities of differentiation efficiency to certain culture parameters across time. As stem cell therapeutics continue to emerge in the clinic, robust processes for 3D differentiation screening and optimization serve to accelerate the pace of discovery and development.

Acknowledgements Thank you to Dr. Mary West of the High-Throughput Screening Facility (HTSF) at UC Berkeley. Additionally, we thank Eric Granlund and the College of Chemistry machine shop for machining custom parts. This research was supported by the California Institute for Regenerative Medicine (DISC-08982) and the National Institutes of Health (R01-ES020903) and Instrumentation Grant (S10OD021828) that provided the Perkin Elmer Opera Phenix microscope.

Chapter 5

Assessment of Stirred Bioreactor Configuration for Upscaling OPC Production: A Pilot Study

5.1 Introduction

The promising outlook for hPSC-OPCs so far leads many to consider the development of manufacturing processes to meet the patient demand for such hPSC-derived therapeutics. Roughly 250,000 patients in the U.S. suffer by some form of SCI, with the total growing annually by an estimated 15,000 new patients. [108] Clinical trials of hPSC-OPCs in humans were recently dosed at 20 million cells per patient, [105] amounting to over 1 trillion OPCs required to meet the total patient demand today. It is therefore imperative to develop systems that enable scalable and GMP-compliant production to follow upstream screening and optimization of these therapies (Figure 5.1).

Toward this aim, various bioreactor configurations, including rocking platforms [124], spinner flasks [125], continuous stirred tank reactors [126], and rotary perfusion vessels [127], have been developed to accomodate larger volumes of hPSC cultures for expansion and/or differentiation into a range of target cell types [128, 129].

Additionally, 3D culture systems, including suspensions of microcarriers [130], cell aggregates, and hydrogel microencapsulations, that are compatible across many bioreactor configurations have demonstrated strong potential for larger scale and higher yield [114, 117, 131] of hPSC expansion and differentiation processes as well as compliance with Good Manufacturing Practice (GMP) [115–117], in contrast to 2D counterparts. Microencapsulation of cells in thermoresponsive hydrogels is of additional interest because they facilitate cell retrieval without harsh chemical or mechanical gel degradation at the end of the production process [115, 132].

Here, we describe a pilot study to assess a stirred bioreactor configuration for the upscaling

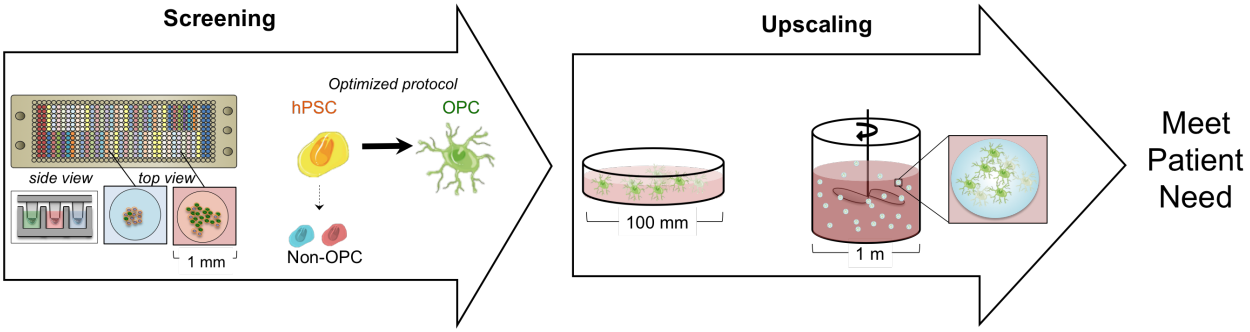

Figure 5.1: Schematic of upstream Screening and downsteam Upscaling for robust production hPSC-derived CRTs. Thousands of culture conditions are screened for optimal marker expression profile of cell type in micro-scale systems and the optimal protocol is translated first to bench-scale systems and ultimately to large-scale culture systems to produce enough volume to meet patient needs.

of 3D thermoreversible gel-encapsulated OPC production from hPSCs. Initially, we use computational modeling to predict and quantify the effect of stirred agitation on glucose concentration and shear stress profiles at a cross-section of the bioreactor vessel. Then, we use a pilot bioreactor system to measure hPSC viability, proliferation, and OPC differentiation with and without stirred agitation.

5.2 Experimental Procedures

5.2.1 Computational Modeling of Fluid and Chemical Dynamics

COMSOL was used to model the physicochemical macroenvironment within our bioreactor to predict the shear rate and glucose consumption rate for stirred and static conditions in the scaled up differentiation. Parameterization details were extracted from experimental data [133] and are found in Table B.3.

5.2.2 hPSC subculture

Human embryonic stem cells (H9s, NIH Stem Cell Registry 0062) were subcultured in monolayer format on a layer of 1% Matrigel and maintained in Essential 8 medium during expansion. At 80% confluency, H9s were passaged using Versene solution and replated at a 1:8 split.

5.2.3 3D thermoreversible hPSC culture and differentiation

Human embryonic stem cells (H9s, NIH Stem Cell Registry 0062) were dissociated with Accutase and single cells suspended in E8 medium with 10 μM Y-27632 were seeded in Mebiol Gel (CosmoBio) in an annulus at the outer perimeter of a 6-well plate at a cell density of 1E5 cells/mL and expanded as previously described [115] for two days prior to

differentiation. For differentiation, cells were cultured in medium containing small molecule combinations and doses according to Table B.1.

5.2.4 Viability and Proliferation Assays

A 200 microliter portion of the 3D gel was resected from the culture and placed in an eppendorf tube containing ice cold PBS to liquify the mebiol gel and release cell aggregates. The eppendorf tube was centrifuged for 1 minute and resuspended in PBS containing Calcein AM, Ethidium Homodimer, and Hoechst (dilution details in Table B.2). The cel aggregates were then replated onto a flat bottom well plate and incubated for 20 minutes prior to imaging using a wide-field fluorescent microscope. The diameter of all cell aggregates was measured and used as a proliferation index between the stirred and static culture conditions. Cell aggregates were imaged using a Zeiss Axio Observer epi-fluorescent microscope.

5.2.5 Immunocytochemistry Analysis

On Day 21, cell aggregates were transplanted into laminin coated culture slides and on Day 22 were fixed in 4% parafomaldehyde for 15 min. Then, cultures were washed twice in PBS for 5 min each and placed permeabilized in 0.25% Triton-X + 5% donkey serum in PBS for 10 min. After permeabilization, the wells were washed 5 times in 5% donkey serum for 5 min each and incubated in primary antibodies of interest diluted in PBS+donkey serum (dilution details in Table S2) and stored overnight at 4°C. After primary staining, wells were washed twice in PBS for 5 min each and then incubated in the corresponding secondary antibodies (dilution details in Table B.2) at 37°C for 2 h. After secondary staining, wells were washed twice in PBS for 5 min each. Cells were imaged using a Zeiss Axio Observer epi-fluorescent microscope and scored for marker expression using FIJI image analysis software [51]. In brief, background fluorescence was removed from all images using a rolling bar radius algorithm and standard feature extraction applications were used to quantify cellular marker expression. Quantified image data was then imported into Python for statistical data analysis and data visualization.

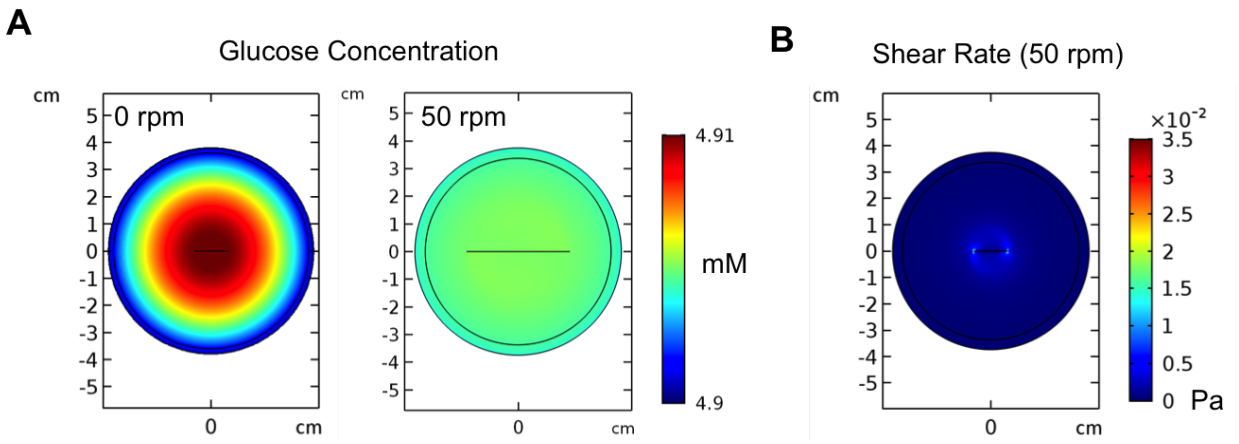

Figure 5.2: Quantitative modeling in COMSOL of physicochemical environment at cross section of bioreactor. A) Glucose concentration with and without agitation (50 RPM) B) Shear stress profile across bioreactor section with 50 RPM stir rate.

5.3 Results and Discussion

5.3.1 Physicochemical modeling of macroenvironment in stirred bioreactor

Computationally, COMSOL was used to create a dynamic quantitative model of the culture environment within a 50 mL bioreactor vessel and provide estimates of the magnitude of chemical and shear force gradients within a stirred setting (Figure 5.2). The model showed significant differences in the chemical environment across the bioreactor with (50 RPM) and without agitation for bioreactor vessels with a diameter of 8 cm. Additionally, the model calculated shear forces caused by the stirring to be on the order of 0.1 Pa, below previously reported limits for neural differentiation from hPSCs in stirred suspension cultures [134].

5.3.2 Effect of agitation on gel-encapsulated hPSC viability, proliferation, and OPC differentiation

Experimentally, we created a pilot scale bioreactor to assess the effect of stirred agitation on hPSC viability, proliferation, and subsequent OPC differentiation. A single well inside a 6-well plate was used as the bioreactor vessel, which has a diameter of 3.5 cm. At this pilot scale and based on previous modeling (Figure 5.2), we did not anticipate major nutrient deficiencies from diffusion limitations across the bioreactor to inhibit cell growth and metabolism, therefore could isolate the effect of stirring on hPSC expansion and differentiaion.

hPSCs were encapsulated in thermoreversible gel in single cell form in the pilot scale bioreactor (Figure 5.3) and were placed in OPC differentiation media starting Day 0. On Day 4, stirring at 0 or 50 RPM was introduced. No observable effects on gel integrity were

observed during the course of agitation. On Day 10, measurements of viability and neurosphere growth were recorded (Figure 5.4). No significant differences were observed between the distribution of neurosphere size in static (0 RPM) and stirred (50 RPM) conditions, however we observed an increased proportion of neurospheres under 50 microns in diameter in the static condition. This could potentially be explained by the predicted glucose levels (Figure 5.2) at the outer edges of the bioreactor in the static condition versus stirred condition, where a depletion and lack of transport of nutrients limits the expansion rate of a select portion of cells positioned on the edges.

We then wanted to determine if the stirred environment would impact the differentiation of hPSCs into OPCs. The OPC differentiation was carried out until Day 21 and Olig2 expression was measured within the pilot stirred bioreactor (Figure 5.5). Qualitatively, we observed aggregates with comparable levels of Olig2+ cells between the static and stirred culture conditions, indicating that the shear forces present at 50 RPM stirring conditions does not inhibit OPC specification. Overall, we found a favorable outlook for the further scale up of OPC differentiation within thermoreversible gel in stirred bioreactors, such as spinner flasks or continuous stirred tanks reactors.

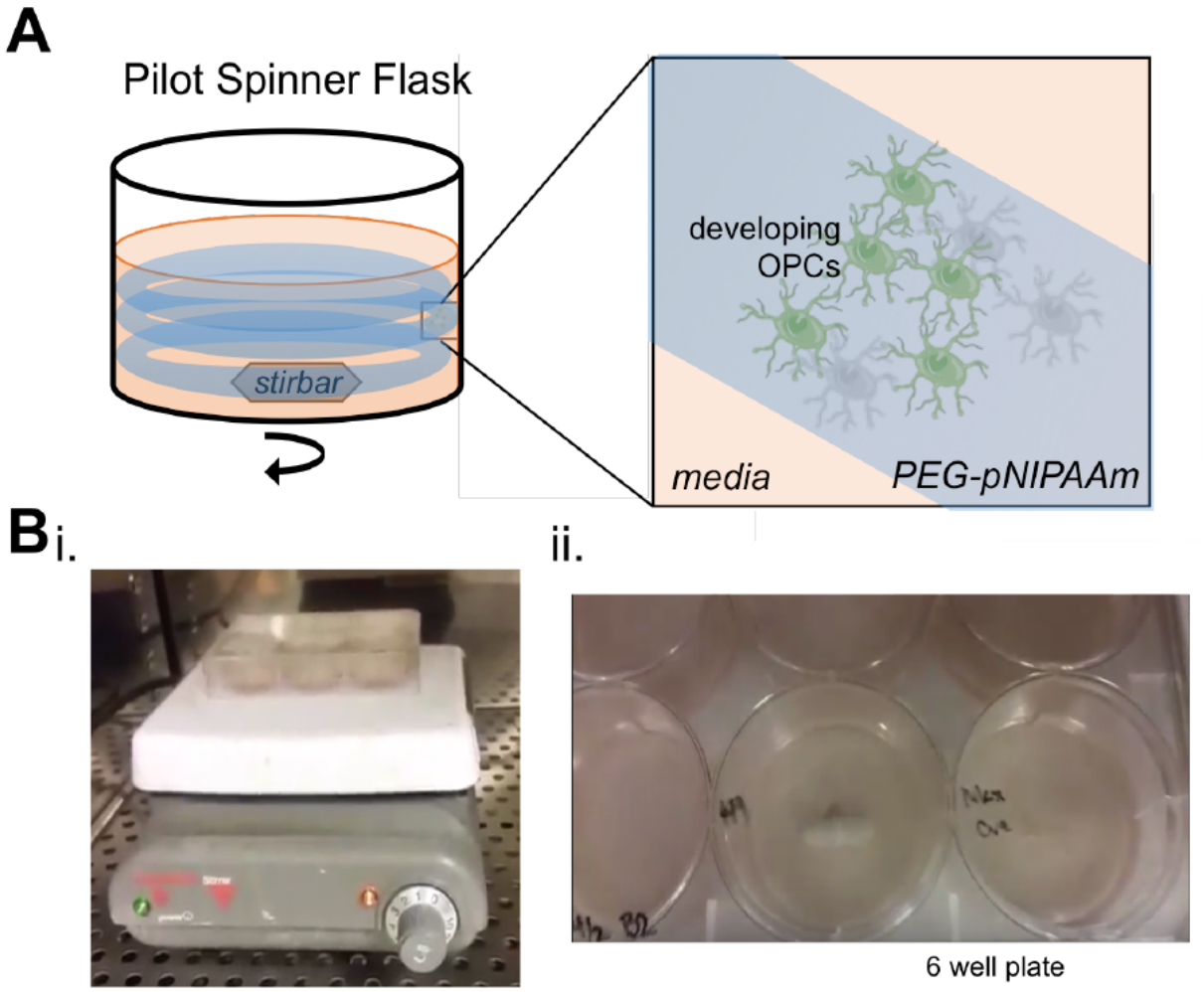

Figure 5.3: A) Schematic of OPCs encapsulated in thermoresponsive gel within spinner flask bioreactor. B) Experimental setup for pilot experiment i. 6 -well dish with hPSCs encapsulated in thermoreversible gel on stirplate. ii. static and stirred 50 RPM wells of 3D hPSC culture in 6-well plate.

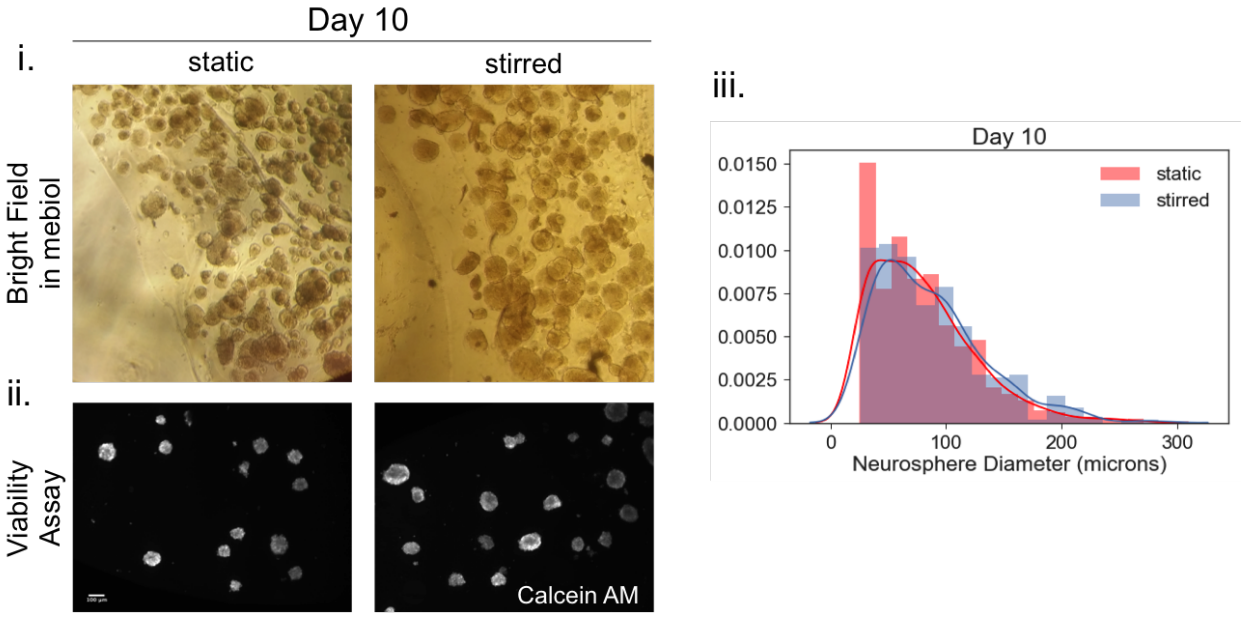

Figure 5.4: i Bright field image of encapsulated neurospheres in bioreactor after 10 days of growth ii. Viability assay iii. Distribution of growth in thermoresponsive gels in stirred 50 RPM and static culture environments measured by neurosphere diameter.

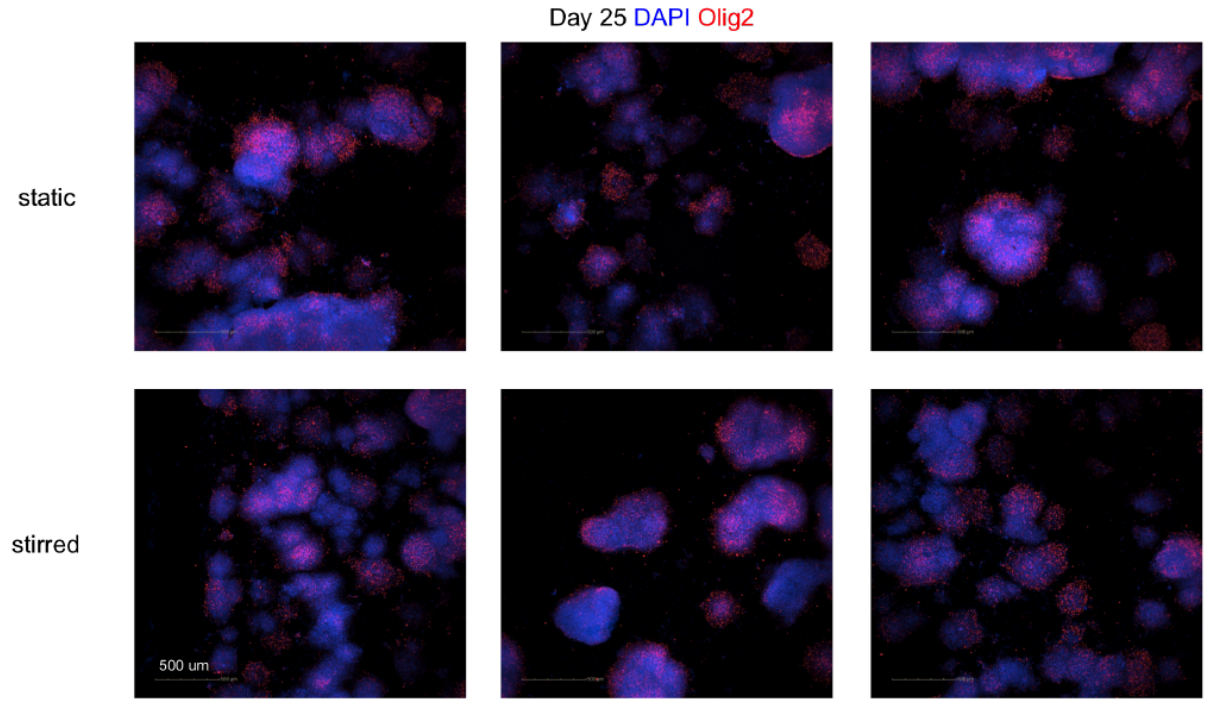

Figure 5.5: Immunocytochemistry images of Olig2 expression in 3D cellular aggregates after 21 days of differentiation in static (top) and stirred 50 RPM (bottom) 3D cultures.

5.4 Conclusion

To work toward meeting the need for robust upscaling strategies for hPSC-derived cell therapies, we describe a pilot scale study to assess the compatibility of stirred agitation bioreactor vessels for thermoreversible gel microencapsulation-based derivation of OPCs from hPSCs. Combining computational and experimental methods, we found that stirred agitation at 50 RPM would help mitigate large concentration gradients in glucose for bioreactors with a diameter of 8 cm, and that the shear forces caused by stirring at 50 RPM would not inhibit hPSC viability, proliferation, or OPC specification. Overall, these results are promising for further upscaling to spinner flask bioreactors.

Acknowledgements Thank you to Anthony Abel for providing COMSOL simulation data and Dr. Mary West of the High-Throughput Screening Facility (HTSF) at UC Berkeley. This research was supported by the California Institute for Regenerative Medicine (DISC-08982) and the National Institutes of Health Instrumentation Grant (S10OD021828) that provided the Perkin Elmer Opera Phenix microscope.

Bibliography

[1] F. H. Gage, P. W. Coates, T. D. Palmer, H. G. Kuhn, L. J. Fisher, J. O. Suhonen, D. A. Peterson, S. T. Suhr, and J. Ray, "Survival and differentiation of adult neuronal progenitor cells transplanted to the adult brain.," *Proceedings of the National Academy of Sciences of the United States of America*, vol. 92, pp. 11879–83, dec 1995.

[2] E. A. Mcculloch and J. E. Till, "Cytological Demonstration of the Clonal Nature of Spleen Colonies Derived From Trans-," vol. 197, pp. 452–454, feb 1963.

[3] A. J. FRIEDENSTEIN, "Humoral nature of osteogenic activity of transitional epithelium.," *Nature*, vol. 194, pp. 698–9, may 1962.

[4] J. E. TILL, E. A. MCCULLOCH, and L. SIMINOVITCH, "A STOCHASTIC MODEL OF STEM CELL PROLIFERATION, BASED ON THE GROWTH OF SPLEEN COLONY-FORMING CELLS.," *Proceedings of the National Academy of Sciences of the United States of America*, vol. 51, pp. 29–36, jan 1964.

[5] M. J. Evans and M. H. Kaufman, "Establishment in culture of pluripotential cells from mouse embryos.," *Nature*, vol. 292, pp. 154–6, jul 1981.

[6] J. A. Thomson, "Embryonic Stem Cell Lines Derived from Human Blastocysts," *Science*, vol. 282, pp. 1145–1147, nov 1998.

[7] K. Takahashi and S. Yamanaka, "Induction of pluripotent stem cells from mouse embryonic and adult fibroblast cultures by defined factors.," *Cell*, vol. 126, pp. 663–76, aug 2006.

[8] K. Takahashi, K. Tanabe, M. Ohnuki, M. Narita, T. Ichisaka, K. Tomoda, and S. Yamanaka, "Induction of pluripotent stem cells from adult human fibroblasts by defined factors.," *Cell*, vol. 131, pp. 861–72, nov 2007.

[9] Y. Kondo, T. Toyoda, N. Inagaki, and K. Osafune, "iPSC technology-based regenerative therapy for diabetes," *Journal of Diabetes Investigation*, vol. 9, pp. 234–243, mar 2018.

[10] M. Parmar, "Towards stem cell based therapies for Parkinson's disease.," *Development (Cambridge, England)*, vol. 145, p. dev156117, jan 2018.

[11] W. Faiella and R. Atoui, "Therapeutic use of stem cells for cardiovascular disease.," *Clinical and translational medicine*, vol. 5, p. 34, dec 2016.

[12] U. G. Thakkar, A. V. Vanikar, and H. L. Trivedi, "Stem cell therapy: An emerging modality in glomerular diseases.," *Cytotherapy*, vol. 19, pp. 333–348, mar 2017.

[13] T. Duncan and M. Valenzuela, "Alzheimer's disease, dementia, and stem cell therapy.," *Stem cell research & therapy*, vol. 8, p. 111, may 2017.

[14] B. Connor, "Concise Review: The Use of Stem Cells for Understanding and Treating Huntington's Disease," *STEM CELLS*, vol. 36, pp. 146–160, feb 2018.

[15] B. X. Ho, N. M. Q. Pek, and B.-S. Soh, "Disease Modeling Using 3D Organoids Derived from Human Induced Pluripotent Stem Cells.," *International journal of molecular sciences*, vol. 19, p. 936, mar 2018.

[16] A. Hoffmann, V. Sportelli, M. Ziller, and D. Spengler, "From the Psychiatrist's Couch to Induced Pluripotent Stem Cells: Bipolar Disease in a Dish," *International Journal of Molecular Sciences*, vol. 19, p. 770, mar 2018.

[17] C. Liu, A. Oikonomopoulos, N. Sayed, and J. C. Wu, "Modeling human diseases with induced pluripotent stem cells: from 2D to 3D and beyond.," *Development (Cambridge, England)*, vol. 145, p. dev156166, mar 2018.

[18] K. Muguruma, "Self-Organized Cerebellar Tissue from Human Pluripotent Stem Cells and Disease Modeling with Patient-Derived iPSCs," *The Cerebellum*, vol. 17, pp. 37–41, feb 2018.

[19] F. M. Watt and B. L. Hogan, "Out of eden: Stem cells and their niches," feb 2000.

[20] S. Bixby, G. M. Kruger, J. T. Mosher, N. M. Joseph, and S. J. Morrison, "Cell-Intrinsic Differences between Stem Cells from Different Regions of the Peripheral Nervous System Regulate the Generation of Neural Diversity," *Neuron*, vol. 35, pp. 643–656, aug 2002.

[21] D. J. Rossi, D. Bryder, J. M. Zahn, H. Ahlenius, R. Sonu, A. J. Wagers, and I. L. Weissman, "Cell intrinsic alterations underlie hematopoietic stem cell aging," *Proceedings of the National Academy of Sciences*, vol. 102, pp. 9194–9199, jun 2005.

[22] R. Jaenisch and A. Bird, "Epigenetic regulation of gene expression: how the genome integrates intrinsic and environmental signals.," *Nature genetics*, vol. 33 Suppl, pp. 245–54, mar 2003.

[23] J. A. Knoblich, "Mechanisms of Asymmetric Stem Cell Division," feb 2008.

[24] J. Peltier and D. V. Schaffer, "Systems biology approaches to understanding stem cell fate choice.," *IET systems biology*, vol. 4, pp. 1–11, jan 2010.

[25] E. Fuchs, T. Tumbar, and G. Guasch, "Socializing with the neighbors: stem cells and their niche.," *Cell*, vol. 116, pp. 769–78, mar 2004.

[26] R. Peerani, B. M. Rao, C. Bauwens, T. Yin, G. A. Wood, A. Nagy, E. Kumacheva, and P. W. Zandstra, "Niche-mediated control of human embryonic stem cell self-renewal and differentiation.," *The EMBO journal*, vol. 26, pp. 4744–55, nov 2007.

[27] C. S. Bjornsson, M. Apostolopoulou, Y. Tian, and S. Temple, "It takes a village: Constructing the neurogenic niche," feb 2015.

[28] K. Raymond, M.-A. Deugnier, M. M. Faraldo, and M. A. Glukhova, "Adhesion within the stem cell niches.," *Current opinion in cell biology*, vol. 21, pp. 623–9, oct 2009.

[29] K. I. Mosher and D. V. Schaffer, "Influence of hippocampal niche signals on neural stem cell functions during aging," *Cell and Tissue Research*, vol. 371, pp. 115–124, jan 2018.

[30] S. Chen, A. W. Bremer, O. J. Scheideler, Y. S. Na, M. E. Todhunter, S. Hsiao, P. R. Bomdica, M. M. Maharbiz, Z. J. Gartner, and D. V. Schaffer, "Interrogating cellular fate decisions with high-throughput arrays of multiplexed cellular communities.," *Nature communications*, vol. 7, p. 10309, jan 2016.

[31] R. S. Ashton, A. Conway, C. Pangarkar, J. Bergen, K.-I. Lim, P. Shah, M. Bissell, and D. V. Schaffer, "Astrocytes regulate adult hippocampal neurogenesis through ephrin-B signaling.," *Nature neuroscience*, vol. 15, pp. 1399–406, oct 2012.

[32] K. Nakashima, M. Yanagisawa, H. Arakawa, N. Kimura, T. Hisatsune, M. Kawabata, K. Miyazono, and T. Taga, "Synergistic signaling in fetal brain by STAT3-Smad1 complex bridged by p300.," *Science (New York, N.Y.)*, vol. 284, pp. 479–82, apr 1999.

[33] M. B. C. V. Goncalves, J. Boyle, D. J. Webber, S. Hall, S. L. Minger, and J. P. T. Corcoran, "Timing of the retinoid-signalling pathway determines the expression of neuronal markers in neural progenitor cells.," *Developmental biology*, vol. 278, pp. 60–70, mar 2005.

[34] C. J. Flaim, D. Teng, S. Chien, and S. N. Bhatia, "Combinatorial signaling microenvironments for studying stem cell fate.," *Stem cells and development*, vol. 17, pp. 29–39, feb 2008.

[35] M. Nakajima, T. Ishimuro, K. Kato, I.-K. Ko, I. Hirata, Y. Arima, and H. Iwata, "Combinatorial protein display for the cell-based screening of biomaterials that direct neural stem cell differentiation," *Biomaterials*, vol. 28, pp. 1048–1060, feb 2007.

[36] Z. Wang, B. Calpe, J. Zerdani, Y. Lee, J. Oh, H. Bae, A. Khademhosseini, and K. Kim, "High-throughput investigation of endothelial-to-mesenchymal transformation (EndMT) with combinatorial cellular microarrays.," *Biotechnology and bioengineering*, vol. 113, pp. 1403–12, jul 2016.

[37] L. Hou, J. Coller, V. Natu, T. J. Hastie, and N. F. Huang, "Combinatorial extracellular matrix microenvironments promote survival and phenotype of human induced pluripotent stem cell-derived endothelial cells in hypoxia.," *Acta biomaterialia*, vol. 44, pp. 188–99, oct 2016.

[38] K. B. Kaylan, V. Ermilova, R. C. Yada, and G. H. Underhill, "Combinatorial microenvironmental regulation of liver progenitor differentiation by Notch ligands, TGFβ, and extracellular matrix.," *Scientific reports*, vol. 6, p. 23490, mar 2016.

[39] D. Zhang, J. Lee, M. B. Sun, Y. Pei, J. Chu, M. U. Gillette, T. M. Fan, and K. A. Kilian, "Combinatorial Discovery of Defined Substrates That Promote a Stem Cell State in Malignant Melanoma," *ACS Central Science*, vol. 3, pp. 381–393, may 2017.

[40] Y. Y. I. Amin, K. Runager, F. Simoes, A. Celiz, V. Taresco, R. Rossi, J. J. Enghild, L. A. Abildtrup, D. C. E. Kraft, D. S. Sutherland, M. R. Alexander, M. Foss, and R. Ogaki, "Combinatorial Biomolecular Nanopatterning for High-Throughput Screening of Stem-Cell Behavior.," *Advanced materials (Deerfield Beach, Fla.)*, vol. 28, pp. 1472–6, feb 2016.

[41] M. D. Cabezas, D. J. Eichelsdoerfer, K. A. Brown, M. Mrksich, and C. A. Mirkin, "Combinatorial screening of mesenchymal stem cell adhesion and differentiation using polymer pen lithography.," *Methods in cell biology*, vol. 119, pp. 261–76, 2014.

[42] M. Tarunina, D. Hernandez, C. J. Johnson, S. Rybtsov, V. Ramathas, M. Jeyakumar, T. Watson, L. Hook, A. Medvinsky, C. Mason, and Y. Choo, "Directed differentiation of embryonic stem cells using a bead-based combinatorial screening method.," *PloS one*, vol. 9, p. e104301, sep 2014.

[43] F. Yang, S.-W. Cho, S. M. Son, S. P. Hudson, S. Bogatyrev, L. Keung, D. S. Kohane, R. Langer, and D. G. Anderson, "Combinatorial extracellular matrices for human embryonic stem cell differentiation in 3D.," *Biomacromolecules*, vol. 11, pp. 1909–14, aug 2010.

[44] A. Dolatshahi-Pirouz, M. Nikkhah, A. K. Gaharwar, B. Hashmi, E. Guermani, H. Aliabadi, G. Camci-Unal, T. Ferrante, M. Foss, D. E. Ingber, and A. Khademhosseini, "A combinatorial cell-laden gel microarray for inducing osteogenic differentiation of human mesenchymal stem cells," *Scientific Reports*, vol. 4, p. 3896, may 2015.

[45] S. L. Vega, M. Y. Kwon, K. H. Song, C. Wang, R. L. Mauck, L. Han, and J. A. Burdick, "Combinatorial hydrogels with biochemical gradients for screening 3D cellular microenvironments," *Nature Communications*, vol. 9, p. 614, feb 2018.

[46] D. M. Titmarsh, N. R. Glass, R. J. Mills, A. Hidalgo, E. J. Wolvetang, E. R. Porrello, J. E. Hudson, and J. J. Cooper-White, "Induction of Human iPSC-Derived Cardiomyocyte Proliferation Revealed by Combinatorial Screening in High Density Microbioreactor Arrays.," *Scientific reports*, vol. 6, p. 24637, jan 2016.

[47] Y. Maury, J. Côme, R. A. Piskorowski, N. Salah-Mohellibi, V. Chevaleyre, M. Peschanski, C. Martinat, and S. Nedelec, "Combinatorial analysis of developmental cues efficiently converts human pluripotent stem cells into multiple neuronal subtypes.," *Nature biotechnology*, vol. 33, pp. 89–96, jan 2015.

[48] A. Ranga, S. Gobaa, Y. Okawa, K. Mosiewicz, A. Negro, and M. P. Lutolf, "3D niche microarrays for systems-level analyses of cell fate.," *Nature communications*, vol. 5, p. 4324, jan 2014.

[49] S. J. Kwon, D. W. Lee, D. A. Shah, B. Ku, S. Y. Jeon, K. Solanki, J. D. Ryan, D. S. Clark, J. S. Dordick, and M.-Y. Lee, "High-throughput and combinatorial gene expression on a chip for metabolism-induced toxicology screening.," *Nature communications*, vol. 5, p. 3739, jan 2014.

[50] D. W. Lee, Y.-S. Choi, Y. J. Seo, M.-Y. Lee, S. Y. Jeon, B. Ku, S. Kim, S. H. Yi, and D.-H. Nam, "High-throughput screening (HTS) of anticancer drug efficacy on a micropillar/microwell chip platform.," *Analytical chemistry*, vol. 86, pp. 535–42, jan 2014.

[51] P. Bankhead, "Analyzing fluorescence microscopy images with ImageJ," *ImageJ*, no. May, pp. 1–195, 2014.

[52] M. Pool, J. Thiemann, A. Bar-Or, and A. E. Fournier, "NeuriteTracer: A novel ImageJ plugin for automated quantification of neurite outgrowth," *Journal of Neuroscience Methods*, vol. 168, pp. 134–139, feb 2008.

[53] N. Malo, J. A. Hanley, S. Cerquozzi, J. Pelletier, and R. Nadon, "Statistical practice in high-throughput screening data analysis.," *Nature biotechnology*, vol. 24, pp. 167–75, feb 2006.

[54] T. Hunter, "Signaling—2000 and Beyond," *Cell*, vol. 100, pp. 113–127, jan 2000.

[55] G. Box, *Statistics for Experimenters*. 2005.

[56] J. W. Lichtman and J.-A. Conchello, "Fluorescence microscopy.," *Nature methods*, vol. 2, pp. 910–9, dec 2005.

[57] T. G. Fernandes, S.-J. Kwon, M.-Y. Lee, D. S. Clark, J. M. S. Cabral, and J. S. Dordick, "On-chip, cell-based microarray immunofluorescence assay for high-throughput analysis of target proteins.," *Analytical chemistry*, vol. 80, pp. 6633–9, sep 2008.

[58] J. Zhang, T. Chung, and K. Oldenburg, "A Simple Statistical Parameter for Use in Evaluation and Validation of High Throughput Screening Assays.," *Journal of biomolecular screening*, vol. 4, pp. 67–73, jan 1999.

[59] A. Diaspro, *Confocal and Two-Photon Microscopy: Founfdations, Applications, and Advances*. Wiley-Liss, 2002.

[60] X. Bao, D. Clark, and D. V. Schaffer, "Gene Editing to Generate Versatile Human Pluripotent Stem Cell Reporter Lines for Analysis of Differentiation and Lineage Tracing," *In revision*, 2018.

[61] J. G. Albeck, G. MacBeath, F. M. White, P. K. Sorger, D. A. Lauffenburger, and S. Gaudet, "Collecting and organizing systematic sets of protein data.," *Nature reviews. Molecular cell biology*, vol. 7, pp. 803–12, nov 2006.

[62] Y. Benjamini and Y. Hochberg, "Controlling the False Discovery Rate: A Practical and Powerful Approach to Multiple Testing," 1995.

[63] Y. Avior, I. Sagi, and N. Benvenisty, "Pluripotent stem cells in disease modelling and drug discovery.," *Nature reviews. Molecular cell biology*, vol. 17, pp. 170–82, mar 2016.

[64] J. Lader, M. Stachel, and L. Bu, "Cardiac stem cells for myocardial regeneration: promising but not ready for prime time," oct 2017.

[65] K. Pelttari, M. Mumme, A. Barbero, and I. Martin, "Nasal chondrocytes as a neural crest-derived cell source for regenerative medicine," *Current Opinion in Biotechnology*, vol. 47, pp. 1–6, oct 2017.

[66] M. T. Rodrigues, M. E. Gomes, and R. L. Reis, "Current strategies for osteochondral regeneration: From stem cells to pre-clinical approaches," oct 2011.

[67] S. L. Rossi and H. S. Keirstead, "Stem cells and spinal cord regeneration," oct 2009.

[68] F. H. Gage, G. Kempermann, T. D. Palmer, D. A. Peterson, and J. Ray, "Multipotent progenitor cells in the adult dentate gyrus.," *Journal of neurobiology*, vol. 36, pp. 249–66, aug 1998.

[69] J. T. Gonçalves, S. T. Schafer, and F. H. Gage, "Adult Neurogenesis in the Hippocampus: From Stem Cells to Behavior," 2016.

[70] T. Palmer, "FGF-2-Responsive Neuronal Progenitors Reside in Proliferative and Quiescent Regions of the Adult Rodent Brain," *Molecular and Cellular Neuroscience*, vol. 6, pp. 474–486, oct 1995.

[71] T. D. Palmer, E. A. Markakis, A. R. Willhoite, F. Safar, and F. H. Gage, "Fibroblast growth factor-2 activates a latent neurogenic program in neural stem cells from diverse regions of the adult CNS.," *The Journal of neuroscience : the official journal of the Society for Neuroscience*, vol. 19, pp. 8487–97, oct 1999.

[72] K. Lai, B. K. Kaspar, F. H. Gage, and D. V. Schaffer, "Sonic hedgehog regulates adult neural progenitor proliferation in vitro and in vivo.," *Nature neuroscience*, vol. 6, pp. 21–7, jan 2003.

[73] K. Lai, M. J. Robertson, and D. V. Schaffer, "The sonic hedgehog signaling system as a bistable genetic switch.," *Biophysical journal*, vol. 86, pp. 2748–57, may 2004.

[74] D.-C. Lie, S. A. Colamarino, H.-J. Song, L. Désiré, H. Mira, A. Consiglio, E. S. Lein, S. Jessberger, H. Lansford, A. R. Dearie, and F. H. Gage, "Wnt signalling regulates adult hippocampal neurogenesis.," *Nature*, vol. 437, pp. 1370–5, oct 2005.

[75] A. M. Bond, C. Y. Peng, E. A. Meyers, T. McGuire, O. Ewaleifoh, and J. A. Kessler, "BMP signaling regulates the tempo of adult hippocampal progenitor maturation at multiple stages of the lineage," *Stem Cells*, vol. 32, pp. 2201–2214, aug 2014.

[76] M. Kandasamy, B. Lehner, S. Kraus, P. R. Sander, J. Marschallinger, F. J. Rivera, D. Trümbach, U. Ueberham, H. A. Reitsamer, O. Strauss, U. Bogdahn, S. Couillard-Despres, and L. Aigner, "TGF-beta signalling in the adult neurogenic niche promotes stem cell quiescence as well as generation of new neurons," *Journal of Cellular and Molecular Medicine*, vol. 18, pp. 1444–1459, jul 2014.

[77] H. Mira, Z. Andreu, H. Suh, D. Chichung Lie, S. Jessberger, A. Consiglio, J. S. Emeterio, R. Hortigüela, M. Á. Marqués-Torrejón, K. Nakashima, D. Colak, M. Götz, I. Fariñas, and F. H. Gage, "Signaling through BMPR-IA regulates quiescence and long-term activity of neural stem cells in the adult hippocampus," *Cell Stem Cell*, vol. 7, pp. 78–89, jul 2010.

[78] H. Yousef, A. Morgenthaler, C. Schlesinger, L. Bugaj, I. M. Conboy, and D. V. Schaffer, "Age-Associated Increase in BMP Signaling inhibits Hippocampal Neurogenesis.," *Stem cells (Dayton, Ohio)*, vol. 33, pp. 1577–88, dec 2014.

[79] H. Yousef, M. J. Conboy, A. Morgenthaler, C. Schlesinger, L. Bugaj, P. Paliwal, C. Greer, I. M. Conboy, and D. Schaffer, "Systemic attenuation of the TGF-β pathway by a single drug simultaneously rejuvenates hippocampal neurogenesis and myogenesis in the same old mammal," jun 2015.

[80] E. S. Lein, M. J. Hawrylycz, N. Ao, M. Ayres, A. Bensinger, A. Bernard, A. F. Boe, M. S. Boguski, K. S. Brockway, E. J. Byrnes, L. Chen, L. Chen, T.-M. Chen, M. Chi Chin, J. Chong, B. E. Crook, A. Czaplinska, C. N. Dang, S. Datta, N. R. Dee, A. L. Desaki, T. Desta, E. Diep, T. A. Dolbeare, M. J. Donelan, H.-W. Dong, J. G. Dougherty, B. J. Duncan, A. J. Ebbert, G. Eichele, L. K. Estin, C. Faber, B. A. Facer, R. Fields, S. R. Fischer, T. P. Fliss, C. Frensley, S. N. Gates, K. J. Glattfelder, K. R. Halverson, M. R. Hart, J. G. Hohmann, M. P. Howell, D. P. Jeung, R. A. Johnson, P. T. Karr, R. Kawal, J. M. Kidney, R. H. Knapik, C. L. Kuan, J. H. Lake, A. R. Laramee, K. D. Larsen, C. Lau, T. A. Lemon, A. J. Liang, Y. Liu, L. T. Luong, J. Michaels, J. J. Morgan, R. J. Morgan, M. T. Mortrud, N. F. Mosqueda, L. L. Ng, R. Ng, G. J. Orta, C. C. Overly, T. H. Pak, S. E. Parry, S. D. Pathak, O. C. Pearson, R. B. Puchalski, Z. L. Riley, H. R. Rockett, S. A. Rowland, J. J. Royall, M. J. Ruiz, N. R. Sarno, K. Schaffnit, N. V. Shapovalova, T. Sivisay, C. R. Slaughterbeck, S. C. Smith, K. A. Smith, B. I. Smith, A. J. Sodt, N. N. Stewart, K.-R. Stumpf, S. M. Sunkin, M. Sutram, A. Tam, C. D. Teemer, C. Thaller, C. L. Thompson, L. R. Varnam, A. Visel, R. M. Whitlock, P. E. Wohnoutka, C. K. Wolkey, V. Y. Wong, M. Wood, M. B. Yaylaoglu, R. C. Young, B. L. Youngstrom, X. Feng Yuan, B. Zhang, T. A. Zwingman, and A. R. Jones, "Genome-wide atlas of gene expression in the adult mouse brain," *Nature*, vol. 445, pp. 168–176, jan 2007.

[81] D. A. Brafman, S. de Minicis, E. Seki, K. D. Shah, D. Teng, D. Brenner, K. Willert, and S. Chien, "Investigating the role of the extracellular environment in modulating hepatic

stellate cell biology with arrayed combinatorial microenvironments.," *Integrative biology : quantitative biosciences from nano to macro*, vol. 1, pp. 513–24, sep 2009.

[82] S. Gobaa, S. Hoehnel, M. Roccio, A. Negro, S. Kobel, and M. P. Lutolf, "Artificial niche microarrays for probing single stem cell fate in high throughput.," *Nature methods*, vol. 8, pp. 949–55, nov 2011.

[83] M. A. LaBarge, C. M. Nelson, R. Villadsen, A. Fridriksdottir, J. R. Ruth, M. R. Stampfer, O. W. Petersen, and M. J. Bissell, "Human mammary progenitor cell fate decisions are products of interactions with combinatorial microenvironments.," *Integrative biology : quantitative biosciences from nano to macro*, vol. 1, pp. 70–9, jan 2009.

[84] S. Rasi Ghaemi, B. Delalat, X. Cetó, F. J. Harding, J. Tuke, and N. H. Voelcker, "Synergistic influence of collagen I and BMP 2 drives osteogenic differentiation of mesenchymal stem cells: A cell microarray analysis.," *Acta biomaterialia*, vol. 34, pp. 41–52, apr 2016.

[85] M. Roccio, S. Gobaa, and M. P. Lutolf, "High-throughput clonal analysis of neural stem cells in microarrayed artificial niches," *Integrative Biology*, vol. 4, p. 391, apr 2012.

[86] Y. Soen, A. Mori, T. D. Palmer, and P. O. Brown, "Exploring the regulation of human neural precursor cell differentiation using arrays of signaling microenvironments.," *Molecular systems biology*, vol. 2, p. 37, jan 2006.

[87] G. J. Nierode, B. C. Perea, S. K. McFarland, J. F. Pascoal, D. S. Clark, D. V. Schaffer, and J. S. Dordick, "High-Throughput Toxicity and Phenotypic Screening of 3D Human Neural Progenitor Cell Cultures on a Microarray Chip Platform," *Stem Cell Reports*, vol. 7, no. 5, pp. 970–982, 2016.

[88] M. Boutros, F. Heigwer, and C. Laufer, "Microscopy-Based High-Content Screening.," *Cell*, vol. 163, pp. 1314–25, dec 2015.

[89] M. Koolpe, R. Burgess, M. Dail, and E. B. Pasquale, "EphB receptor-binding peptides identified by phage display enable design of an antagonist with ephrin-like affinity.," *The Journal of biological chemistry*, vol. 280, pp. 17301–11, apr 2005.

[90] A. Conway, T. Vazin, D. P. Spelke, N. A. Rode, K. E. Healy, R. S. Kane, and D. V. Schaffer, "Multivalent ligands control stem cell behaviour in vitro and in vivo.," *Nature nanotechnology*, vol. 8, pp. 831–8, nov 2013.

[91] T. Vazin, R. S. Ashton, A. Conway, N. A. Rode, S. M. Lee, V. Bravo, K. E. Healy, R. S. Kane, and D. V. Schaffer, "The effect of multivalent Sonic hedgehog on differentiation of human embryonic stem cells into dopaminergic and GABAergic neurons.," *Biomaterials*, vol. 35, pp. 941–8, jan 2014.

[92] T. J. Schwarz, B. Ebert, and D. C. Lie, "Stem cell maintenance in the adult mammalian hippocampus: a matter of signal integration?," *Developmental neurobiology*, vol. 72, pp. 1006–15, jul 2012.

[93] D. A. Lim, A. D. Tramontin, J. M. Trevejo, D. G. Herrera, J. M. García-Verdugo, and A. Alvarez-Buylla, "Noggin Antagonizes BMP Signaling to Create a Niche for Adult Neurogenesis," *Neuron*, vol. 28, pp. 713–726, dec 2000.

[94] E. Batlle, J. T. Henderson, H. Beghtel, M. M. W. van den Born, E. Sancho, G. Huls, J. Meeldijk, J. Robertson, M. van de Wetering, T. Pawson, and H. Clevers, "Beta-catenin and TCF mediate cell positioning in the intestinal epithelium by controlling the expression of EphB/ephrinB.," *Cell*, vol. 111, pp. 251–63, oct 2002.

[95] K. A. Janes and D. A. Lauffenburger, "Models of signalling networks - what cell biologists can gain from them and give to them.," *Journal of cell science*, vol. 126, pp. 1913–21, may 2013.

[96] M. Bonaguidi, M. Wheeler, J. Shapiro, R. Stadel, G. Sun, G.-l. Ming, and H. Song, "In Vivo Clonal Analysis Reveals Self-Renewing and Multipotent Adult Neural Stem Cell Characteristics," *Cell*, vol. 145, pp. 1142–1155, jun 2011.

[97] G.-A. Pilz, S. Bottes, M. Betizeau, D. J. Jörg, S. Carta, B. D. Simons, F. Helmchen, and S. Jessberger, "No Title," vol. 359, pp. 658–662, feb 2018.

[98] Y. He, H. Zhang, A. Yung, S. A. Villeda, P. A. Jaeger, O. Olayiwola, N. Fainberg, and T. Wyss-Coray, "ALK5-dependent TGF-β 2 signaling is a major determinant of late-stage adult neurogenesis," *Nature Neuroscience*, vol. 17, pp. 943–952, jul 2014.

[99] E. F. Jacobson and E. S. Tzanakakis, "Human pluripotent stem cell differentiation to functional pancreatic cells for diabetes therapies: Innovations, challenges and future directions," *Journal of Biological Engineering*, vol. 11, p. 21, dec 2017.

[100] F. Fang, Z. Li, Q. Zhao, H. Li, and C. Xiong, "Human induced pluripotent stem cells and male infertility: an overview of current progress and perspectives," *Human Reproduction*, vol. 33, pp. 188–195, feb 2018.

[101] A. Oikonomopoulos, T. Kitani, and J. C. Wu, "Pluripotent Stem Cell-Derived Cardiomyocytes as a Platform for Cell Therapy Applications: Progress and Hurdles for Clinical Translation.," *Molecular therapy : the journal of the American Society of Gene Therapy*, vol. 26, pp. 1624–1634, jul 2018.

[102] L. A. Jevons, F. D. Houghton, and R. S. Tare, "Augmentation of musculoskeletal regeneration: role for pluripotent stem cells," *Regenerative Medicine*, vol. 13, pp. 189–206, mar 2018.

[103] S. A. Goldman, "Stem and Progenitor Cell-Based Therapy of the Central Nervous System: Hopes, Hype, and Wishful Thinking," *Cell Stem Cell*, vol. 18, pp. 174–188, feb 2016.

[104] J. Sharp, J. Frame, M. Siegenthaler, G. Nistor, and H. S. Keirstead, "Human embryonic Stem Cell-Derived Oligodendrocyte Progenitor Cell Transplants Improve Recovery after Cervical Spinal Cord Injury," *Stem Cells*, vol. 28, no. 1, pp. N/A–N/A, 2009.

[105] C. A. Priest, N. C. Manley, J. Denham, E. D. Wirth, and J. S. Lebkowski, "Preclinical safety of human embryonic stem cell-derived oligodendrocyte progenitors supporting clinical trials in spinal cord injury," *Regenerative Medicine*, vol. 10, pp. 939–958, nov 2015.

[106] N. C. Manley, C. A. Priest, J. Denham, E. D. Wirth, and J. S. Lebkowski, "Human Embryonic Stem Cell-Derived Oligodendrocyte Progenitor Cells: Preclinical Efficacy and Safety in Cervical Spinal Cord Injury," *Stem Cells Translational Medicine*, vol. 6, pp. 1917–1929, oct 2017.

[107] P. Douvaras, J. Wang, M. Zimmer, S. Hanchuk, M. O'Bara, S. Sadiq, F. J. Sim, J. Goldman, V. Fossati, M. A. O'Bara, S. Sadiq, F. J. Sim, J. Goldman, and V. Fossati, "Efficient generation of myelinating oligodendrocytes from primary progressive multiple sclerosis patients by induced pluripotent stem cells," *Stem Cell Reports*, vol. 3, pp. 250–259, aug 2014.

[108] D. D. French, R. R. Campbell, S. Sabharwal, A. L. Nelson, P. A. Palacios, and D. Gavin-Dreschnack, "Health care costs for patients with chronic spinal cord injury in the Veterans Health Administration.," *The journal of spinal cord medicine*, vol. 30, no. 5, pp. 477–81, 2007.

[109] Y. Tao and S.-C. Zhang, "Neural Subtype Specification from Human Pluripotent Stem Cells," *Cell Stem Cell*, vol. 19, pp. 573–586, nov 2016.

[110] S. A. Goldman and N. J. Kuypers, "How to make an oligodendrocyte.," *Development (Cambridge, England)*, vol. 142, no. 23, pp. 3983–95, 2015.

[111] Q. Zhou, G. Choi, and D. J. Anderson, "The bHLH transcription factor Olig2 promotes oligodendrocyte differentiation in collaboration with Nkx2.2.," *Neuron*, vol. 31, pp. 791–807, sep 2001.

[112] G. I. Nistor, M. O. Totoiu, N. Haque, M. K. Carpenter, and H. S. Keirstead, "Human embryonic stem cells differentiate into oligodendrocytes in high purity and myelinate after spinal cord transplantation," *GLIA*, vol. 49, pp. 385–396, feb 2005.

[113] P. Douvaras and V. Fossati, "Generation and isolation of oligodendrocyte progenitor cells from human pluripotent stem cells.," *Nature protocols*, vol. 10, no. 8, pp. 1143–54, 2015.

[114] M. Serra, C. Brito, C. Correia, and P. M. Alves, "Process engineering of human pluripotent stem cells for clinical application," 2012.

[115] Y. Lei and D. V. Schaffer, "A fully defined and scalable 3D culture system for human pluripotent stem cell expansion and differentiation.," *Proceedings of the National*

Academy of Sciences of the United States of America, vol. 110, pp. E5039–48, dec 2013.

[116] G. M. Rodrigues, T. Gaj, M. M. Adil, J. Wahba, A. T. Rao, F. K. Lorbeer, R. U. Kulkarni, M. M. Diogo, J. M. Cabral, E. W. Miller, D. Hockemeyer, and D. V. Schaffer, "Defined and Scalable Differentiation of Human Oligodendrocyte Precursors from Pluripotent Stem Cells in a 3D Culture System," *Stem Cell Reports*, vol. 8, pp. 1770–1783, jun 2017.

[117] M. M. Adil and D. V. Schaffer, "Expansion of human pluripotent stem cells," *Current Opinion in Chemical Engineering*, vol. 15, pp. 24–35, feb 2017.

[118] S. C. Desbordes, D. G. Placantonakis, A. Ciro, N. D. Socci, G. Lee, H. Djaballah, and L. Studer, "High-throughput screening assay for the identification of compounds regulating self-renewal and differentiation in human embryonic stem cells.," *Cell stem cell*, vol. 2, pp. 602–12, jun 2008.

[119] S. C. Desbordes and L. Studer, "Adapting human pluripotent stem cells to high-throughput and high-content screening," *Nature Protocols*, vol. 8, pp. 111–130, dec 2012.

[120] A. Ranga and M. P. Lutolf, "High-throughput approaches for the analysis of extrinsic regulators of stem cell fate.," *Current opinion in cell biology*, vol. 24, pp. 236–44, apr 2012.

[121] S. M. Chambers, C. A. Fasano, E. P. Papapetrou, M. Tomishima, M. Sadelain, and L. Studer, "Highly efficient neural conversion of human ES and iPS cells by dual inhibition of SMAD signaling," *Nature Biotechnology*, vol. 27, pp. 275–280, mar 2009.

[122] R. Pal, M. K. Mamidi, A. K. Das, and R. Bhonde, "Diverse effects of dimethyl sulfoxide (DMSO) on the differentiation potential of human embryonic stem cells," *Archives of Toxicology*, vol. 86, pp. 651–661, apr 2012.

[123] K. Saha and D. V. Schaffer, "Signal dynamics in Sonic hedgehog tissue patterning.," *Development (Cambridge, England)*, vol. 133, pp. 889–900, mar 2006.

[124] S. Ting, A. Chen, S. Reuveny, and S. Oh, "An intermittent rocking platform for integrated expansion and differentiation of human pluripotent stem cells to cardiomyocytes in suspended microcarrier cultures.," *Stem cell research*, vol. 13, pp. 202–13, sep 2014.

[125] M. Vosough, E. Omidinia, M. Kadivar, M.-A. Shokrgozar, B. Pournasr, N. Aghdami, and H. Baharvand, "Generation of Functional Hepatocyte-Like Cells from Human Pluripotent Stem Cells in a Scalable Suspension Culture," *Stem Cells and Development*, vol. 22, pp. 2693–2705, oct 2013.

[126] H. Kempf, C. Kropp, R. Olmer, U. Martin, and R. Zweigerdt, "Cardiac differentiation of human pluripotent stem cells in scalable suspension culture," *Nature Protocols*, vol. 10, pp. 1345–1361, aug 2015.

[127] T. DiStefano, H. Y. Chen, C. Panebianco, K. D. Kaya, M. J. Brooks, L. Gieser, N. Y. Morgan, T. Pohida, and A. Swaroop, "Accelerated and Improved Differentiation of Retinal Organoids from Pluripotent Stem Cells in Rotating-Wall Vessel Bioreactors," *Stem Cell Reports*, vol. 10, pp. 300–313, jan 2018.

[128] K. G. Chen, B. S. Mallon, R. D. McKay, and P. G. Robey, "Human Pluripotent Stem Cell Culture: Considerations for Maintenance, Expansion, and Therapeutics," *Cell Stem Cell*, vol. 14, pp. 13–26, jan 2014.

[129] C. Kropp, D. Massai, and R. Zweigerdt, "Progress and challenges in large-scale expansion of human pluripotent stem cells," *Process Biochemistry*, vol. 59, pp. 244–254, aug 2017.

[130] D. E. Kehoe, D. Jing, L. T. Lock, and E. S. Tzanakakis, "Scalable Stirred-Suspension Bioreactor Culture of Human Pluripotent Stem Cells," *Tissue Engineering Part A*, vol. 16, pp. 405–421, feb 2010.

[131] R. Olmer, L. Engels, A. Usman, S. Menke, M. N. H. Malik, F. Pessler, G. Göhring, D. Bornhorst, S. Bolten, S. Abdelilah-Seyfried, T. Scheper, H. Kempf, R. Zweigerdt, and U. Martin, "Differentiation of Human Pluripotent Stem Cells into Functional Endothelial Cells in Scalable Suspension Culture.," *Stem cell reports*, vol. 10, pp. 1657–1672, may 2018.

[132] H. Lin, Q. Li, and Y. Lei, "An Integrated Miniature Bioprocessing for Personalized Human Induced Pluripotent Stem Cell Expansion and Differentiation into Neural Stem Cells," *Scientific Reports*, vol. 7, p. 40191, dec 2017.

[133] C. Kropp, H. Kempf, C. Halloin, D. Robles-Diaz, A. Franke, T. Scheper, K. Kinast, T. Knorpp, T. O. Joos, A. Haverich, U. Martin, R. Zweigerdt, and R. Olmer, "Impact of Feeding Strategies on the Scalable Expansion of Human Pluripotent Stem Cells in Single-Use Stirred Tank Bioreactors," *STEM CELLS Translational Medicine*, vol. 5, pp. 1289–1301, oct 2016.

[134] S. Abbasalizadeh, M. R. Larijani, A. Samadian, and H. Baharvand, "Bioprocess Development for Mass Production of Size-Controlled Human Pluripotent Stem Cell Aggregates in Stirred Suspension Bioreactor," *Tissue Engineering Part C: Methods*, vol. 18, pp. 831–851, nov 2012.

Appendix A

Supplemental Material for Adult Neural Stem Cell Study

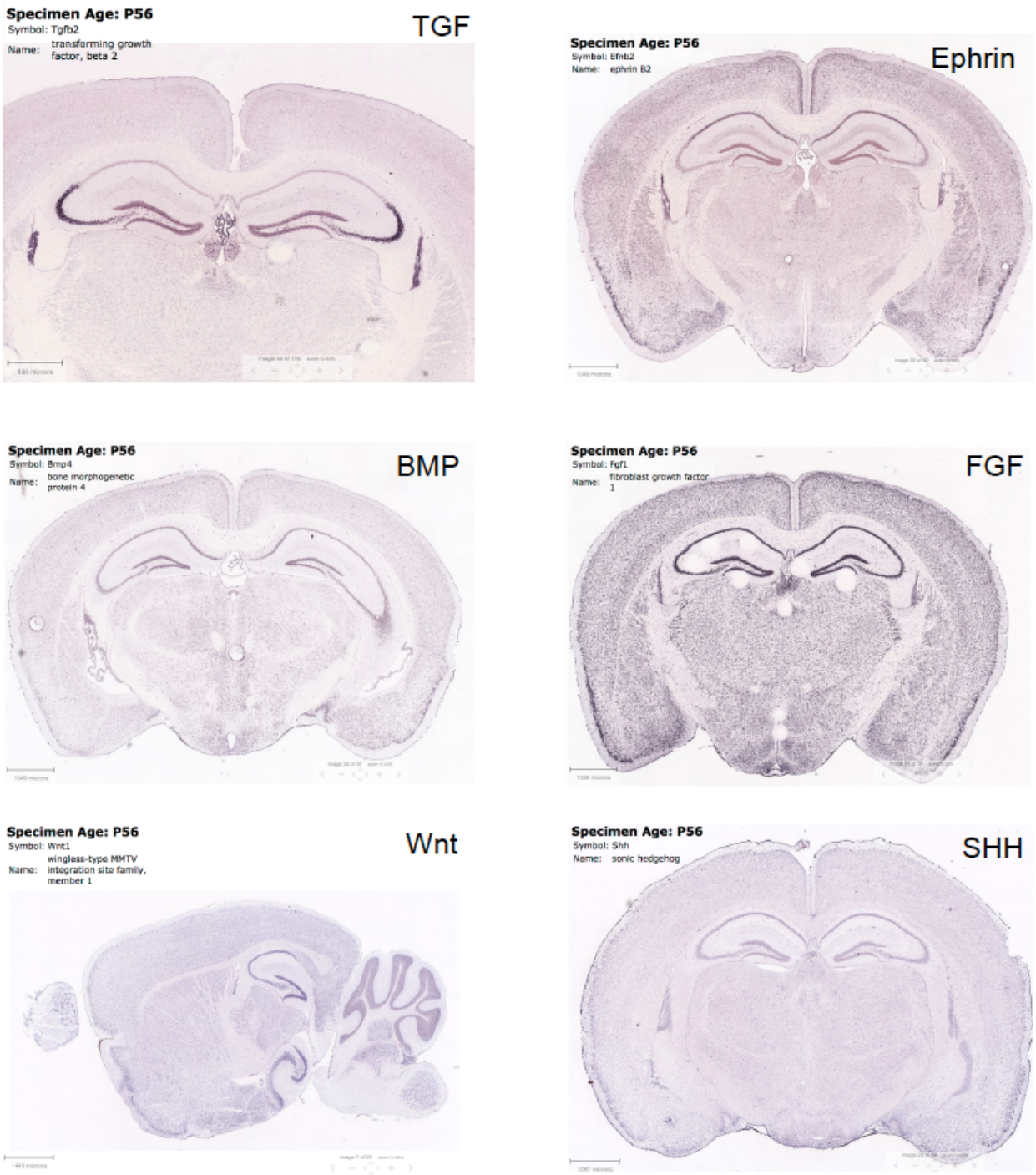

Figure A.1: Collection of in situ hybridization (ISH) data from the Allen Mouse Brain Atlas for mRNA expression of select signaling cues in the adult mouse hippocampus

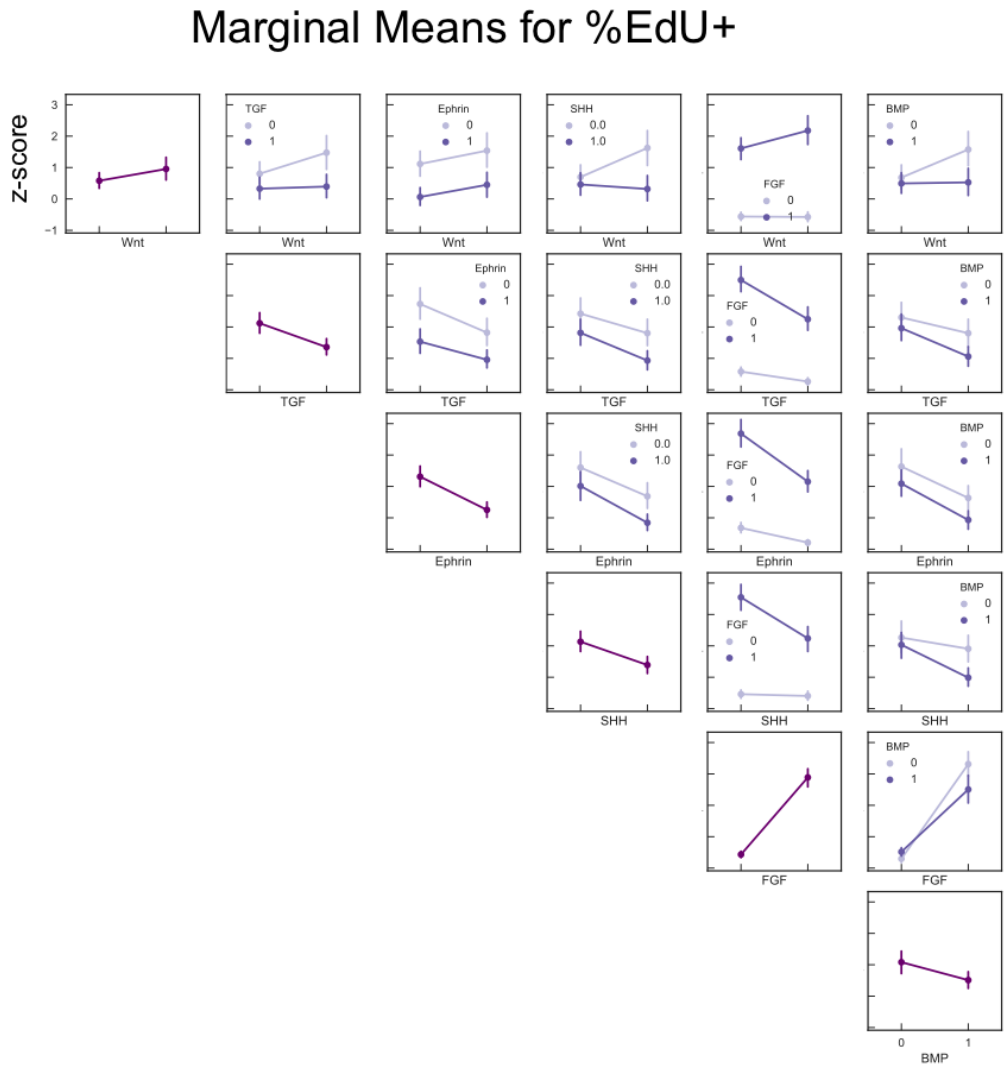

Figure A.2: Complete marginal means interaction grid for Edu+.

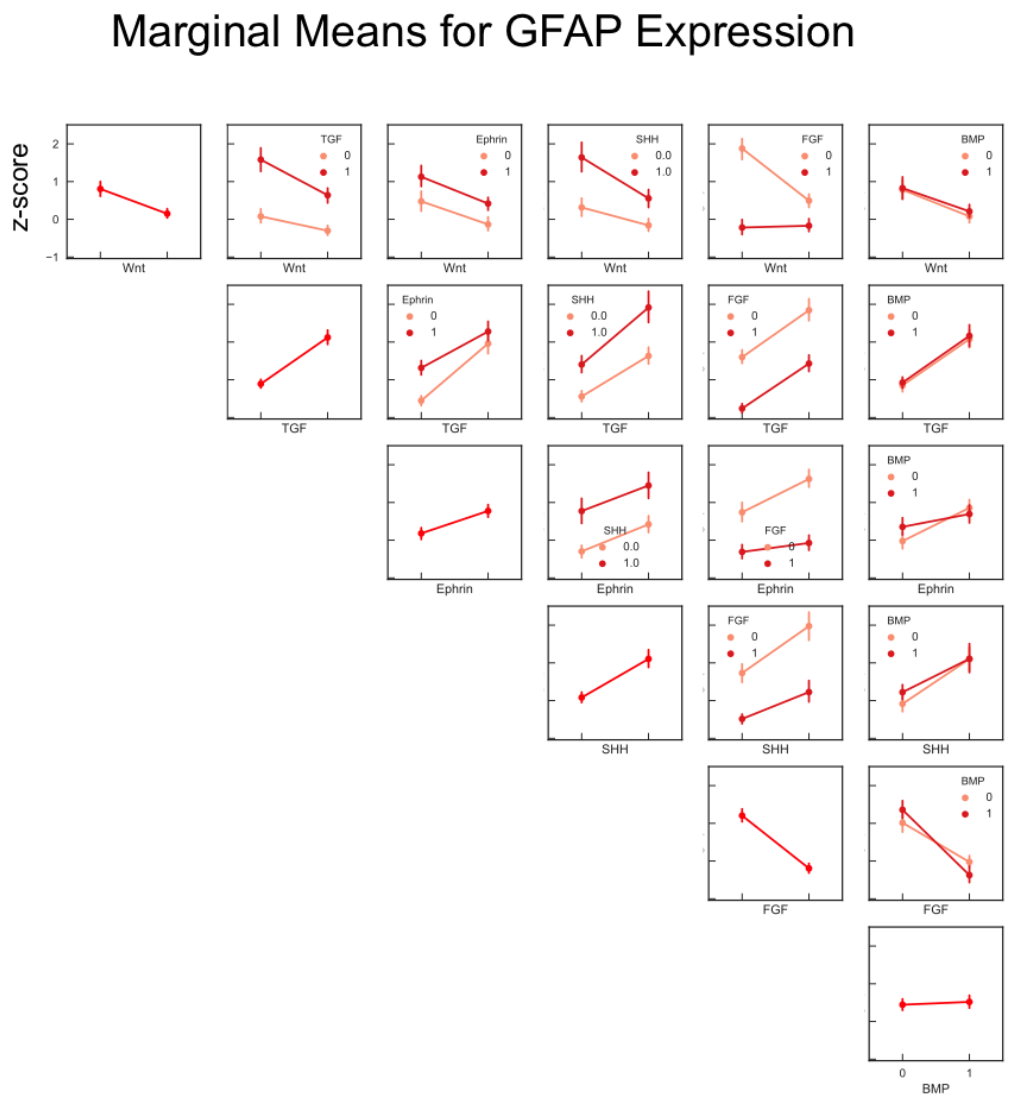

Figure A.3: Complete marginal means interaction grid for GFAP expression.

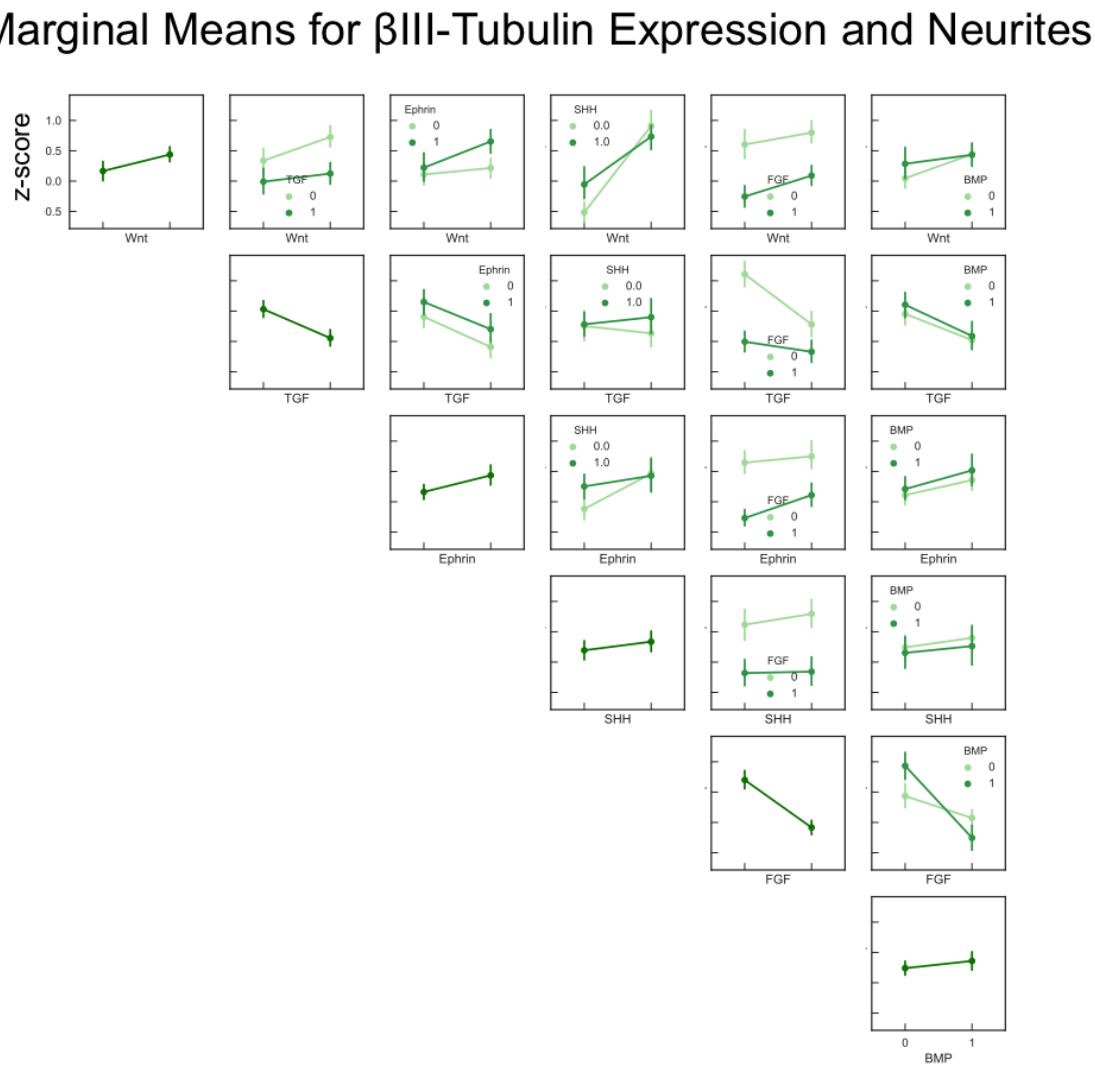

Figure A.4: Complete marginal means interaction grid for βIII-Tubulin expression.

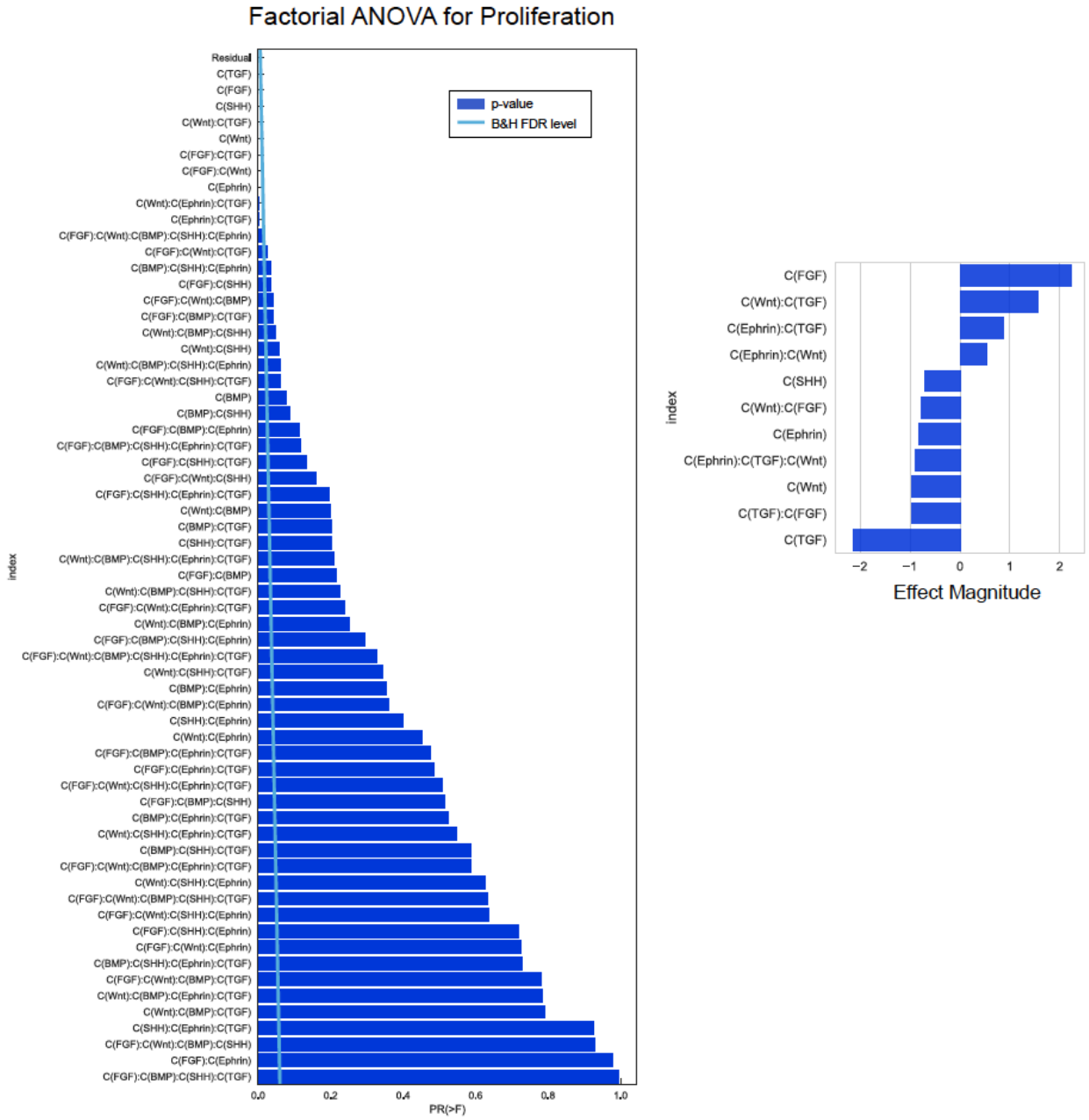

Figure A.5: Factorial ANOVA for proliferation with the Benjamini - Hochberg threshold for multiple comparisons at a significance level of 0.05 and effect magnitudes of significant combinations.

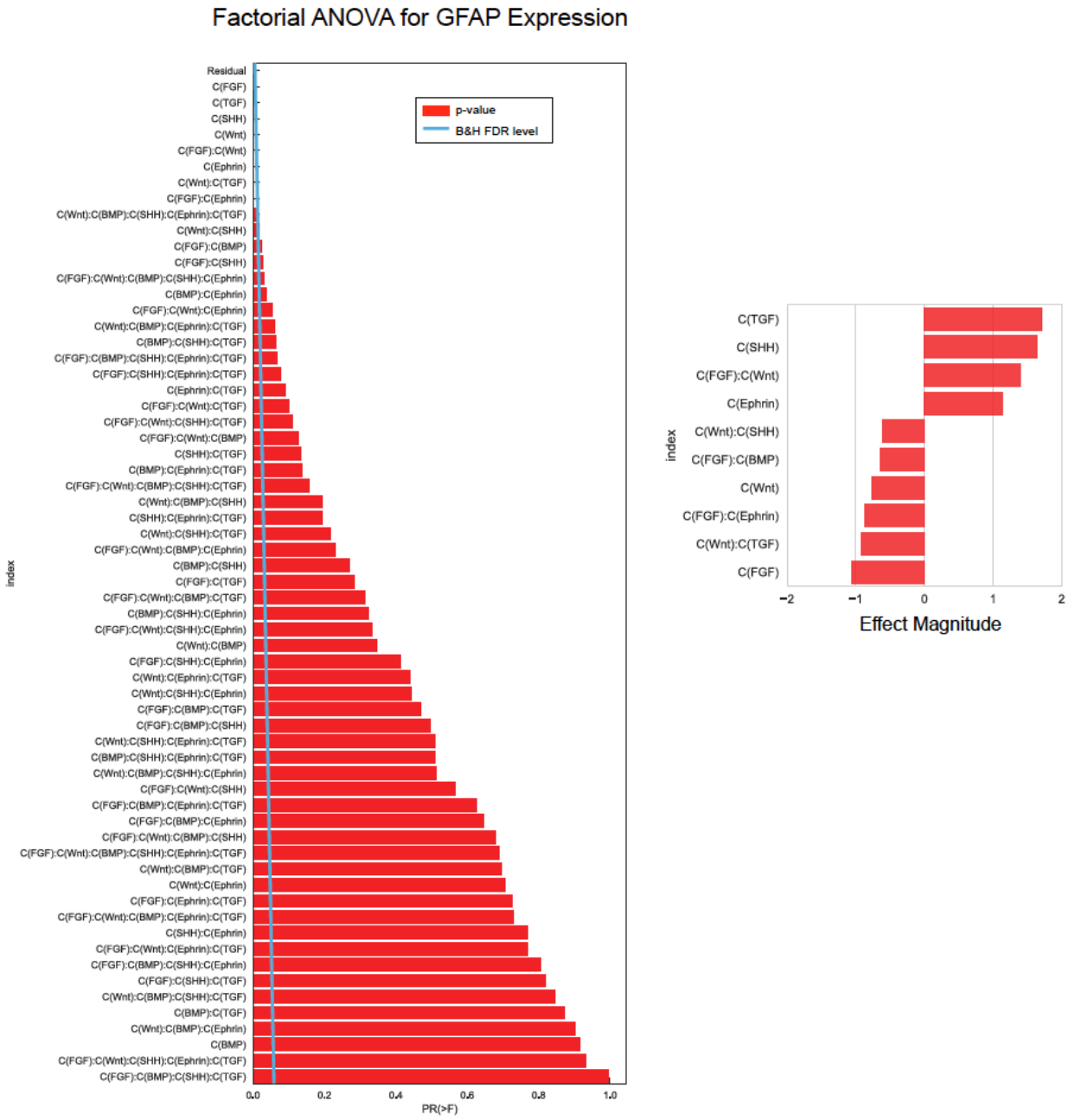

Figure A.6: Factorial ANOVA for GFAP expression with the Benjamini - Hochberg threshold for multiple comparisons at a significance level of 0.05 and effect magnitudes of significant combinations.

Table A.1: Adult Hippocampal Neural Progenitor Cell Culture Reagent Details

Cell Culture Reagents	**Experimental Details**	**Manufacturer, Cat. No**
Human FGF-2	1-20 ng/mL	Peptrotech, 100-18B
Mouse SHH C25II, N-Terminus	1 μg/mL	R&D, 464-SH-025/CF
Multivalent Ephrin	400 nM	C. Yang, Schaffer Lab
Human Wnt-3a	200 ng/mL	R&D, 5036-WN-010/CF
Bovine Serum Albumin	0.5%	Sigma, A4503-100G
Human BMP-4	50 ng/mL	R&D, 314-BP-010/CF
Human TGF-β 1	50 ng/mL	R&D, 240-B-002/CF
N-2 Supplement	1:50	Life Technologies, 17502-048
Accutase	-	Life Technologies, A11105-01
poly-L-Ornithine HBr	10 μg/mL	Sigma, P3655-100MG
Natural mouse Laminin	5-100 μg/mL	Invitrogen, 23017-015
Retinoic Acid, all trans	1 μM	Enzo, BML-GR100-0500
Fetal Bovine Serum	1%	Fischer, SH3007001
DMEM-F12	-	Life Technologies, 11039-047

Table A.2: Fluorescence Cytochemistry Reagents Details

Staining Reagents	**Dilution Details**	**Manufacturer, Cat. No**
Hoechst	1:2000	Life Technologies, H3570
Calcein AM	1:2000	Invitrogen, L-3224
Ethidium Homodimer	1:500	Invitrogen, L-3224
Click-It EdU kit	As described in kit	Life Technologies, C10340
Rabbit anti-GFAP	1:1000	Abcam, ab7260
Mouse anti-βIII Tubulin	1:1000	Sigma, T8578-200UL
Donkey anti-Rabbit Cy3	1:250	Jackson, 711-165-152
Donkey anti-Rabbit 647	1:250	Jackson, 711-605-152
Donkey anti-Mouse 488	1:250	Jackson, 711-545-152
Donkey Serum	5%	Sigma, D9663-10ML
Triton X-100	0.25%	Sigma, X100-100ML

Appendix B

Supplemental Material for Pluripotent Stem Cell Study

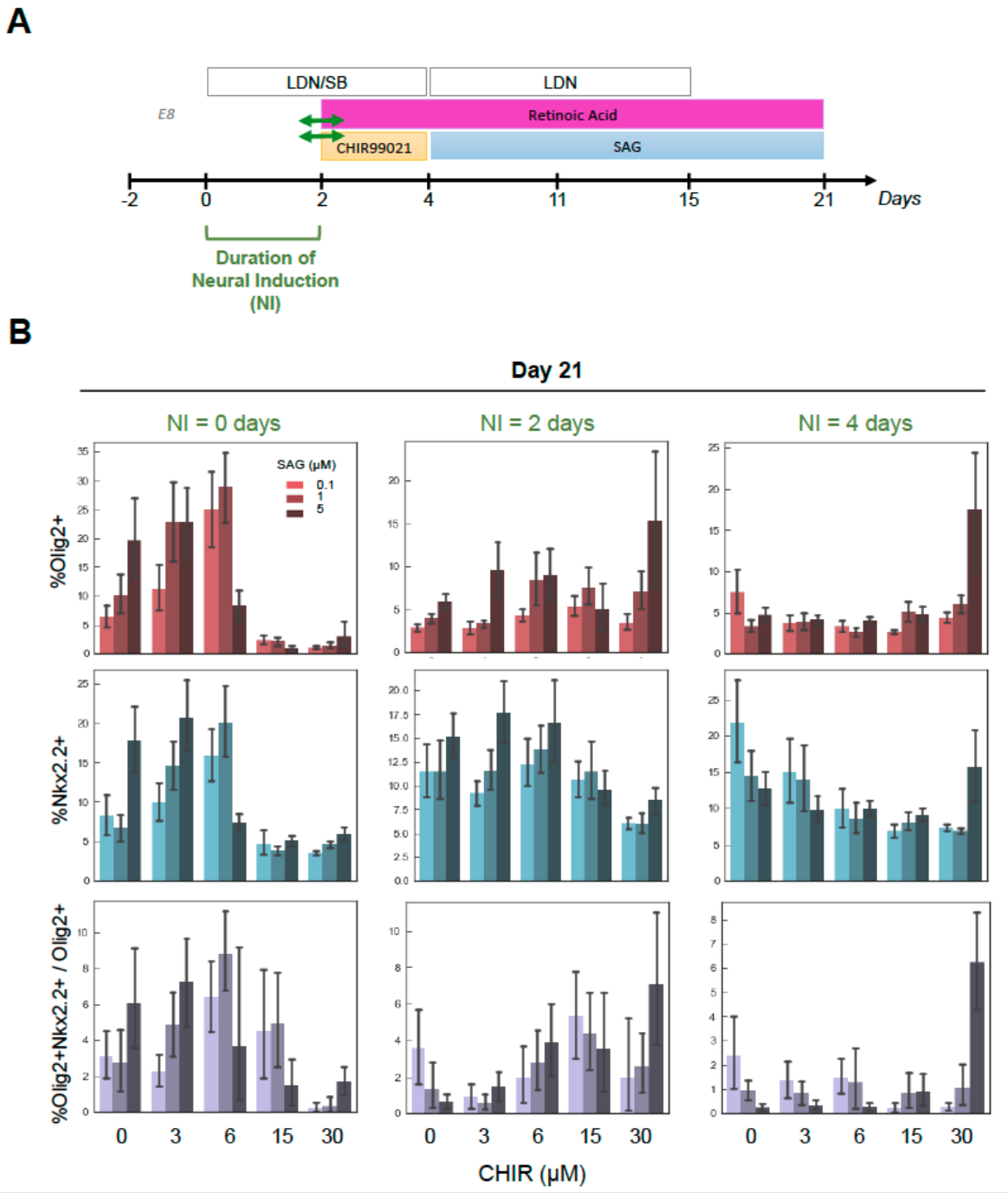

Figure B.1: Duration of Neural Induction affects OPC differentiation efficiency. A) Timeline of soluble signaling cues and three different durations of neural induction before addition of additional patterning cues CHIR, RA, and SAG. B). Olig2, Nkx2.2, proportion of Nkx2.2+ Olig2+ cells in total Olig2+ population at Day 21.

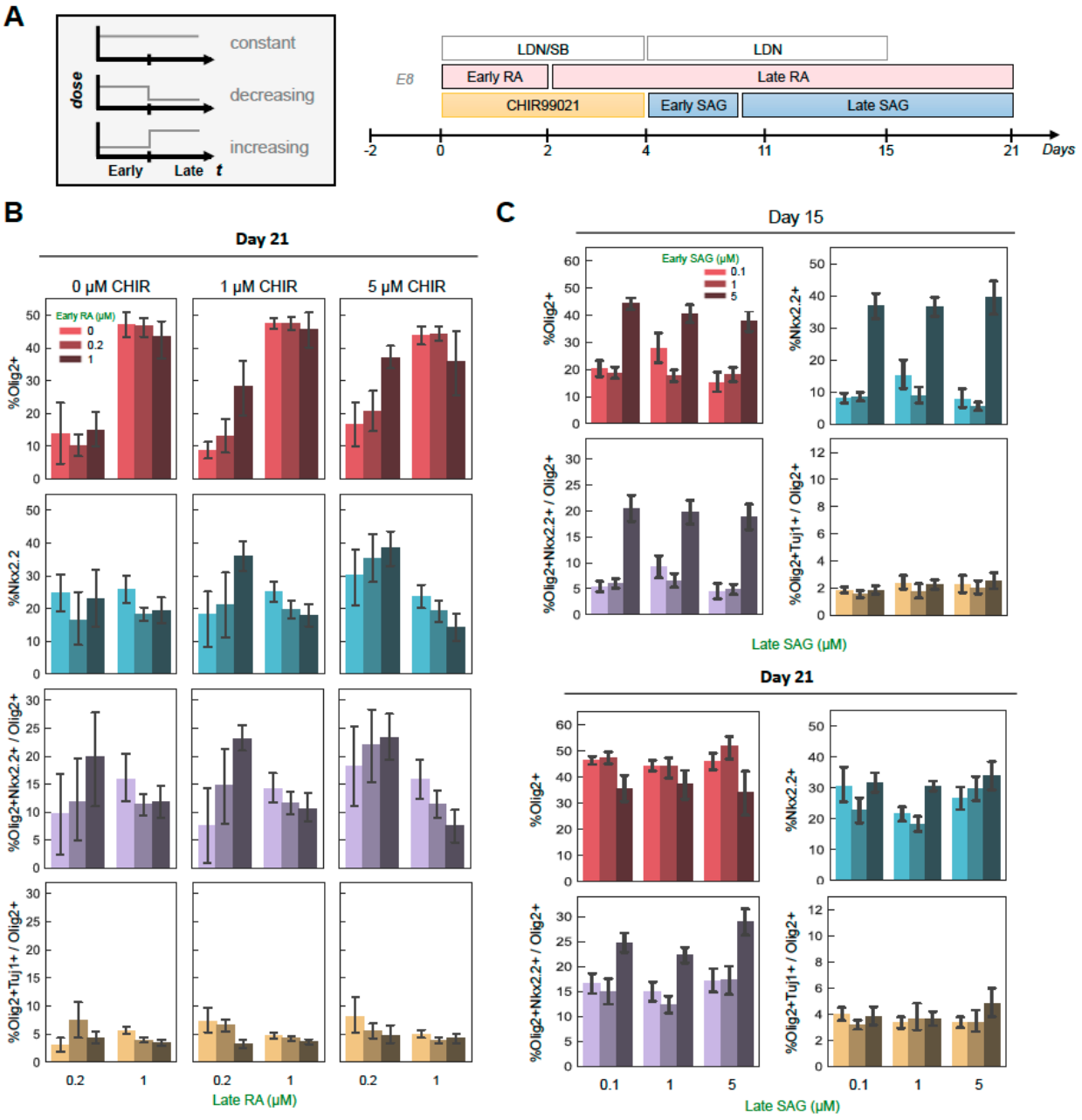

Figure B.2: Temporal profiles of RA and SAG influence OPC specification. A) Timeline of early and late windows for RA and SAG exposure. B) Olig2, Nkx2.2, and proportion of Nkx2.2+ Olig2+ cells in total Olig2 at Day 21 in response to time-varying doses of RA and different CHIR concentrations. C) Olig2, Nkx2.2, proportion of Nkx2.2+ Olig2+ cells in total Olig2+, and proportion of Tuj1+ Olig2+ cells in total Olig2+ population at Day 15 and Day 21 in response to time-varying doses of SAG.

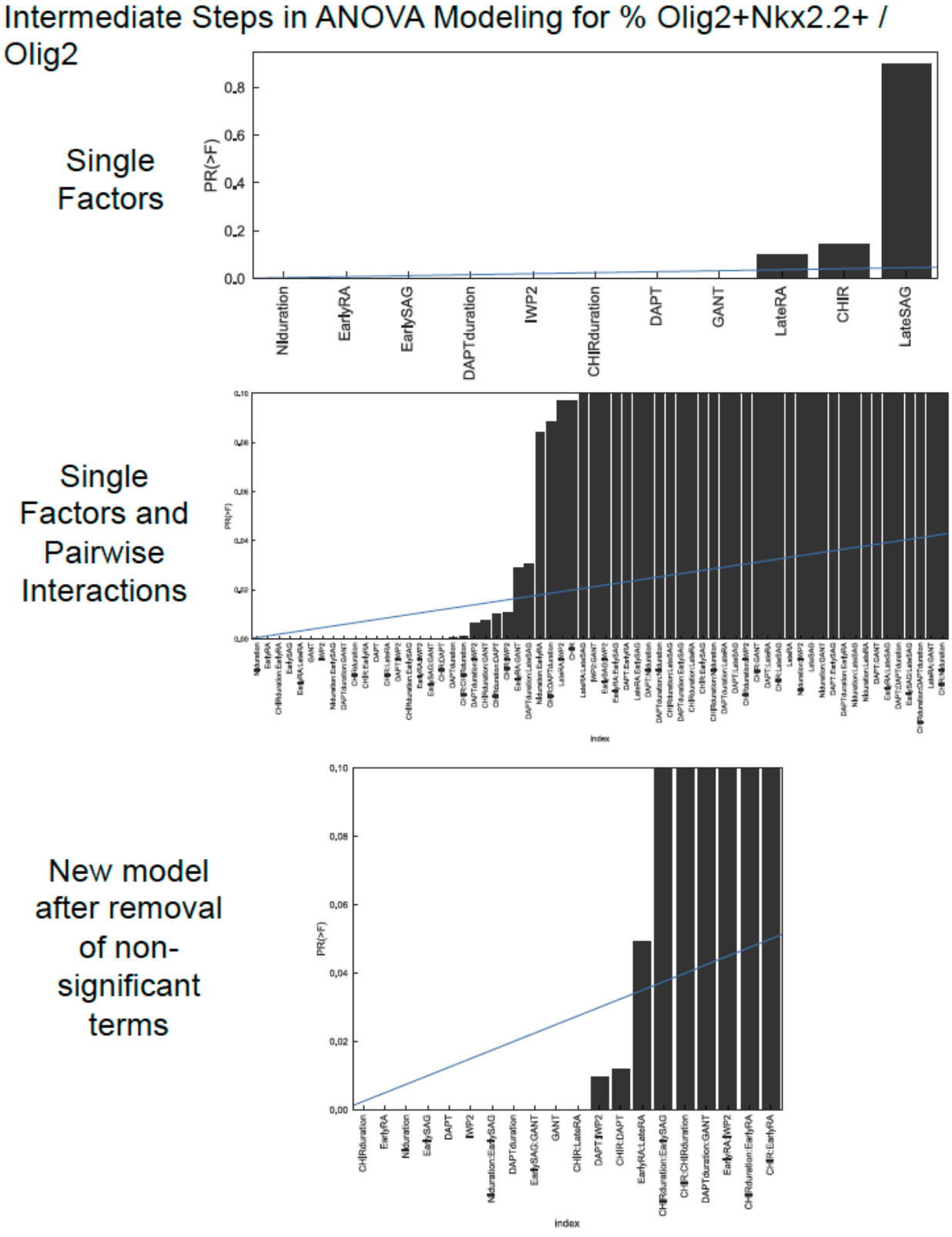

Figure B.3: Iterative process to improve Factorial ANOVA model.

Table B.1: Human Pluripotent Stem Cell Culture Reagents

Cell Culture Reagents	**Dosing**	**Manufacturer, Cat. No**
Y-27632 (Rock Inhibitor)	10 μM	SelleckChem, S1049
CHIR-99011	varied	Tocris, 4423
Retinoic Acid, all trans	varied	Enzo, BML-GR100-0500
SAG dihydrochloride	varied	Xcessbio, M60081-2
DAPT	varied	SelleckChem, S2215
IWP-2	varied	Tocris, 3533
GANTT61	varied	Enzo, ALX-270-482-M001
DMSO	100%	Sigma, D2650-5X5ML
Glutamax Supplement	1:100	ThermoFisher, 35050061
B27 supplement	1:50	ThermoFisher, 17504-044
N-2 Supplement	1:50	Life Technologies, 17502-048
Accutase Solution	-	Life Technologies, A11105-01
Versene Solution	-	ThermoFisher, 15040066
Essential-8 Media	100%	Life Technologies, A1517001
DMEM-F12	50%	Life Technologies, 11039-047
Neurobasal Media	50%	ThermoFisher, 10888022
hESC-qualified Matrigel	50%	Corning, 354277
Penicillin/Streptomycin	0.50%	ThermoFisher, 15140122

Table B.2: Fluoresence Cytochemistry Reagent Details

Staining Reagents	**Dilution Details**	**Manufacturer, Cat. No**
Hoechst	1:2000	Life Technologies, H3570
Calcein AM	1:2000	Invitrogen, L-3224
Ethidium Homodimer	1:500	Invitrogen, L-3224
Mouse anti-Nkx2.2	1:200	DSHB, 74.5A5
Goat anti-Olig2	1:40	R&D Systems, AF2418
Mouse anti-TH	1:1000	Pel-Freez, P40101-150
Mouse anti-Tuj1	1:1000	Sigma, T8578-200UL
Donkey anti-Rabbit Cy3	1:250	Jackson, 711-165-152
Donkey anti-Goat 647	1:250	Jackson, 705-605-147
Donkey anti-Mouse 488	1:250	Jackson, 711-545-152
Donkey Serum	5%	Sigma, D9663-10ML

Table B.3: Parameterization Details for Computational Fluid and Chemical Dynamics Modeling of Stirred Bioreactor in COMSOL

Biological	
PSC conc_0, cells/mL gel	1.00E+05
n, days	10
growth rate, daysˆ1	0.4
PSCs_0, cells	5.00E+05
PSCs_n, cells	1.45E+07
viability fraction	0.8
PSC conc_0, cells/mL media	1.00E+04
PSC conc_n, cells/mL media	2.89E+05

Chemical	
Glucose_0, mM	13
Glucose_7, mM	5
Glucose degradation, mM/cell/day	-5.53E-07
Lactate_0, mM	0.5
Lactate_7, mM	14
Lactate production, mM/cell/day	9.33E-07
Dissolved O2_0, %	100
Dissolved O2_7, %	20
Dissolved O2 rate %/cell/day	-5.53E-06
Incubator CO2, %	5
pH_0	7.2
pH_7	6.5
pH change rate /cell/day	-4.84E-08

Physical	
Gel Volume, mL	5
Media Volume, mL	50
Media density, g/mL	1
Media viscosity, Pa*s	8.90E-04
Media height, cm	1.1
Vessel radius, cm	3.8
Stir bar length, cm	1.25
Stir bar width, cm	0.3
Stirrer setting	1
Stir Bar rotational velocity, rpm	36.6

Legend
_0 = at time 0
_n = at time n
calculated
measured